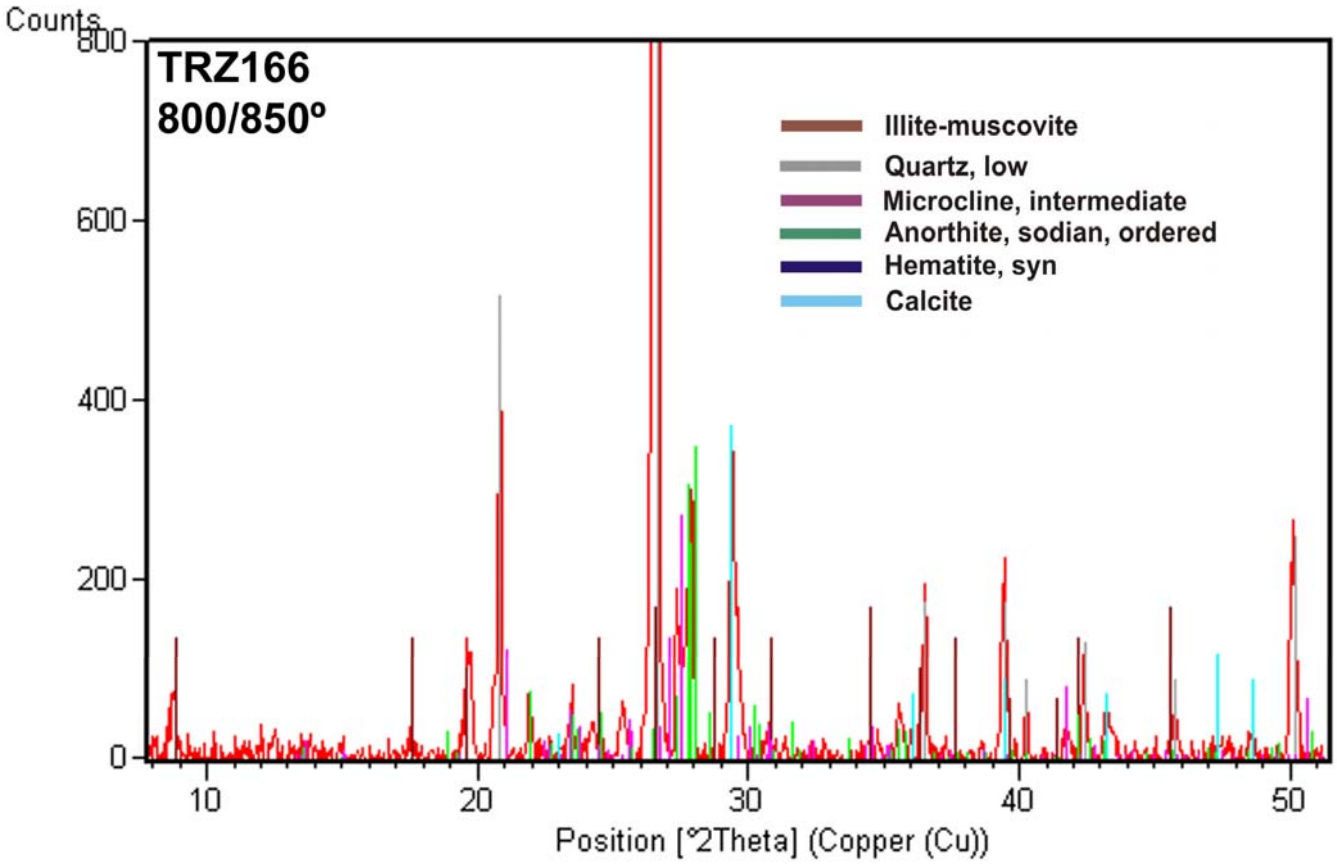

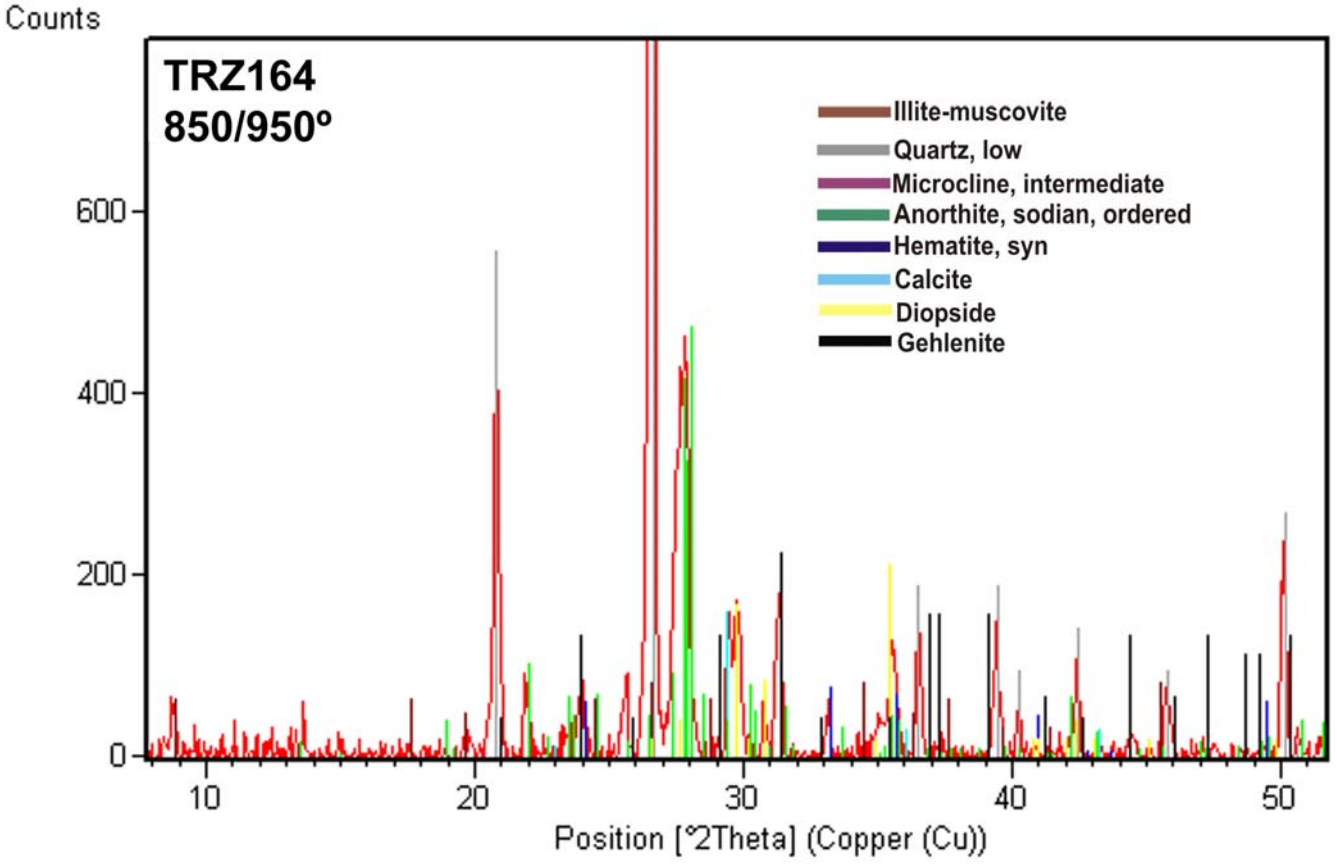

Figure 29: Difractograms of the individuals TRZ0166 and TRZ164, representing the chemical group TRZ

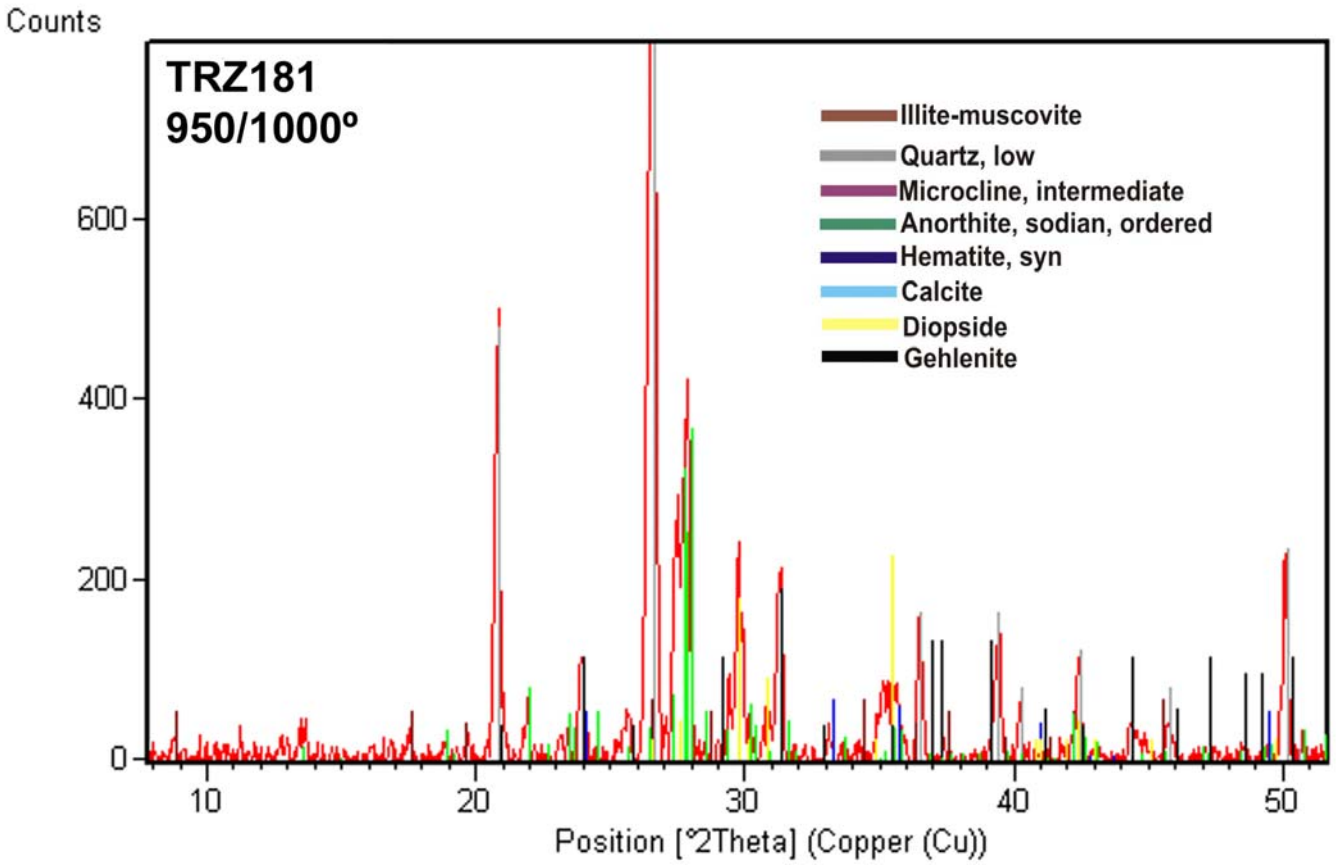

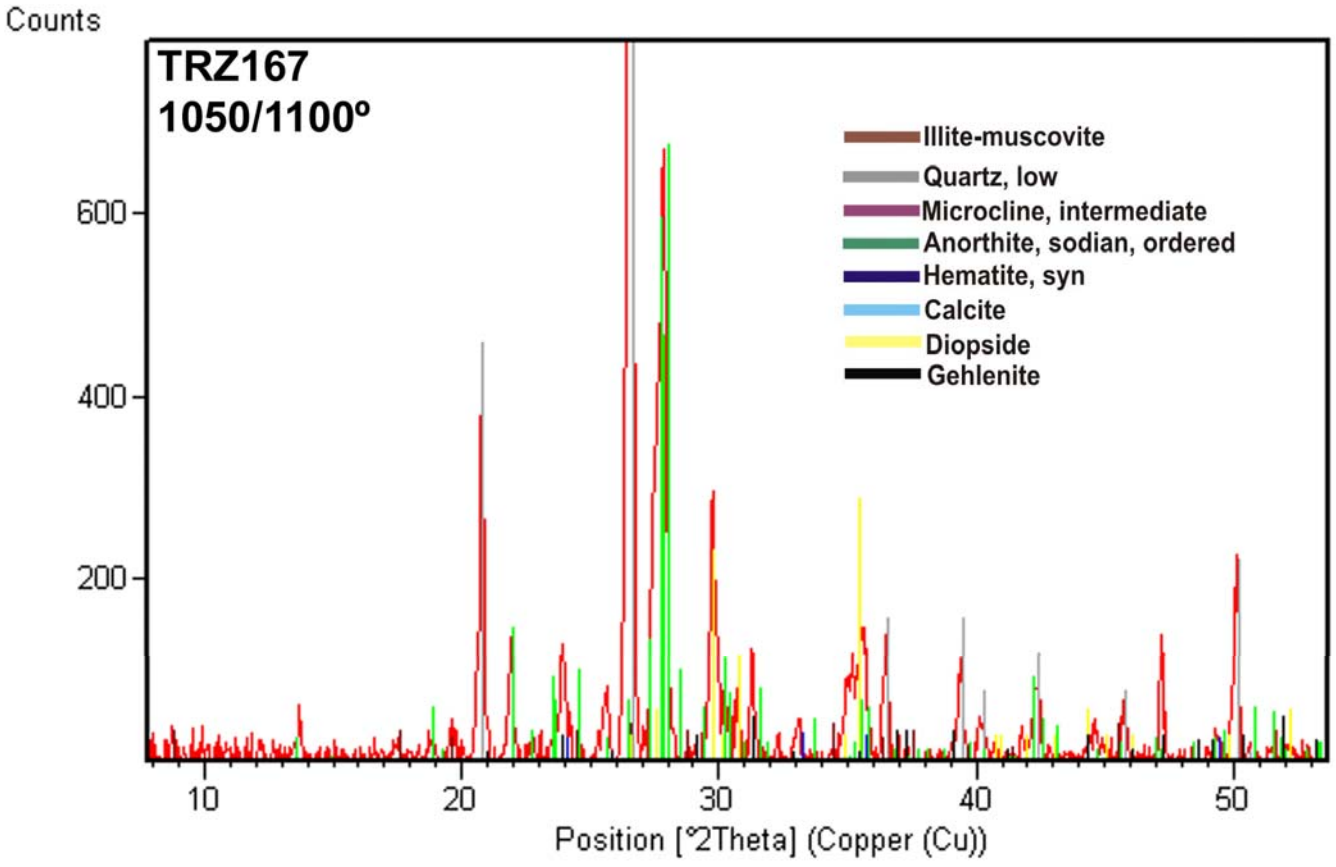

Figure 30: Difractograms of the individuals TRZ181 and TRZ167 representing the chemical group TRZ

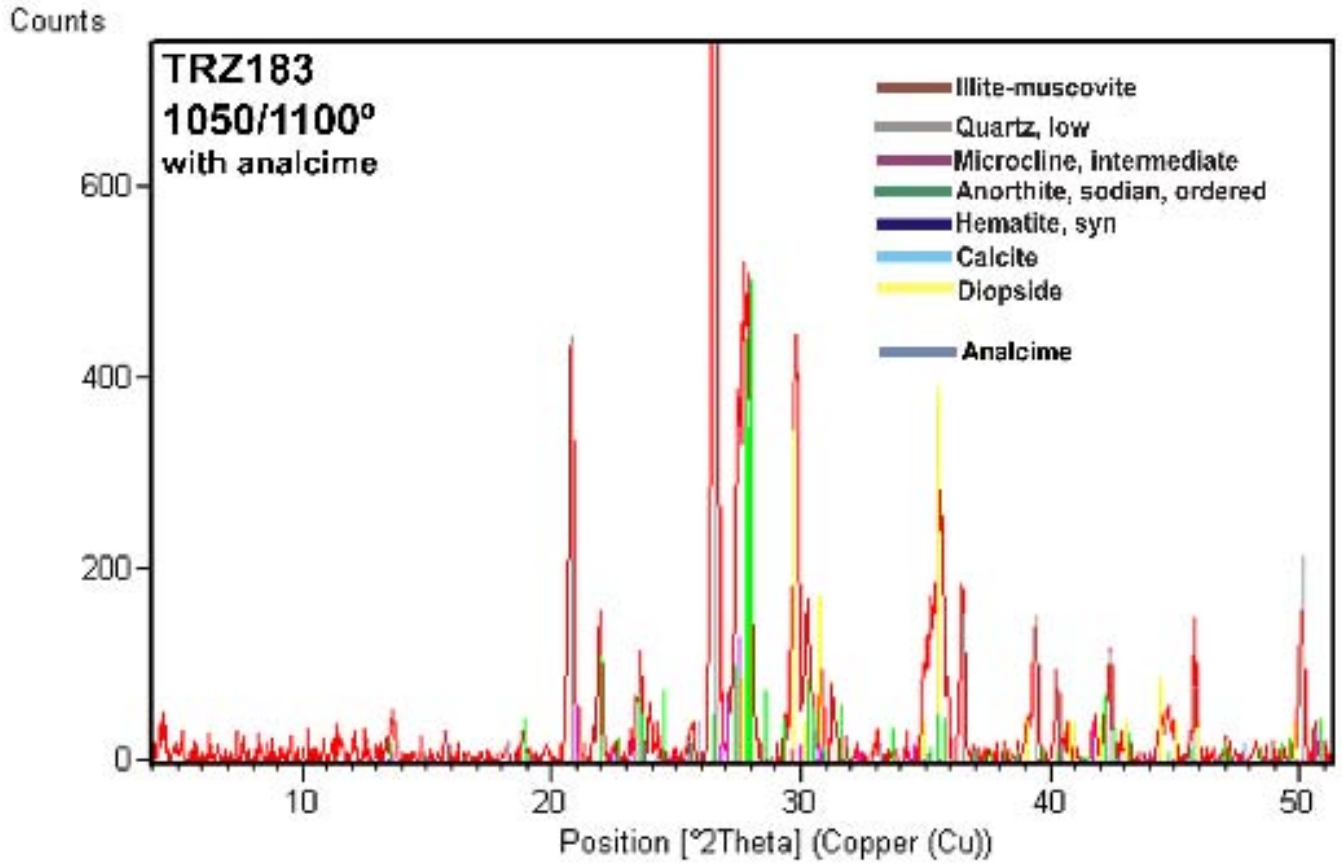

Figure 31: Difractogram of the individual TRZ183 with analcime representing the chemical group TRZ

Analysis of the surface treatment

The study of the reddish-orange slip that covers some of the common wares was performed on TRZ074 and TRZ084 sherds from Kara Tepe. The quantitative micro-chemical analysis that carried out by SEM-EDS in 3 different points of the slip and different areas of the body at 2 different sherds re-veal slight differences between TRZ074 and TRZ084 ceramics (Figure 32). Clay of TRZ074 is richer in Si

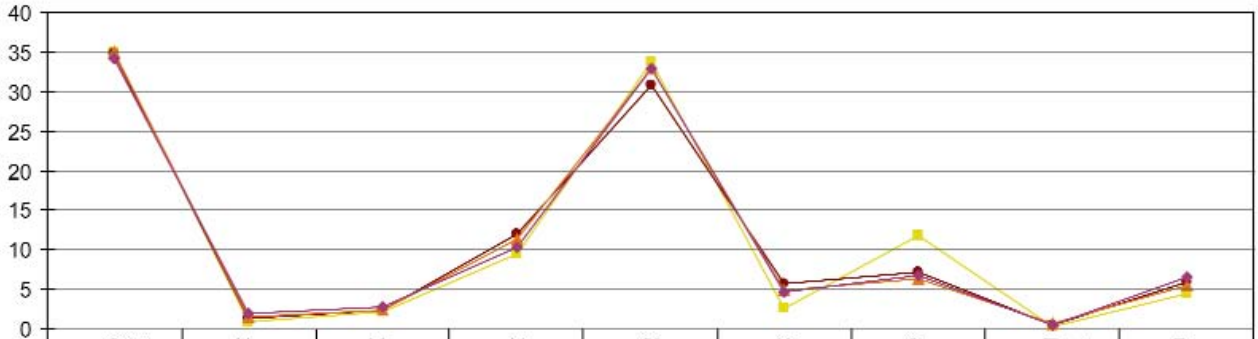

	O (%)	Na (%)	Mg (%)	Al (%)	Si (%)	K (%)	Ca (%)	Ti (%)	Fe (%)
TRZ074c	35.03	0.9	2.04	9.34	33.69	2.57	11.65	0.3	4.48
TRZ074s	34.82	1.17	2.36	11.99	30.72	5.67	7.05	0.42	5.79
TRZ084c	35.06	1.38	2.36	11.26	32.78	4.86	6.37	0.54	5.38
TRZ084s	34.15	1.85	2.77	10.21	32.97	4.53	6.64	0.35	6.52

Figure 32: Mean chemical composition of clay (c) and slip (s) of the common ware TRZ074, associated to TT-K1 pottery production and of the common ware TRZ084 considered an outlier

and Ca whereas the clay matrix of TRZ084 is richer in Al and K. In both cases, the clay matrix and the red slip had a similar composition but Al and K values are higher in the slip of TRZ074 whereas on the case of TRZ084, the Si content is higher. The similarity in the composition between clays and slip in both cases probably means that a finer fracture of the clay used to fabricate the pots was applied to produce the red slip.

The microphotographs of the polished sections show a fine and homogeneous layer of an irregular thickness, from 150 to 450µm, on the ceramic body's surface (Figure 33). Looking at the interface between the red slip and the clay matrix, no clear separation line could be observed but the existence of a 10 to 50µm insertion zone. That clearly indicates a biscuit, just fired at ones, and no glaze firing. No clear differences are observed in the firing process between painted and unpainted common wares (Figure 34). Five bowls and one jar from the Citadell are painted. Most of them were fired around 850-950ºC and only two bowls (TRZ098 and 101) were fired at higher temperature. Painted kushan-sassanian ceramics from Tchinguiz Tepe appears in all ranges of estimated temperatures. Bowls were normally fired around 850-950ºC whereas big plates and coups were fired up to 950ºC. Painted jars from the kiln 2 of Kara Tepe were fired in a large range of temperatures, from 900 to 1000ºC. Firing temperature estimated for painted big containers and bowls from Kara Tepe is 900-950ºC whereas all big plates and one lamp were fired up to 950ºC.

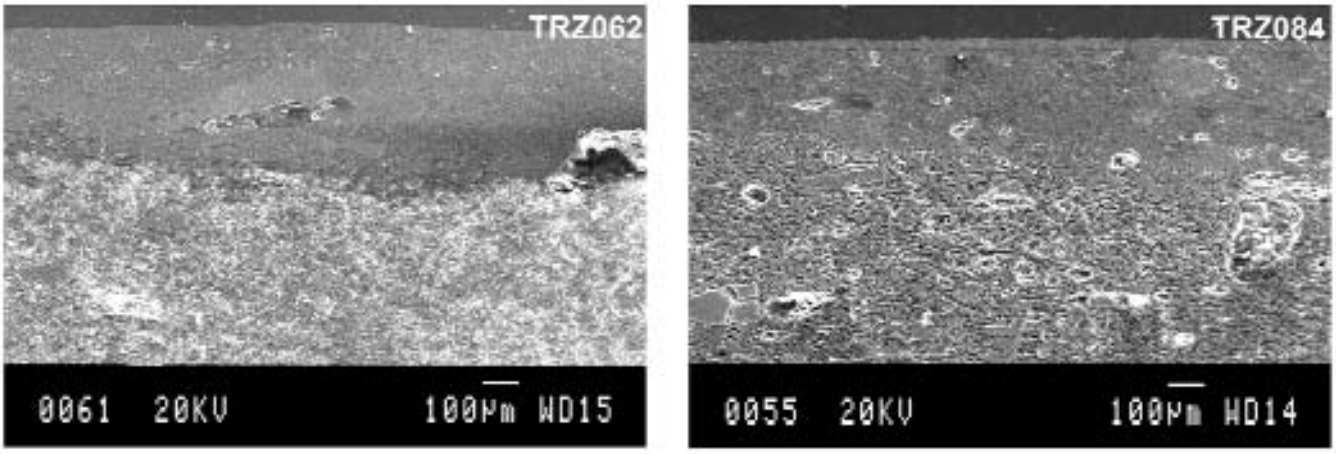

Figure 33: SEM photomicrographs of the polished sections of the red slip and paste area observed in SEM-EDS upon the common wares TRZ062 and TRZ084

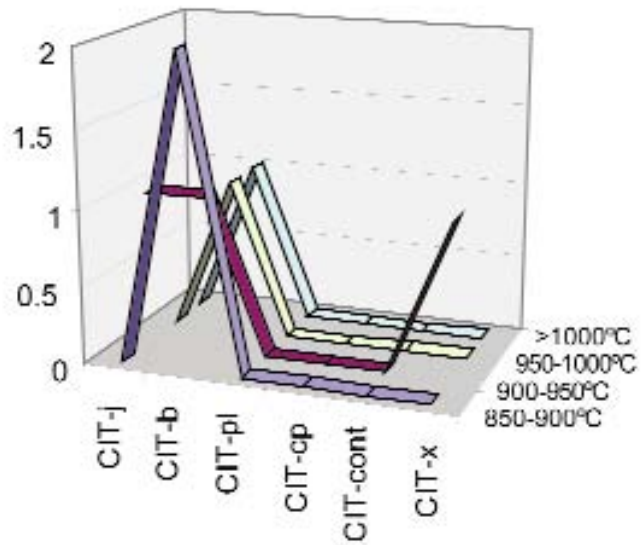

Figure 34: Graphics representing the different typologies of the painted common wares (j: jars, b:bowls, pl: plates, cp: coup, cont: container, x: unknown) from the Citadel (CIT), Tchinguiz Tepe (TT-K1) and Kara Tepe (KR-K2) and the firing temperatures associated to each typology

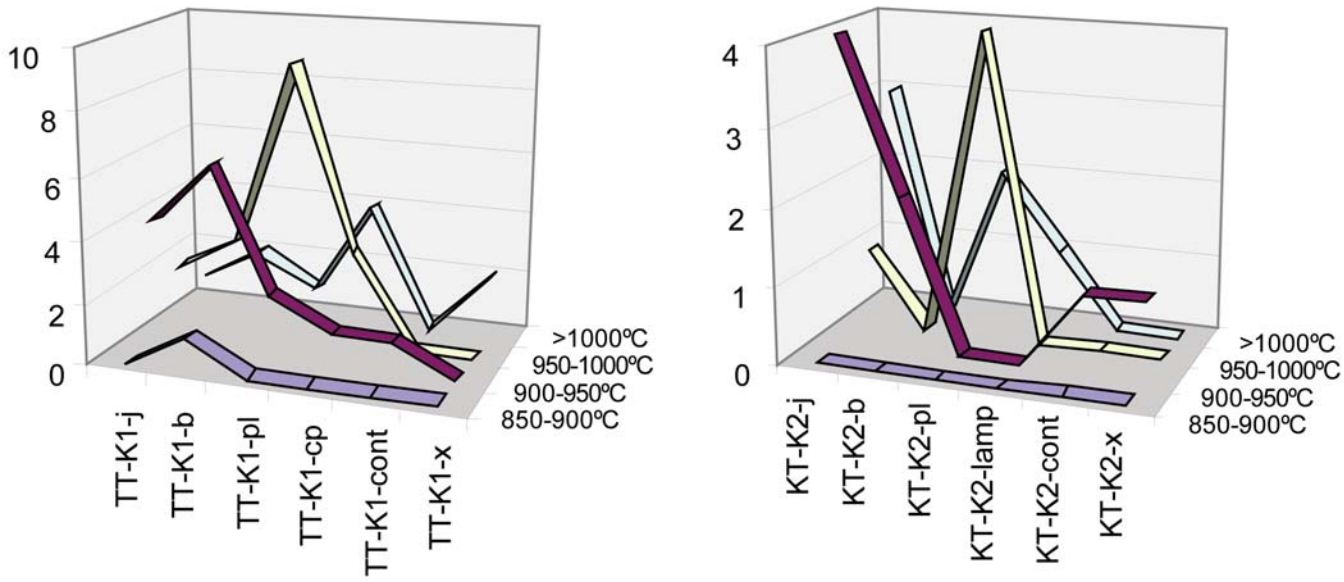

Figure 34: Graphics representing the different typologies of the painted common wares (j: jars, b:bowls, pl: plates, cp: coup, cont: container, x: unknown) from the Citadel (CIT), Tchinguiz Tepe (TT-K1) and Kara Tepe (KR-K2) and the firing temperatures associated to each typology

Integrated chemical and petrographic results for Kampyr Tepe ceramics

An important general observation can be made on the data set. First, all the analysed material is calcareous without any exception. Second, the Na_2O concentrations are clearly high in all the individuals exactly like in the case of the ceramics from ***Termez***. Due to the burial conditions in this desert area, there are salt (NaCl) contaminations in all the samples of ***Kampyr Tepe*** and in one individual (TRZ204) the presence of analcyme ($Na_2AlSi_2O_6 \times H_2O$) could be observed.

The CVM calculated for ***Kampyir Tepe's*** data set can be seen in Table 11. It has been calculated without considering the following elements: Mo, Sn, Co, W, MnO P_2O_5 and Pb. As it has been already explained before, the first two elements have been left out in the cause of analytical imprecision, as both of them are under their regression limits in ceramics. MnO is an element with problems of analytical accuracy. Co and W have been left out from the calculation because of the possibility of contamination due to the sample preparation process and, the last two because they are elements which are very susceptible to suffer post-depositional contaminations. Therefore they can introduce a false variability in the data set.

The total variation (vt) in this data set according to the CVM is 0.2363, which generally, indicates a very homogeneous geochemical character (similar or common raw materials) for all the analysed material. At the first site, the variability introduced by the majority of the elements is relatively low. In Table 11 we pointed out by yellow the elements which introduce more than the 50% of the variability in this data set and which are Sr, CaO, Na_2O, Ce, Cu and Ni. From these elements in the case of Na_2O the high variability is due to post-depositional contaminations. The first one is altered almost in the whole data set, as above explained, because of the presence of NaCl (salt) and in the case of TRZ204 because of the presence of analcime ($Na_2AlSi_2O_6 \times H_2O$), which affects also the K_2O and Rb concentrations in this specific individual. Therefore to avoid the chemical differences introduced by the above mentioned alte-rations and/or contaminations dominate the statistical treatment of the data we ignored Na_2O, K_2O, Rb concentrations of the rest of the statistical treatment.

In the new CVM, the vt is equal to 0.1885 and the most variable elements in this new CVM are maintained, CaO, Sr, Ce, Ni and Cu.The normalised chemical composition of the analysed ceramic material from ***Kampyr Tepe*** can be seen in Table 12. Looking at the chemical data, CaO, Sr and Ce are chemically associated elements and this kind of variability can be natural in calcareous raw material sources. A total variation of this range indicates that all the sampled individuals from ***Kampyr Tepe*** are probably representing one single production, or, at the same way as in the case of ***Termez***, it this might be owed to the low geological variability in this area if we accept that they are local productions.

To continue the statistical treatment, the chemical data were transformed into logratios following the consideration of Aitchison (1986) and Buxeda (1999) on compositional data. The logratio transformation was performed upon the subcomposition: Fe_2O_3 TiO_2, SiO_2, Zr, Y, Ce, Ga, V, Nb, Zn, Cu, Ni and Cr of the 40 analysed individuals, where Al_2O_3 was used as divisor. As according to the CVM it was the element less contributing to the chemical variability. Beside the elements we did not considered above in the statistical treatment we also excluded CaO, Sr, MgO, Th and Ce from the logratio transformation to avoid that possible natural variability in these specific elements dominate the multivariate analysis. The chemical results are summarized in the dendrogram of Figure 35, resulting from the cluster analysis performed by S-plus2000 (MathSoft, 1999) upon the previous subcomposition, using the Square Euclidean distance and the centroid algorithm. The main group of the analysed material indicted by a discontinuous green rectangle in the dendrogram of Figure 35 is very similar chemically and probably represents one single production which can be separated into two smaller subgroups **$KPT_{(A)}$** (TRZ203, 204, 208, 209, 210, 211, 212, 213, 214, 215, 217, 219, 222, 228, 232, 233, 237, 239) and **$KPT_{(B)}$** (TRZ205, 206, 207, 220, 221, 224, 226, 227, 234, 236, 238, 240, 241, 242) due to small differences in the trace element composition (biplot of Figure 36). By looking at the chemical composition **$KPT_{(A)}$** contains individuals with slightly higher Ga, V, Cu, Ni and Cr concentrations. These differences, however, are not so significant that to indicate the existence of two different productions or Paste Compositional Reference Units (PCRU's). TRZ223 is a chemical outlier of **$KPT_{(B)}$** and TRZ230 is a chemical outlier of **$KPT_{(A)}$** TRZ225 and TRZ231 are chemical outliers of both of these subgroups. The mean chemical composition and the standard deviation of both subgroups can be seen at Table 13 and at Figures 37 and 38 the typology of each subgroup can be distinguished. Crosschecking these results with the mineralogical study, a slight difference in the firing temperature can be observed between the two subgroups and this might be the reason of their separation following the multivariate analysis. Finally we can say that **$KPT_{(A)}$** and **$KPT_{(B)}$** correspond in fact to the same production. Their chemical similarity also can be confirmed by the mean chemical composition presented at Table 13.

In the dendrogram can be distinguished four individuals located in a marginal position at the left side of the dendrogram (TRZ229, TRZ216, TRZ235 and TRZ228), outliers from Kampir Tepe represented in Figure 39. To visualize the chemical differences that these individuals present regarding the rest of the analysed material of **Kampyr Tepe** in Figure 37, 38 we present the biplot of the two first principal component result of the principal component analysis applied upon the subcomposition Fe_2O_3 TiO_2, SiO_2, Zr, Y, Ce, Ga, V, Nb, Zn, Cu, Ni and Cr using Al_2O_3 as divisor of the logratio transformation of the chemical data of the 40 analysed individuals sampled at ***Kampyr Tepe***. This graph contains the 42% of the variability present in this data set. According to this graph TRZ229 (KPT-08-AC-2) can be distinguished from the rest of the material due to significant differences in Ce and slight differences in the other trace elements, these differences can be confirmed by its chemical composition (Table 12). TRZ216 (KPT-08-IN-4) presents slightly lower Ni, Cu and Cr content while the cooking pot TRZ235 (KPT-08-IN-2) a part from the same differences that TRZ216 also present slightly higher concentrations of V. Finally, the cooking pot TRZ218 (KPT-08-IN-6) is precisely separated because of its lower Ce content.

El.	Fe2O3	Al2O3	TiO2	MgO	CaO	Na2O	K2O	SiO2	Ba	Rb	Th
Fe2O3	0,0000	0,0016	0,0038	0,0054	0,0443	0,0351	0,0155	0,0104	0,0125	0,0070	0,0101
Al2O3	0,0016	0,0000	0,0016	0,0054	0,0395	0,0279	0,0116	0,0053	0,0110	0,0053	0,0087
TiO2	0,0038	0,0016	0,0000	0,0064	0,0331	0,0248	0,0107	0,0030	0,0095	0,0082	0,0091
MgO	0,0054	0,0054	0,0064	0,0000	0,0342	0,0303	0,0173	0,0117	0,0101	0,0127	0,0100
CaO	0,0443	0,0395	0,0331	0,0342	0,0000	0,0531	0,0455	0,0314	0,0333	0,0504	0,0402
Na2O	0,0351	0,0279	0,0248	0,0303	0,0531	0,0000	0,0432	0,0201	0,0268	0,0463	0,0303
K2O	0,0155	0,0116	0,0107	0,0173	0,0455	0,0432	0,0000	0,0110	0,0151	0,0080	0,0212
SiO2	0,0104	0,0053	0,0030	0,0117	0,0314	0,0201	0,0110	0,0000	0,0079	0,0114	0,0102
Ba	0,0125	0,0110	0,0095	0,0101	0,0333	0,0268	0,0151	0,0079	0,0000	0,0168	0,0118
Rb	0,0070	0,0053	0,0082	0,0127	0,0504	0,0463	0,0080	0,0114	0,0168	0,0000	0,0152
Th	0,0101	0,0087	0,0091	0,0100	0,0402	0,0303	0,0212	0,0102	0,0118	0,0152	0,0000
Nb	0,0050	0,0028	0,0014	0,0060	0,0298	0,0282	0,0105	0,0032	0,0073	0,0082	0,0086
Zr	0,0211	0,0150	0,0082	0,0180	0,0267	0,0244	0,0161	0,0050	0,0136	0,0215	0,0170
Y	0,0061	0,0036	0,0013	0,0065	0,0266	0,0257	0,0109	0,0032	0,0076	0,0094	0,0089
Sr	0,0714	0,0633	0,0589	0,0553	0,0286	0,0596	0,0592	0,0542	0,0500	0,0749	0,0677
Ce	0,0303	0,0266	0,0223	0,0311	0,0647	0,0322	0,0319	0,0221	0,0285	0,0364	0,0333
Ga	0,0020	0,0012	0,0039	0,0060	0,0438	0,0324	0,0123	0,0082	0,0121	0,0047	0,0101
V	0,0052	0,0037	0,0061	0,0098	0,0496	0,0308	0,0147	0,0105	0,0155	0,0092	0,0141
Zn	0,0171	0,0135	0,0125	0,0167	0,0356	0,0338	0,0141	0,0134	0,0173	0,0164	0,0230
Cu	0,0104	0,0135	0,0190	0,0164	0,0573	0,0616	0,0304	0,0278	0,0280	0,0158	0,0214
Ni	0,0072	0,0117	0,0161	0,0108	0,0604	0,0535	0,0277	0,0250	0,0223	0,0161	0,0168
Cr	0,0035	0,0032	0,0055	0,0069	0,0495	0,0276	0,0171	0,0085	0,0099	0,0096	0,0094
t.i	0,3248	0,2763	0,2654	0,3269	0,8774	0,7475	0,4441	0,3034	0,3670	0,4036	0,3970
vt/t.i	0,7276	0,8553	0,8906	0,7230	0,2694	0,3161	0,5322	0,7789	0,6440	0,5856	0,5953
r v,t	0,9489	0,9788	0,9955	0,9683	0,1813	0,7322	0,9575	0,9559	0,9817	0,9565	0,9830

El.	Nb	Zr	Y	Sr	Ce	Ga	V	Zn	Cu	Ni	Cr
Fe2O3	0,0050	0,0211	0,0061	0,0714	0,0303	0,0020	0,0052	0,0171	0,0104	0,0072	0,0035
Al2O3	0,0028	0,0150	0,0036	0,0633	0,0266	0,0012	0,0037	0,0135	0,0135	0,0117	0,0032
TiO2	0,0014	0,0082	0,0013	0,0589	0,0223	0,0039	0,0061	0,0125	0,0190	0,0161	0,0055
MgO	0,0060	0,0180	0,0065	0,0553	0,0311	0,0060	0,0098	0,0167	0,0164	0,0108	0,0069
CaO	0,0298	0,0267	0,0266	0,0286	0,0647	0,0438	0,0496	0,0356	0,0573	0,0604	0,0495
Na2O	0,0282	0,0244	0,0257	0,0596	0,0322	0,0324	0,0308	0,0338	0,0616	0,0535	0,0276
K2O	0,0105	0,0161	0,0109	0,0592	0,0319	0,0123	0,0147	0,0141	0,0304	0,0277	0,0171
SiO2	0,0032	0,0050	0,0032	0,0542	0,0221	0,0082	0,0105	0,0134	0,0278	0,0250	0,0085
Ba	0,0073	0,0136	0,0076	0,0500	0,0285	0,0121	0,0155	0,0173	0,0280	0,0223	0,0099
Rb	0,0082	0,0215	0,0094	0,0749	0,0364	0,0047	0,0092	0,0164	0,0158	0,0161	0,0096
Th	0,0086	0,0170	0,0089	0,0677	0,0333	0,0101	0,0141	0,0230	0,0214	0,0168	0,0094
Nb	0,0000	0,0077	0,0012	0,0561	0,0243	0,0043	0,0084	0,0151	0,0185	0,0151	0,0058
Zr	0,0077	0,0000	0,0065	0,0519	0,0217	0,0189	0,0221	0,0215	0,0426	0,0370	0,0199
Y	0,0012	0,0065	0,0000	0,0517	0,0244	0,0053	0,0091	0,0128	0,0204	0,0178	0,0079
Sr	0,0561	0,0519	0,0517	0,0000	0,0862	0,0680	0,0637	0,0535	0,0930	0,0977	0,0710
Ce	0,0243	0,0217	0,0244	0,0862	0,0000	0,0287	0,0290	0,0320	0,0490	0,0413	0,0253
Ga	0,0043	0,0189	0,0053	0,0680	0,0287	0,0000	0,0046	0,0149	0,0120	0,0092	0,0034
V	0,0084	0,0221	0,0091	0,0637	0,0290	0,0046	0,0000	0,0155	0,0212	0,0189	0,0050
Zn	0,0151	0,0215	0,0128	0,0535	0,0320	0,0149	0,0155	0,0000	0,0310	0,0315	0,0182
Cu	0,0185	0,0426	0,0204	0,0930	0,0490	0,0120	0,0212	0,0310	0,0000	0,0097	0,0169
Ni	0,0151	0,0370	0,0178	0,0977	0,0413	0,0092	0,0189	0,0315	0,0097	0,0000	0,0095
Cr	0,0058	0,0199	0,0079	0,0710	0,0253	0,0034	0,0050	0,0182	0,0169	0,0095	0,0000
t.i	0,2675	0,4365	0,2672	1,3358	0,7213	0,3061	0,3666	0,4593	0,6160	0,5553	0,3337
vt/t.i	0,8834	0,5415	0,8845	0,1769	0,3277	0,7721	0,6447	0,5146	0,3837	0,4256	0,7082
r v,t	0,9939	0,7986	0,9897	0,0601	0,9287	0,9608	0,9679	0,9656	0,9098	0,9177	0,9566

vt	0,2363

Table 11: Compositional Variation Matrix (CVM) calculated upon the 40 individuals sampled at Kampyr Tepe and upon the subcomposition: Fe_2O_3 Al_2O_3 TiO_2 MgO CaO Na_2O K_2O SiO_2 Ba Rb Th Nb Zr Y Sr Ce Ga V Zn Cu Ni Cr

ID.	Fe2O3	Al2O3	TiO2	MgO	CaO	Na2O	K2O	SiO2	Ba	Rb	Th
TRZ203	6,73	17,03	0,74	3,78	7,62	1,55	4,35	58,04	0,0458	0,0144	0,0015
TRZ204	6,26	16,11	0,72	3,65	10,00	2,64	2,30	58,16	0,0464	0,0091	0,0015
TRZ205	5,79	15,35	0,70	2,73	9,16	1,55	4,29	60,28	0,0456	0,0125	0,0012
TRZ206	5,19	14,42	0,60	2,91	9,84	1,71	3,50	61,67	0,0488	0,0122	0,0014
TRZ207	5,60	14,95	0,67	2,80	8,87	1,53	3,68	61,73	0,0493	0,0129	0,0012
TRZ208	6,47	16,66	0,71	3,69	8,69	1,46	3,81	58,34	0,0481	0,0144	0,0013
TRZ209	6,38	15,59	0,67	3,57	12,28	1,68	3,75	55,90	0,0528	0,0131	0,0014
TRZ210	6,67	16,49	0,70	3,23	7,36	1,53	3,64	60,21	0,0549	0,0132	0,0013
TRZ211	6,76	15,90	0,70	3,39	8,42	1,70	3,71	59,24	0,0557	0,0133	0,0016
TRZ212	6,47	16,43	0,70	3,58	8,32	1,48	3,76	59,10	0,0549	0,0144	0,0012
TRZ213	6,35	16,49	0,69	3,43	8,26	1,55	3,54	59,51	0,0484	0,0143	0,0014
TRZ214	6,53	16,46	0,69	3,64	8,72	1,82	3,68	58,28	0,0534	0,0133	0,0013
TRZ215	6,27	16,20	0,70	3,57	8,71	1,36	3,64	59,38	0,0496	0,0142	0,0013
TRZ216	5,26	14,37	0,66	2,94	11,46	1,56	3,71	59,84	0,0573	0,0114	0,0012
TRZ217	6,28	16,49	0,70	3,51	7,09	2,37	4,07	59,31	0,0551	0,0144	0,0015
TRZ218	5,84	15,59	0,67	3,26	10,05	1,64	3,58	59,22	0,0481	0,0134	0,0013
TRZ219	5,92	15,53	0,67	3,51	10,47	1,50	3,55	58,68	0,0532	0,0133	0,0015
TRZ220	5,63	15,15	0,68	2,81	9,77	1,52	3,35	60,93	0,0470	0,0131	0,0016
TRZ221	5,57	14,90	0,67	3,07	10,11	1,56	3,68	60,27	0,0486	0,0128	0,0015
TRZ222	6,35	16,05	0,70	3,16	7,05	1,67	3,83	61,02	0,0532	0,0134	0,0014
TRZ223	5,73	14,85	0,68	3,13	11,26	1,49	3,70	58,99	0,0472	0,0121	0,0015
TRZ224	5,28	14,19	0,63	3,25	12,38	1,83	3,73	58,52	0,0493	0,0118	0,0012
TRZ225	5,74	15,24	0,68	3,27	9,80	1,80	3,70	59,58	0,0482	0,0117	0,0012
TRZ226	4,84	14,19	0,65	3,22	8,95	1,98	4,29	61,70	0,0522	0,0114	0,0013
TRZ227	5,49	14,72	0,66	3,05	7,96	1,87	3,82	62,25	0,0515	0,0116	0,0013
TRZ228	6,00	16,30	0,66	3,22	6,46	1,76	3,80	61,64	0,0488	0,0143	0,0015
TRZ229	5,22	13,98	0,65	3,25	8,57	2,19	3,37	62,60	0,0578	0,0115	0,0015
TRZ230	6,84	17,71	0,71	3,64	7,75	1,35	4,07	57,77	0,0470	0,0155	0,0016
TRZ231	5,85	15,56	0,67	3,41	10,77	1,74	3,53	58,30	0,0453	0,0117	0,0013
TRZ232	6,45	16,19	0,71	3,61	9,32	1,27	3,91	58,37	0,0515	0,0139	0,0016
TRZ233	6,19	15,98	0,64	3,39	9,54	1,76	3,45	58,87	0,0559	0,0125	0,0016
TRZ234	5,55	14,78	0,67	3,20	10,29	1,60	3,38	60,37	0,0484	0,0122	0,0014
TRZ235	5,52	15,87	0,67	2,72	7,73	2,12	3,42	61,78	0,0403	0,0132	0,0012
TRZ236	5,66	14,91	0,68	3,44	12,63	1,72	3,56	57,20	0,0525	0,0123	0,0013
TRZ237	6,00	16,16	0,70	3,09	9,76	1,54	3,62	58,97	0,0414	0,0143	0,0013
TRZ238	5,70	14,87	0,66	3,40	11,72	1,62	3,59	58,25	0,0501	0,0126	0,0013
TRZ239	6,35	16,38	0,67	3,69	11,27	1,54	3,79	56,13	0,0557	0,0138	0,0015
TRZ240	5,80	15,13	0,69	3,15	9,52	1,64	3,57	60,34	0,0464	0,0126	0,0014
TRZ241	5,46	14,58	0,66	3,12	10,15	1,57	3,13	61,18	0,0507	0,0117	0,0013
TRZ242	5,53	14,63	0,68	3,37	9,91	1,64	3,74	60,33	0,0471	0,0122	0,0013

Table 12: The normalised chemical composition of the analysed ceramic material from Kampiyr Tepe

ID.	Nb	Zr	Y	Sr	Ce	Ga	V	Zn	Cu	Ni	Cr
TRZ203	0,0016	0,0162	0,0028	0,0339	0,0069	0,0019	0,0115	0,0124	0,0030	0,0051	0,0077
TRZ204	0,0015	0,0166	0,0027	0,0364	0,0071	0,0017	0,0102	0,0091	0,0029	0,0048	0,0080
TRZ205	0,0015	0,0174	0,0026	0,0334	0,0081	0,0016	0,0098	0,0106	0,0027	0,0043	0,0068
TRZ206	0,0014	0,0158	0,0023	0,0393	0,0057	0,0016	0,0090	0,0106	0,0023	0,0039	0,0068
TRZ207	0,0016	0,0175	0,0027	0,0318	0,0064	0,0017	0,0086	0,0101	0,0027	0,0040	0,0066
TRZ208	0,0015	0,0167	0,0027	0,0334	0,0073	0,0019	0,0111	0,0100	0,0033	0,0051	0,0076
TRZ209	0,0015	0,0153	0,0027	0,0592	0,0061	0,0018	0,0100	0,0109	0,0033	0,0049	0,0073
TRZ210	0,0015	0,0153	0,0025	0,0301	0,0071	0,0019	0,0110	0,0101	0,0030	0,0046	0,0081
TRZ211	0,0016	0,0163	0,0026	0,0361	0,0054	0,0018	0,0101	0,0106	0,0028	0,0051	0,0078
TRZ212	0,0016	0,0166	0,0027	0,0298	0,0080	0,0020	0,0110	0,0119	0,0031	0,0054	0,0080
TRZ213	0,0015	0,0165	0,0026	0,0323	0,0063	0,0018	0,0107	0,0100	0,0033	0,0049	0,0079
TRZ214	0,0016	0,0156	0,0026	0,0443	0,0069	0,0019	0,0101	0,0102	0,0037	0,0058	0,0079
TRZ215	0,0016	0,0175	0,0028	0,0361	0,0058	0,0018	0,0098	0,0097	0,0033	0,0046	0,0070
TRZ216	0,0015	0,0179	0,0026	0,0668	0,0050	0,0015	0,0099	0,0094	0,0021	0,0030	0,0063
TRZ217	0,0015	0,0179	0,0027	0,0315	0,0075	0,0019	0,0100	0,0102	0,0028	0,0046	0,0073
TRZ218	0,0016	0,0164	0,0026	0,0337	0,0041	0,0018	0,0093	0,0092	0,0028	0,0044	0,0068
TRZ219	0,0016	0,0164	0,0027	0,0433	0,0048	0,0017	0,0103	0,0097	0,0029	0,0048	0,0077
TRZ220	0,0016	0,0187	0,0027	0,0339	0,0069	0,0018	0,0095	0,0099	0,0028	0,0042	0,0067
TRZ221	0,0015	0,0192	0,0026	0,0393	0,0075	0,0017	0,0092	0,0100	0,0026	0,0042	0,0069
TRZ222	0,0016	0,0167	0,0026	0,0345	0,0079	0,0018	0,0110	0,0114	0,0032	0,0048	0,0080
TRZ223	0,0015	0,0184	0,0027	0,0433	0,0050	0,0016	0,0093	0,0102	0,0028	0,0043	0,0063
TRZ224	0,0015	0,0183	0,0025	0,0568	0,0066	0,0017	0,0092	0,0105	0,0025	0,0040	0,0066
TRZ225	0,0015	0,0186	0,0026	0,0476	0,0065	0,0017	0,0097	0,0108	0,0020	0,0043	0,0069
TRZ226	0,0014	0,0188	0,0024	0,0514	0,0069	0,0015	0,0090	0,0117	0,0024	0,0035	0,0065
TRZ227	0,0016	0,0189	0,0026	0,0453	0,0074	0,0017	0,0094	0,0092	0,0024	0,0040	0,0073
TRZ228	0,0015	0,0155	0,0025	0,0382	0,0058	0,0019	0,0107	0,0096	0,0028	0,0047	0,0080
TRZ229	0,0015	0,0194	0,0026	0,0460	0,0080	0,0015	0,0096	0,0090	0,0020	0,0038	0,0074
TRZ230	0,0017	0,0153	0,0025	0,0367	0,0059	0,0020	0,0120	0,0097	0,0032	0,0055	0,0086
TRZ231	0,0016	0,0173	0,0026	0,0581	0,0069	0,0017	0,0100	0,0083	0,0027	0,0039	0,0063
TRZ232	0,0017	0,0168	0,0028	0,0362	0,0064	0,0019	0,0103	0,0102	0,0037	0,0051	0,0072
TRZ233	0,0014	0,0142	0,0025	0,0411	0,0057	0,0018	0,0104	0,0119	0,0035	0,0048	0,0075
TRZ234	0,0015	0,0181	0,0026	0,0381	0,0071	0,0016	0,0090	0,0103	0,0026	0,0041	0,0069
TRZ235	0,0014	0,0155	0,0024	0,0433	0,0064	0,0017	0,0116	0,0120	0,0024	0,0030	0,0067
TRZ236	0,0015	0,0176	0,0027	0,0635	0,0069	0,0016	0,0097	0,0129	0,0025	0,0039	0,0070
TRZ237	0,0016	0,0169	0,0026	0,0427	0,0052	0,0018	0,0096	0,0105	0,0031	0,0042	0,0070
TRZ238	0,0015	0,0180	0,0026	0,0569	0,0063	0,0016	0,0101	0,0119	0,0027	0,0038	0,0066
TRZ239	0,0016	0,0154	0,0027	0,0595	0,0060	0,0019	0,0095	0,0118	0,0036	0,0052	0,0074
TRZ240	0,0016	0,0192	0,0026	0,0333	0,0072	0,0016	0,0091	0,0090	0,0028	0,0045	0,0071
TRZ241	0,0015	0,0180	0,0025	0,0348	0,0066	0,0015	0,0076	0,0089	0,0028	0,0042	0,0066
TRZ242	0,0015	0,0176	0,0026	0,0377	0,0063	0,0016	0,0088	0,0126	0,0025	0,0041	0,0064

Table 12: The normalised chemical composition of the analysed ceramic material from Kampiyr Tepe

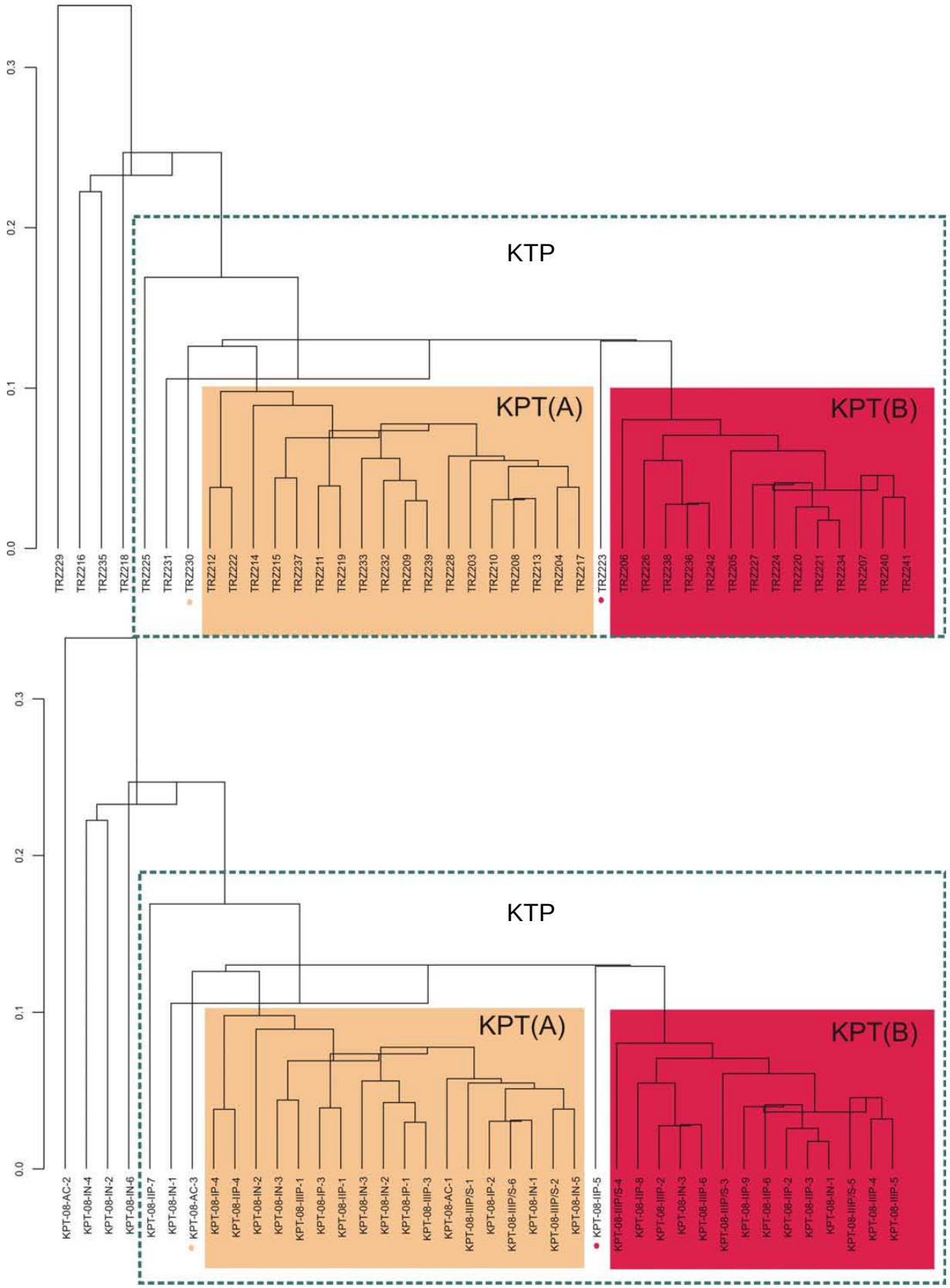

Figure 35: Dendrogram resulted from the cluster analysis performed on the subcomposition Fe_2O_3 TiO_2, SiO_2, Zr, Y, Ce, Ga, V, Nb, Zn, Cu, Ni and Cr using Al_2O_3 as divisor in the logratio transformation of the data of the 40 individuals of Kampyr Tepe using the Square Euclidean distance and the centroid algorithm, performed by S-plus2000 (MathSoft, 1999)

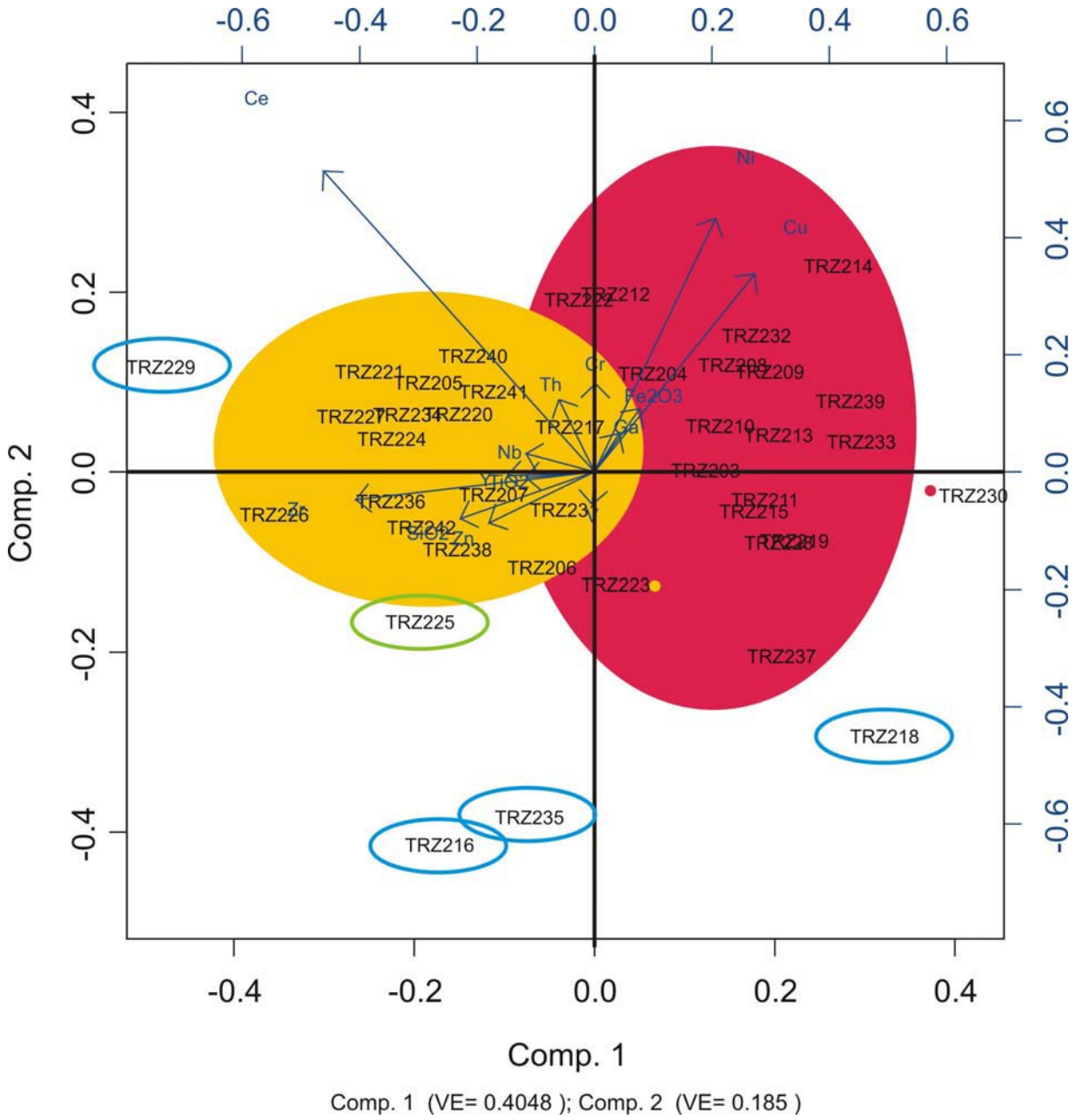

Figure 36: Biplot of the first two principal components, result of the principal component analysis applied upon the subcomposition Fe_2O_3 TiO_2, SiO_2, Zr, Y, Ce, Ga, V, Nb, Zn, Cu, Ni and Cr using Al_2O_3 as divisor of the logratio transformation of the data of the 40 individuals of Kampyr Tepe

KPT(A) n=18		
EL.	Mean	Stan.dev
Fe2O3%	6,11	0,27
Al2O3%	15,60	0,49
TiO2%	0,67	0,03
MgO%	3,34	0,20
CaO%	8,49	1,42
Na2O%	1,61	0,33
K2O%	3,53	0,38
SiO2%	56,50	1,72
Ba ppm	493	41
Rb ppm	130	12
Th ppm	14	1
Nb ppm	15	1
Zr ppm	156	10
Y ppm	25	1
Sr ppm	372	80
Ce ppm	62	9
Ga ppm	18	1
V ppm	100	6
Zn ppm	101	9
Cu ppm	30	3
Ni ppm	47	3
Cr ppm	73	4

KPT(B) n=14		
EL.	Mean	Stan.dev
Fe2O3%	5,16	0,30
Al2O3%	13,84	0,52
TiO2%	0,62	0,03
MgO%	2,91	0,20
CaO%	9,45	1,16
Na2O%	1,56	0,11
K2O%	3,43	0,25
SiO2%	56,58	2,31
Ba ppm	460	21
Rb ppm	115	6
Th ppm	13	1
Nb ppm	14	1
Zr ppm	169	10
Y ppm	24	1
Sr ppm	397	91
Ce ppm	64	6
Ga ppm	15	1
V ppm	86	5
Zn ppm	99	10
Cu ppm	24	2
Ni ppm	38	3
Cr ppm	63	3

Table 13: The mean chemical composition and the standard deviation of each element of $KPT_{(A)}$ and $KPT_{(B)}$

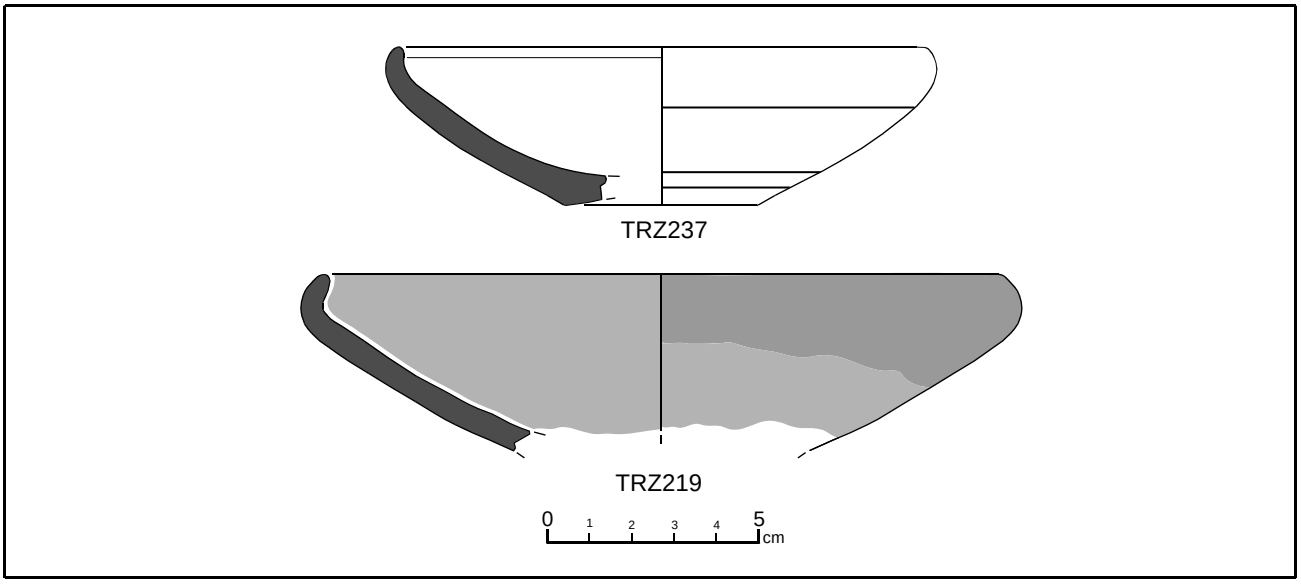

Figure 37: Typology of the group $KPT_{(A)}$

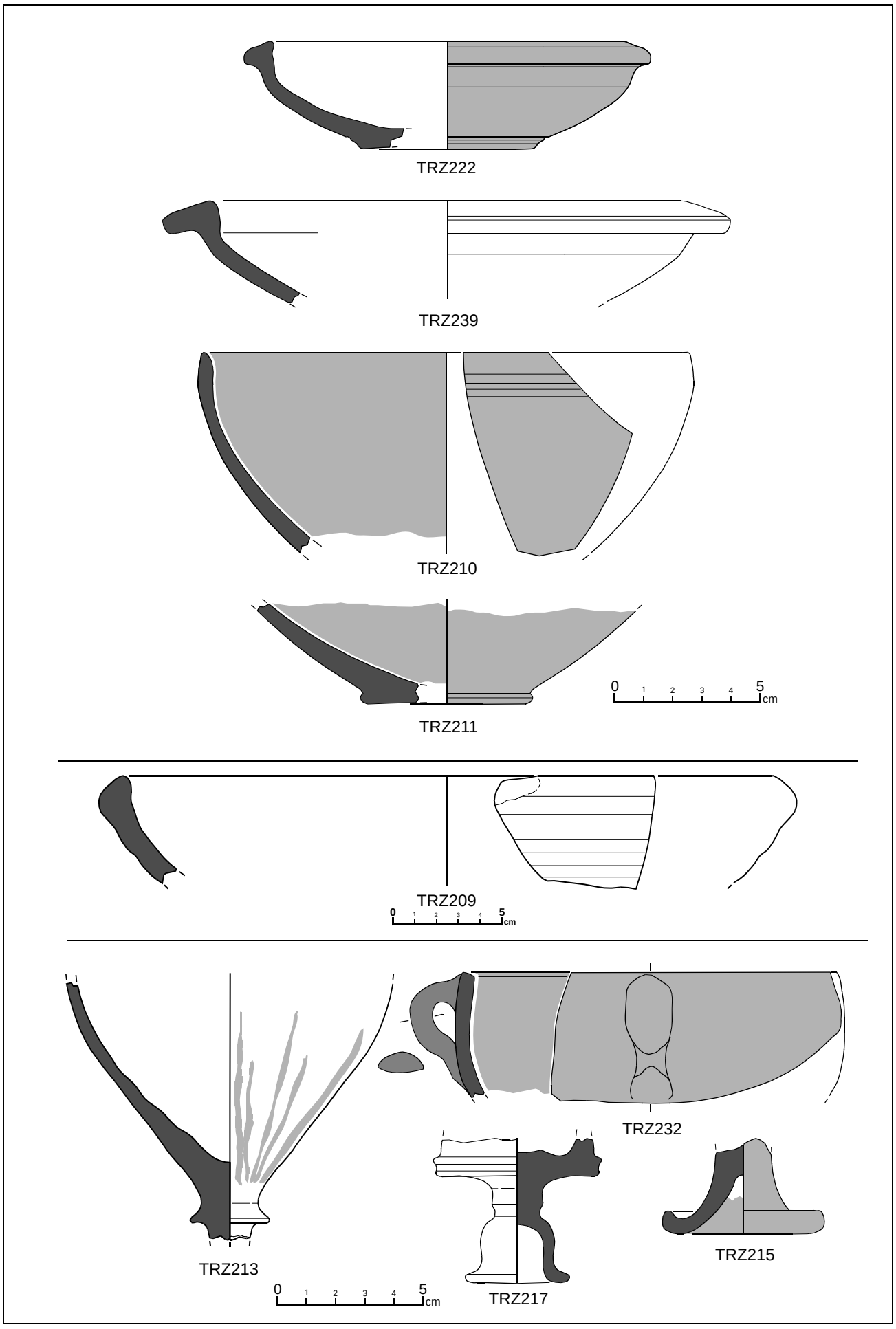

Figure 37: Typology of the group $KPT_{(A)}$

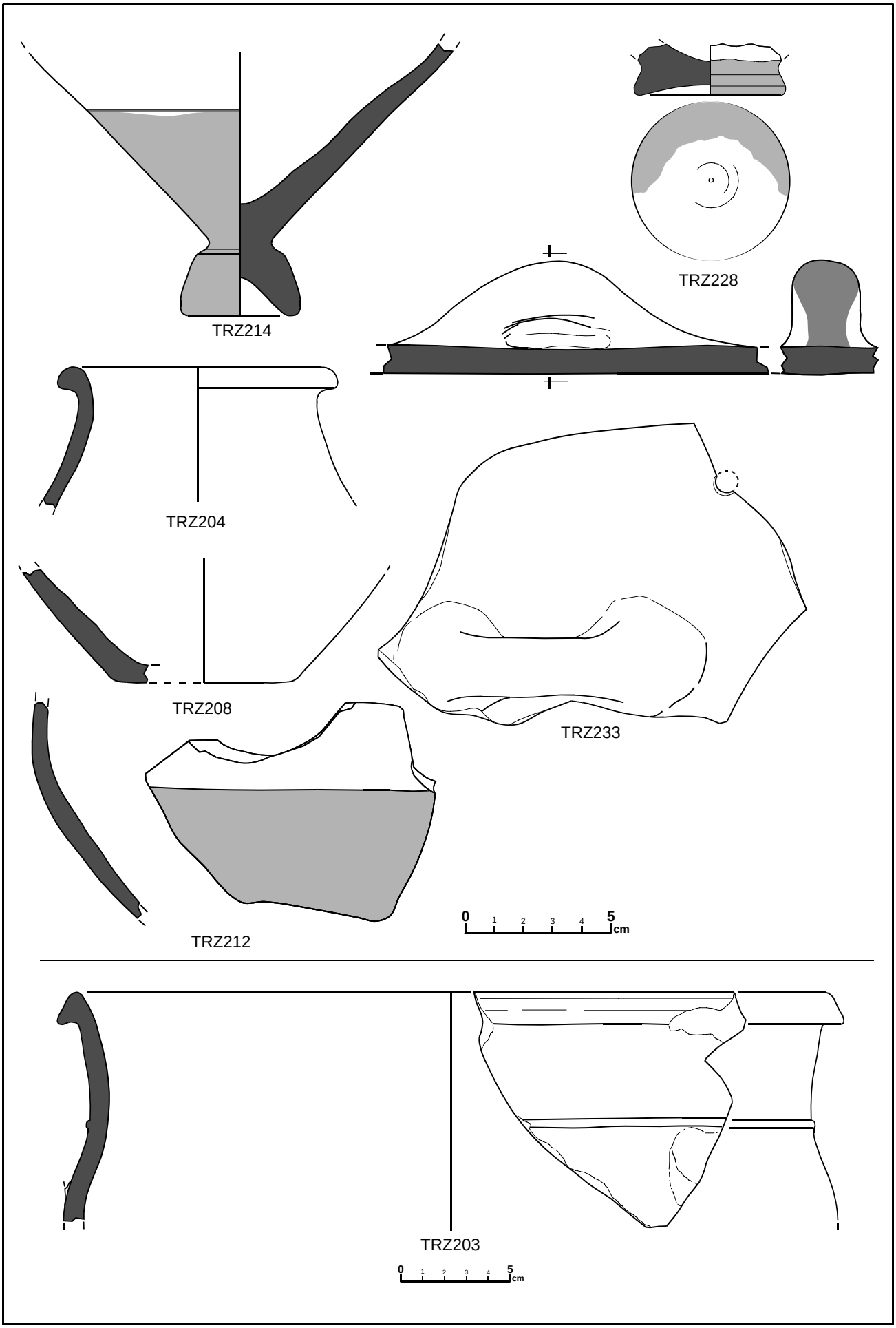

Figure 37: Typology of the group $KPT_{(A)}$

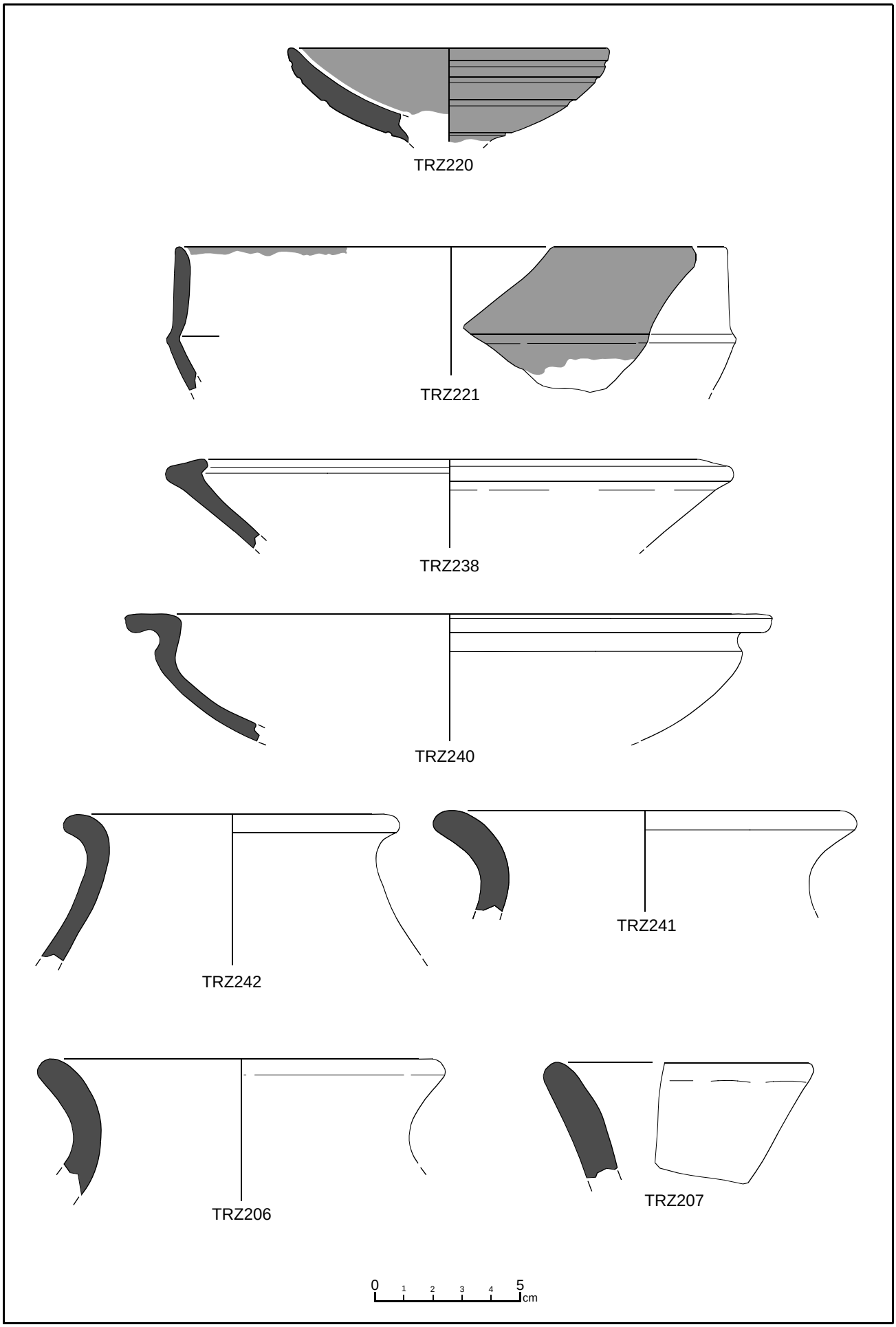

Figure 38: Typology of the group $KPT_{(B)}$

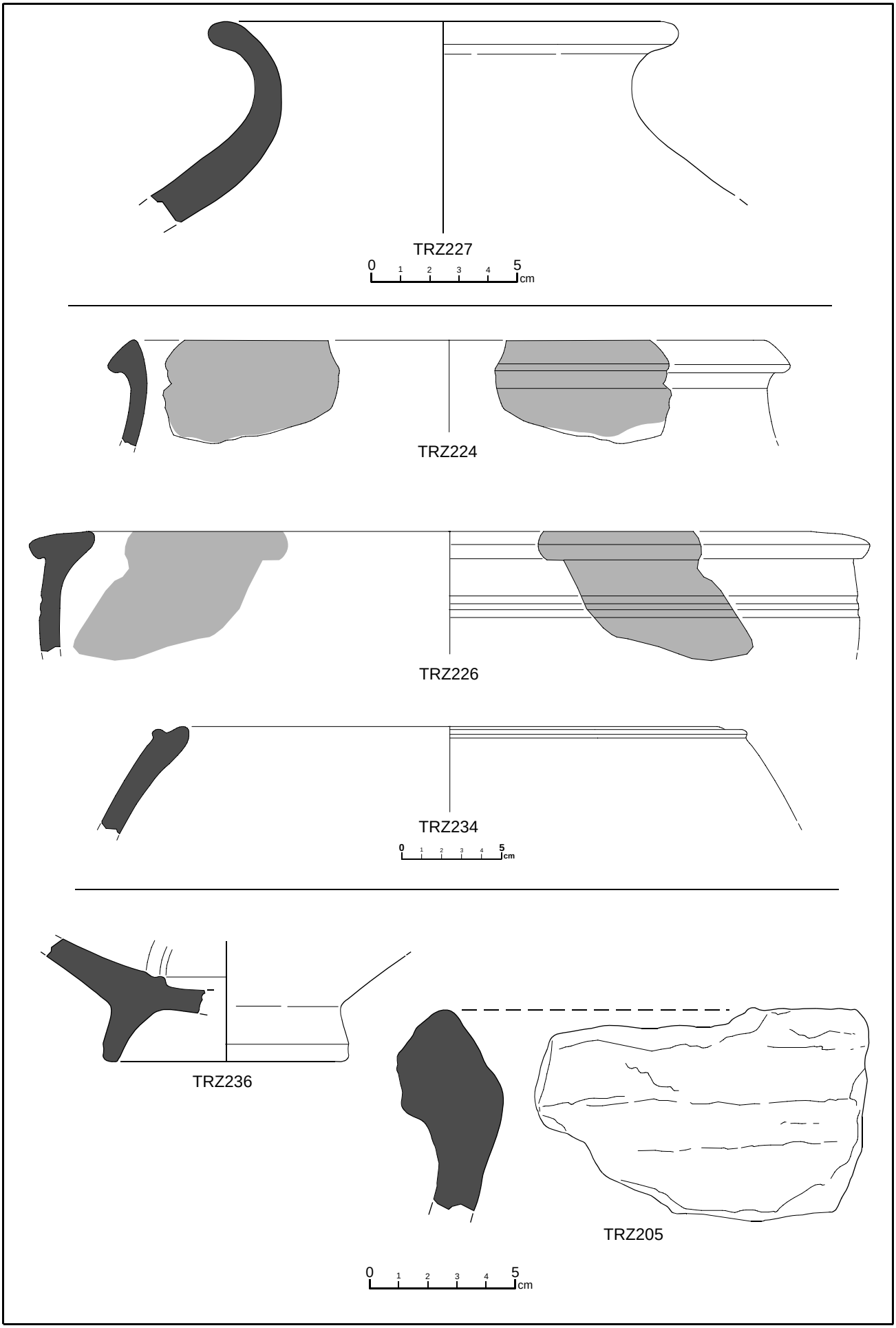

Figure 38: Typology of the group $KPT_{(B)}$

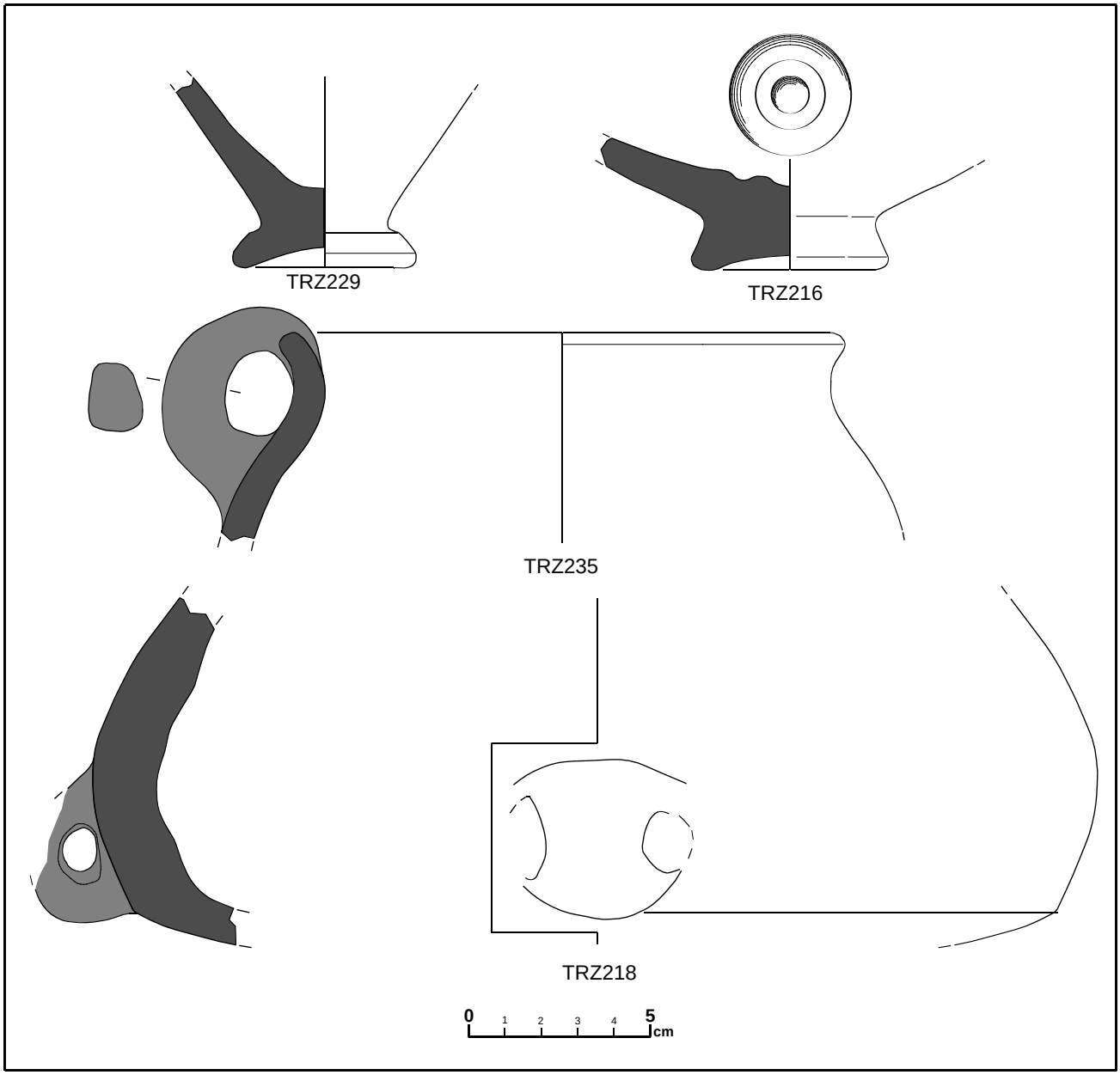

Figure 39: Outliers from Kampyr Tepe

In thin section, the composition of the ceramics sampled at ***Kampyr Tepe*** is similar with the petrographical fabrics identified for ***Tchinguiz Tepe***. The individual TRZ233 identified into the chemical group **KTP$_{(A)}$** is a cooking ware and it corresponds to a medium-coarse fabric (**KPT$_{(A)}$**). Its micromass is heterogeneous, rich in iron oxides and it is darker on the margins of the vessel walls (Figure 40). The inclusions are frequent, sub-rounded, poorly-sorted and single-spaced, showing a bimodal grain-size distribution (Table 5). The coarse fraction presents a grain size lower to 700µm long at both axis dimension, is formed essentially by quartz (200µm), plagioclase (300µm), big mica-muscovite (700µm) and quartz-mica schist (600µm). Other metamorphic rocks as mica-schist are also frequent, together with sandstones (400µm) and other isolated minerals as k-feldspars and amphiboles. Few cherts and opaques are presented as accessory rocks. Porosity is basically constituted by few meso-vesicles and mesovughs.

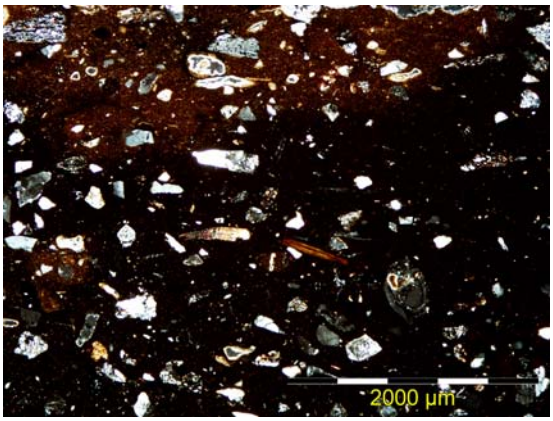

TRZ 233 40 X

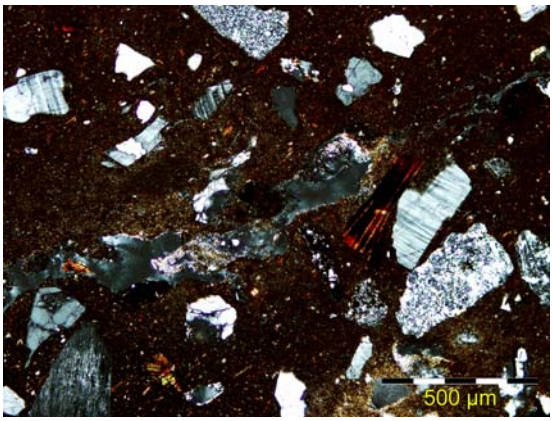

TRZ 233 100 X

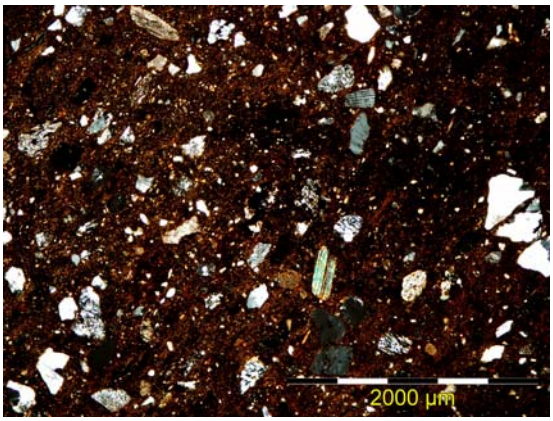

TRZ 235 40 X

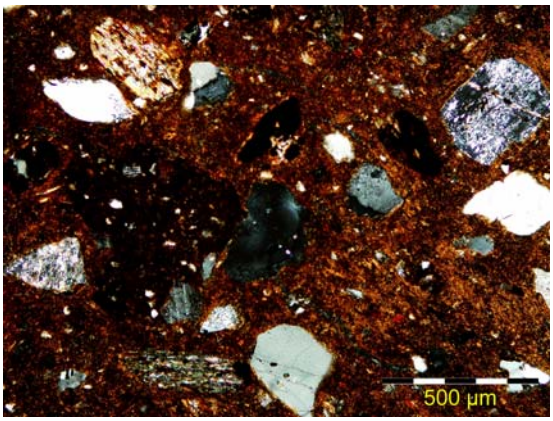

TRZ 235 100 X

Figure 40: A microphotograph by crossed polars of the sample TRZ233 bellowing to $KPT_{(A)}$ fabric and TRZ235 corresponding a chemical loner from Kampyr Tepe

The chemical similarity between all the individuals from ***Kampyr Tepe*** is also revealed in thin section analysis. One of the chemical loners, the cooking ware TRZ235, is petrographically compatible with **$KPT_{(A)}$** fabric and only few differences in composition and dimension of non plastic inclusions can be highlighted. Its micromass is more calcareous than TRZ233, homogeneous and orange-brown/yellowish under PPL. This fabric can be considered as medium-coarse because of non-plastic inclusions are frequent, sub-angular but smaller than in TRZ033. The maximum long axis dimension of coarse fraction is always inferior to 500µm (Figure 40). Quartz fragments, plagioclase, quart-mica schist, mica schist, mica-muscovite and opaques are the predominant non plastic inclusions together with frequent K-feldspars and amphiboles (Table 5). However, TRZ235 contains microfossils and shell fragments that have not been observed in TRZ233. Voids are more frequent than in TRZ233, but porosity is also characterised by the presence of few meso-vesicles and mesovughs.

Firing temperature and mineralogical aspects of KPT (A and B) groups

According to the mineralogical analysis, the 35 individuals representing the group KTP can be divided into four mineralogical categories. The first category's EFT is estimated between 800/850°C which correspond to low firing temperature because of the presence of primary mineral phases and the total absence of clear firing phases and it contains the individuals: TRZ203, TRZ210 (Figure 41), TRZ222, TRZ225, TRZ226, TRZ227 and TRZ228. In the second category, illite-muscovite and alkaline feldspars coexist with gehlenite and pyroxene which situates the EFT of this category around 850/950°C. This category is configured by: TRZ209, TRZ211, TRZ212, TRZ214, TRZ217, TRZ219 (Figure 41), TRZ220,

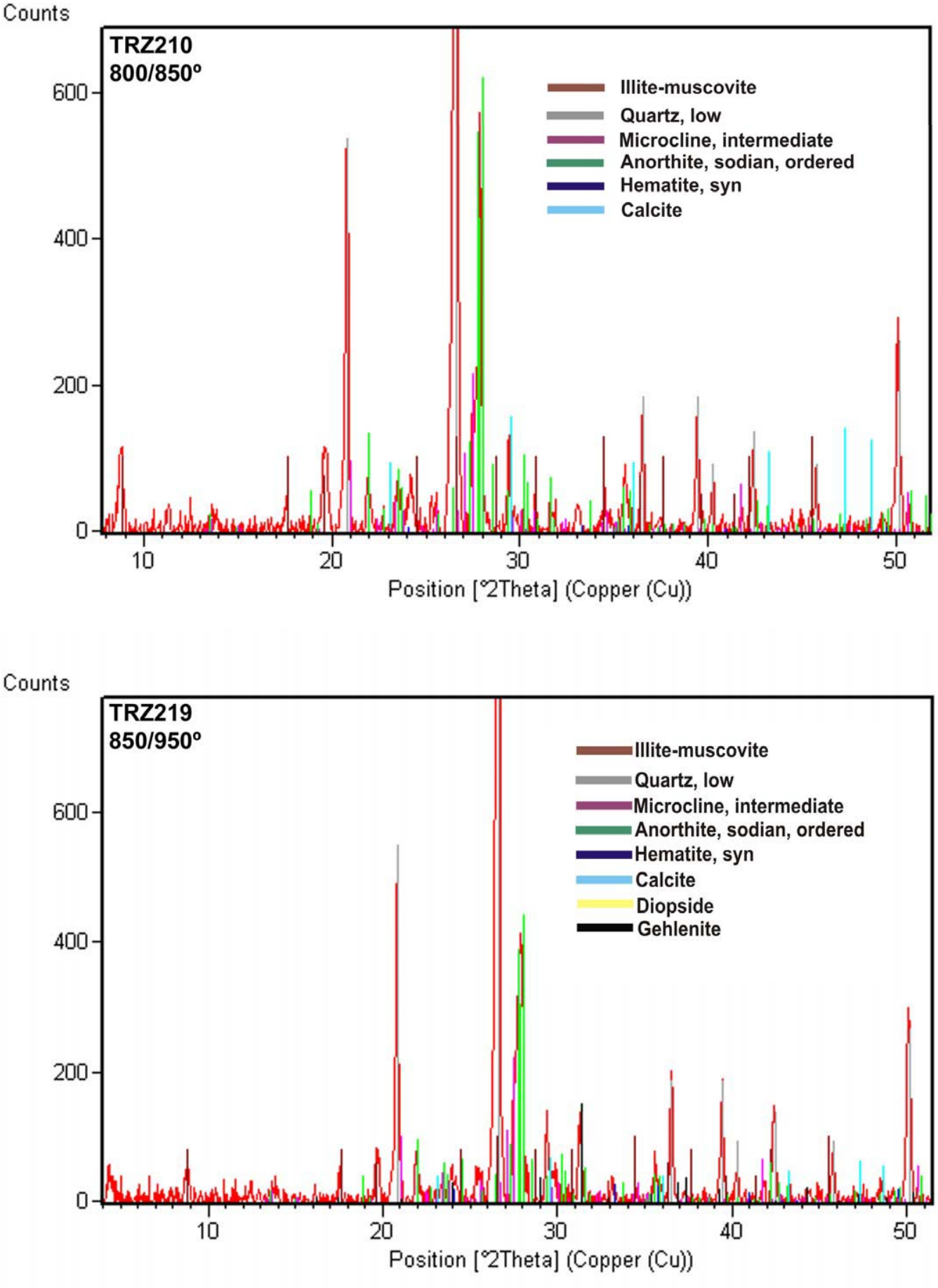

Figure 41: Difractograms of the individuals TRZ210 and TRZ219, representing the chemical group KPT

TRZ221, TRZ224, TRZ232, TRZ236 and TRZ238. In the third category, the development of the firing phases is much more advanced but the existence of illite-muscovite in the difractograms of the individuals in this category indicate a EFT between 950°C and 1000°C. The individuals that belong to this fabric are: TRZ207, TRZ213, TRZ215, TRZ223, TRZ228, TRZ233, TRZ234 and TRZ242 (Figure 42). Finally, the last mineralogical category's ETF can be estimated in the rang of 1050/1110°C as it is characterised by the advanced decomposition of illite-muscovite and gehlenite and the total decomposition of calcite with the parallel clear increment of the pyroxenes. It includes: TRZ204, TRZ230, TRZ231 (Figure 42) and TRZ241. From the above mentioned individuals, TRZ204 (Figure 43) presents also analcime in its difractogram.

To resume it can be pointed out that the 56% of the individuals fired at good temperature, between 850/1000°C and only the 12% are overfired (more than 1000ºC), the the atmosfere seem to have been mainly oxidising. The four outlayers are exception to this rule as most of them were predominantly fired under reduction condition. Four of them low fired (800/850ºC) and only one is fired in the range of 850/950ºC.

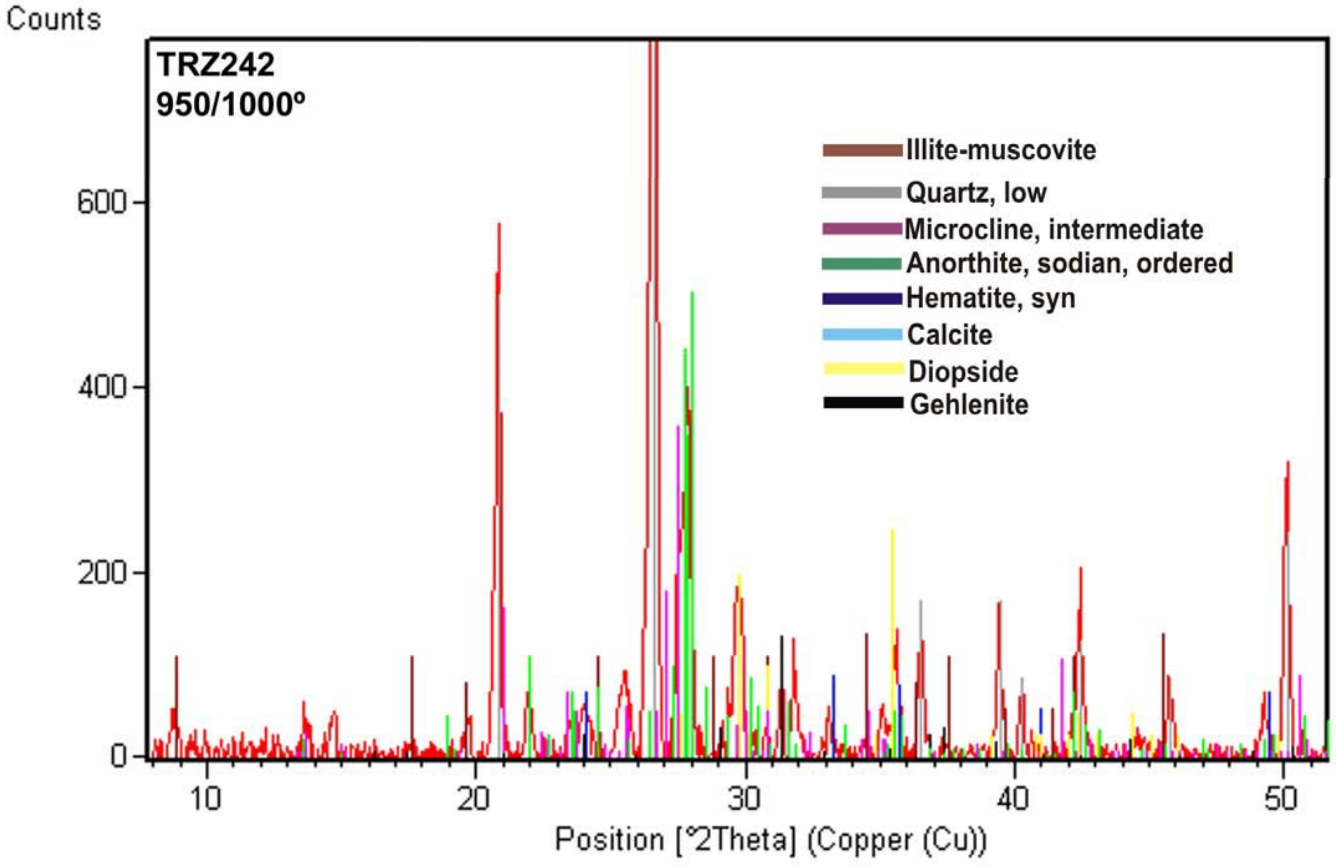

Figure 42: Difractograms of the individuals TRZ242 and TRZ231 representing the chemical group KPT

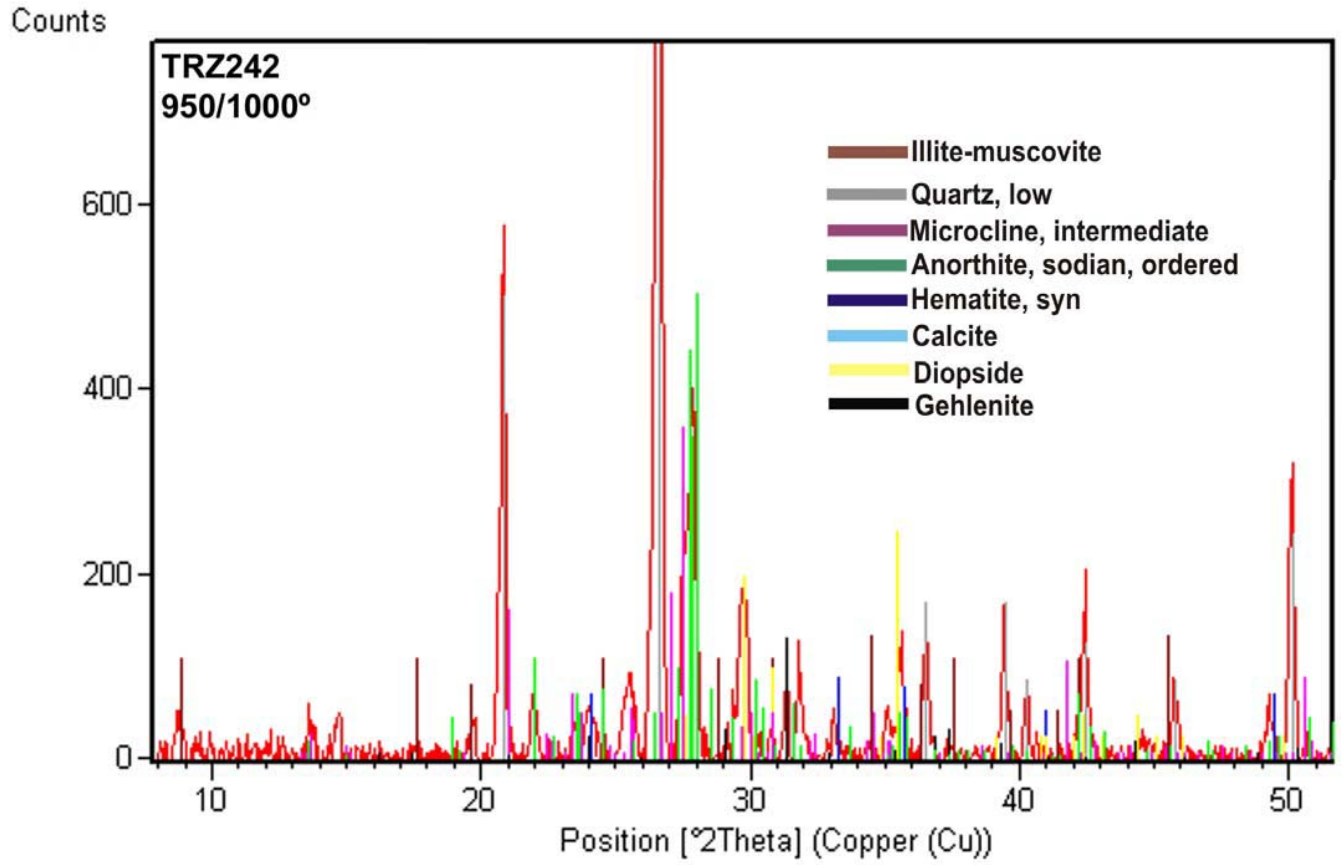

Figure 42: Difractograms of the individuals TRZ242 and TRZ231 representing the chemical group KPT

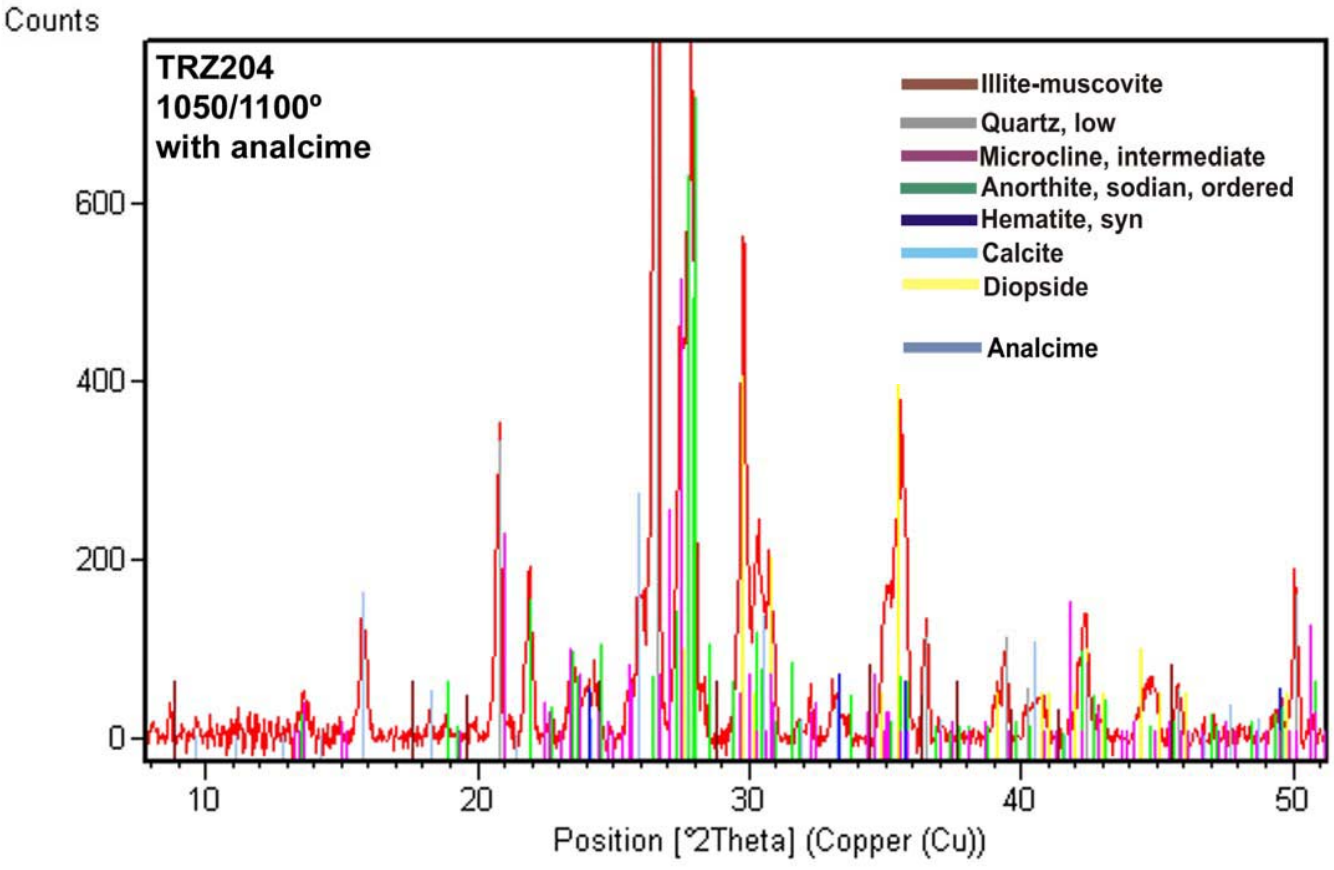

Figure 43: Difractogram of the individual TRZ204 representing the chemical group KPT

Integrated chemical and petrographic results Results for Zar Tepe ceramics:

At first site, the same observations than in the two above described cases can be made on the data set. All the analysed material is calcareous without any exception and the Na_2O concentrations are clearly high in all the individuals as there are salt (NaCl) contaminations in all the samples of ***Zar Tepe*** and in two cases (TRZ283 and TRZ246) the presence of analcyme ($Na_2AlSi_2O_6 \times H_2O$) could be observed.

The CVM calculated for ***Zar Tepe's*** data set can be seen in Table 14. It has been calculated without considering the elements: Mo, Sn, Co, W, MnO P_2O_5 and Pb. For reasons we have already explained in the two previous cases.

The total variation (vt) in this data set, according to the CVM is 0.3457 which generally indicates a polygenetic data (the presence of more than one production in the data set). But it is sufficiently low to point to similar geochemical character (the raw materials possibly come from areas with similar geological character) for all the analysed material. At the first site, the variability introduced by the majority of the elements is relatively low. In Table 14 we pointed out by yellow the elements which introduce more than the 50% of the variability in this data set and these are Na_2O, Ba, Sr, CaO, and Ce. From these elements, in the case of Na_2O, the high variability is due to post-depositional contaminations. The first one is almost altered in the whole data as above explained because of the presence of NaCl (salt) and in some cases (TRZ246 and TRZ283) because of the presence of analcime ($Na_2AlSi_2O_6 \times H_2O$), which affects specific individuals altering the Na_2O, also the K_2O and Rb concentrations.

The normalised chemical composition of the 48 analysed ceramic materials from ***Zar Tepe*** can be seen in Table 15. By looking at the chemical data it can be observed the values of Ba are variable but without being clear if there are some individuals possibly contaminated. On the other hand, in the CVM (Table 14) can be observed that the highest value in the column of Ba that is the one of this element with Na_2O (0.2036), which indicates that the contamination in Na_2O element affects probably Ba values. Therefore, to avoid that the chemical differences introduced by the above mentioned alterations and/or contaminations dominate the statistical treatment, we ignored Na_2O, K_2O, Rb and Ba in the rest of the process.

In the new CVM, the vt is equal to 0.1734 and the elements which introduce now more than the 50% of the variability in the data set are: Sr, CaO, MgO and Ce. All of them are chemically associated elements with generally high natural variability in calcareous raw material sources. A total variation of this range indicates a very homogeneous data set representing probably one single production. At the same way as in the case of ***Termez*** and ***Kampyr Tepe***, in geochemical terms, this vt might point towards a very similar geochemical origin of the raw materials used for the production of all the analysed individuals. It might be due to the fact that this area is very invariable geologically.

In continuation, the chemical data were transformed into logratios following the consideration of Aitchison (1986) and Buxeda (1999) on compositional data. The logratio transformation was performed upon the subcomposition: Fe_2O_3, Al_2O_3, TiO_2, SiO_2, Zr, Ce, Ga, V, Nb, Zn, Cu, Ni and Cr of the 48 analysed individuals from ***Zar Tepe*** where Y was used as divisor, as according to the CVM it was the element less contributing to the chemical variability. CaO, Sr, MgO, Th and Ce have been excluded from logratio transformation to avoid the domination of a possible natural variability upon the multivariate analysis. The chemical results are summarized in the dendrogram of Figure 44, resulting from the cluster analysis performed upon the previous subcomposition, using the Square Euclidean distance and the centroid algorithm. Although the chemical variability indicates one single production in this dendrogram

EL.	Fe2O3	Al2O3	TiO2	MgO	CaO	Na2O	K2O	SiO2	Ba	Rb	Th
Fe2O3	0,0000	0,0011	0,0015	0,0334	0,0416	0,1080	0,0204	0,0081	0,0648	0,0035	0,0099
Al2O3	0,0011	0,0000	0,0015	0,0396	0,0422	0,1018	0,0176	0,0051	0,0624	0,0019	0,0092
TiO2	0,0015	0,0015	0,0000	0,0325	0,0399	0,1024	0,0171	0,0042	0,0555	0,0037	0,0090
MgO	0,0334	0,0396	0,0325	0,0000	0,0701	0,1372	0,0541	0,0408	0,0643	0,0474	0,0445
CaO	0,0416	0,0422	0,0399	0,0701	0,0000	0,1311	0,0610	0,0371	0,1018	0,0481	0,0417
Na2O	0,1080	0,1018	0,1024	0,1372	0,1311	0,0000	0,0739	0,0933	0,2036	0,1056	0,0999
K2O	0,0204	0,0176	0,0171	0,0541	0,0610	0,0739	0,0000	0,0157	0,0794	0,0169	0,0223
SiO2	0,0081	0,0051	0,0042	0,0408	0,0371	0,0933	0,0157	0,0000	0,0526	0,0072	0,0125
Ba	0,0648	0,0624	0,0555	0,0643	0,1018	0,2036	0,0794	0,0526	0,0000	0,0675	0,0603
Rb	0,0035	0,0019	0,0037	0,0474	0,0481	0,1056	0,0169	0,0072	0,0675	0,0000	0,0102
Th	0,0099	0,0092	0,0090	0,0445	0,0417	0,0999	0,0223	0,0125	0,0603	0,0102	0,0000
Nb	0,0032	0,0033	0,0014	0,0304	0,0356	0,1038	0,0175	0,0037	0,0549	0,0064	0,0112
Zr	0,0089	0,0082	0,0042	0,0360	0,0336	0,1030	0,0195	0,0028	0,0530	0,0102	0,0142
Y	0,0038	0,0041	0,0019	0,0308	0,0324	0,1027	0,0204	0,0037	0,0551	0,0062	0,0084
Sr	0,0520	0,0484	0,0482	0,0751	0,0493	0,1081	0,0506	0,0489	0,0828	0,0515	0,0423
Ce	0,0227	0,0206	0,0201	0,0673	0,0572	0,1232	0,0324	0,0186	0,0751	0,0197	0,0294
Ga	0,0024	0,0020	0,0040	0,0415	0,0446	0,1100	0,0250	0,0088	0,0645	0,0037	0,0089
V	0,0036	0,0038	0,0052	0,0384	0,0555	0,1259	0,0269	0,0120	0,0587	0,0059	0,0133
Zn	0,0038	0,0059	0,0052	0,0265	0,0330	0,1113	0,0257	0,0111	0,0683	0,0092	0,0141
Cu	0,0097	0,0117	0,0106	0,0306	0,0351	0,1122	0,0341	0,0160	0,0675	0,0147	0,0188
Ni	0,0020	0,0041	0,0037	0,0271	0,0426	0,1136	0,0254	0,0117	0,0638	0,0071	0,0109
Cr	0,0049	0,0046	0,0037	0,0358	0,0369	0,1091	0,0226	0,0056	0,0592	0,0066	0,0122
t.i	0,4092	0,3992	0,3755	1,0033	1,0704	2,3798	0,6787	0,4193	1,5153	0,4532	0,5029
vt/t.i	0,8447	0,8659	0,9205	0,3445	0,3229	0,1452	0,5093	0,8243	0,2281	0,7627	0,6873
r v,t	0,9948	0,9941	0,9973	0,9409	0,9379	0,7272	0,9137	0,9890	0,9403	0,9891	0,9943

EL.	Nb	Zr	Y	Sr	Ce	Ga	V	Zn	Cu	Ni	Cr
Fe2O3	0,0032	0,0089	0,0038	0,0520	0,0227	0,0024	0,0036	0,0038	0,0097	0,0020	0,0049
Al2O3	0,0033	0,0082	0,0041	0,0484	0,0206	0,0020	0,0038	0,0059	0,0117	0,0041	0,0046
TiO2	0,0014	0,0042	0,0019	0,0482	0,0201	0,0040	0,0052	0,0052	0,0106	0,0037	0,0037
MgO	0,0304	0,0360	0,0308	0,0751	0,0673	0,0415	0,0384	0,0265	0,0306	0,0271	0,0358
CaO	0,0356	0,0336	0,0324	0,0493	0,0572	0,0446	0,0555	0,0330	0,0351	0,0426	0,0369
Na2O	0,1038	0,1030	0,1027	0,1081	0,1232	0,1100	0,1259	0,1113	0,1122	0,1136	0,1091
K2O	0,0175	0,0195	0,0204	0,0506	0,0324	0,0250	0,0269	0,0257	0,0341	0,0254	0,0226
SiO2	0,0037	0,0028	0,0037	0,0489	0,0186	0,0088	0,0120	0,0111	0,0160	0,0117	0,0056
Ba	0,0549	0,0530	0,0551	0,0828	0,0751	0,0645	0,0587	0,0683	0,0675	0,0638	0,0592
Rb	0,0064	0,0102	0,0062	0,0515	0,0197	0,0037	0,0059	0,0092	0,0147	0,0071	0,0066
Th	0,0112	0,0142	0,0084	0,0423	0,0294	0,0089	0,0133	0,0141	0,0188	0,0109	0,0122
Nb	0,0000	0,0035	0,0019	0,0478	0,0214	0,0060	0,0074	0,0061	0,0116	0,0046	0,0029
Zr	0,0035	0,0000	0,0026	0,0546	0,0195	0,0120	0,0148	0,0102	0,0154	0,0114	0,0059
Y	0,0019	0,0026	0,0000	0,0488	0,0199	0,0057	0,0087	0,0053	0,0102	0,0046	0,0030
Sr	0,0478	0,0546	0,0488	0,0000	0,0661	0,0533	0,0609	0,0524	0,0547	0,0524	0,0537
Ce	0,0214	0,0195	0,0199	0,0661	0,0000	0,0221	0,0274	0,0274	0,0300	0,0267	0,0212
Ga	0,0060	0,0120	0,0057	0,0533	0,0221	0,0000	0,0045	0,0064	0,0120	0,0035	0,0063
V	0,0074	0,0148	0,0087	0,0609	0,0274	0,0045	0,0000	0,0106	0,0187	0,0054	0,0083
Zn	0,0061	0,0102	0,0053	0,0524	0,0274	0,0064	0,0106	0,0000	0,0076	0,0043	0,0070
Cu	0,0116	0,0154	0,0102	0,0547	0,0300	0,0120	0,0187	0,0076	0,0000	0,0093	0,0114
Ni	0,0046	0,0114	0,0046	0,0524	0,0267	0,0035	0,0054	0,0043	0,0093	0,0000	0,0063
Cr	0,0029	0,0059	0,0030	0,0537	0,0212	0,0063	0,0083	0,0070	0,0114	0,0063	0,0000
t.i	0,3844	0,4437	0,3802	1,2018	0,7678	0,4472	0,5159	0,4513	0,5417	0,4406	0,4272
vt/t.i	0,8991	0,7791	0,9092	0,2876	0,4502	0,7730	0,6699	0,7659	0,6380	0,7845	0,8091
r v,t	0,9972	0,9878	0,9962	0,9132	0,9879	0,9926	0,9856	0,9878	0,9845	0,9901	0,9962
vt	0,3457										

Table 14: Compositional Variation Matrix (CVM) calculated upon the 40 individuals sampled at Zar Tepe and upon the sub-composition: Fe_2O_3 Al_2O_3 TiO_2 MgO CaO Na_2O K_2O SiO_2 Ba Rb Th Nb Zr Y Sr Ce Ga V Zn Cu Ni Cr

different subgroups can be distinguished (indicated by rectangles of different colour and the letters A, B, C, D, E and F in the dendrogram). To visualize the chemical differences between this subgroups, at Figure 40 we present the biplot of the two first principal component as result of the principal components analysis applied upon the subcomposition Fe_2O_3, Al_2O_3, TiO_2, SiO_2, Zr, Ce, Ga, V, Nb, Zn, Cu, Ni and Cr of the 48 analysed individuals from ***Zar Tepe*** where Y was used as divisor. This graph contains the

ID	Fe2O3	Al2O3	TiO2	MgO	CaO	Na2O	K2O	SiO2	Ba	Rb	Th
TRZ243	6,34	16,82	0,68	3,57	8,04	2,13	4,03	58,23	0,0463	0,0144	0,0015
TRZ244	6,28	16,06	0,69	4,83	9,15	1,71	4,64	56,41	0,0769	0,0134	0,0016
TRZ245	5,32	14,51	0,63	3,89	7,47	2,34	3,95	61,71	0,0635	0,0119	0,0012
TRZ246	5,83	15,75	0,62	4,30	8,30	2,64	3,21	59,15	0,0782	0,0110	0,0013
TRZ247	5,78	15,83	0,64	3,50	6,03	4,12	5,06	58,90	0,0427	0,0137	0,0013
TRZ248	5,84	16,22	0,63	3,27	7,16	2,45	4,43	59,86	0,0428	0,0141	0,0012
TRZ249	6,49	17,08	0,67	3,62	8,90	2,76	3,84	56,49	0,0401	0,0134	0,0013
TRZ250	5,43	14,97	0,60	4,20	8,08	3,28	3,94	59,33	0,0438	0,0124	0,0013
TRZ251	6,47	16,84	0,68	4,72	8,96	1,36	3,81	56,98	0,0615	0,0135	0,0014
TRZ252	5,90	15,13	0,65	5,21	10,77	2,88	3,84	55,46	0,0451	0,0119	0,0012
TRZ253	5,94	16,15	0,66	3,44	6,93	2,01	4,15	60,55	0,0441	0,0139	0,0013
TRZ254	6,64	17,41	0,71	3,64	8,49	1,39	3,60	57,97	0,0401	0,0150	0,0013
TRZ255	6,26	16,21	0,69	5,52	6,15	1,16	3,84	59,99	0,0731	0,0133	0,0013
TRZ256	6,52	16,94	0,68	4,23	8,32	2,26	4,36	56,50	0,0459	0,0144	0,0015
TRZ257	6,58	17,31	0,68	4,11	7,00	1,85	4,16	58,15	0,0494	0,0153	0,0015
TRZ258	5,65	14,77	0,63	4,95	7,68	2,24	4,67	59,24	0,0524	0,0122	0,0014
TRZ259	5,44	14,61	0,63	4,24	8,89	3,33	4,67	58,01	0,0486	0,0123	0,0013
TRZ260	5,40	14,46	0,65	4,72	8,06	1,84	3,66	61,00	0,0992	0,0118	0,0013
TRZ261	6,14	15,89	0,67	3,61	7,05	2,17	5,78	58,55	0,0433	0,0129	0,0013
TRZ262	5,94	15,23	0,65	5,95	10,15	1,48	3,79	56,63	0,0670	0,0126	0,0013
TRZ263	5,95	16,09	0,65	3,46	7,17	2,45	4,08	59,98	0,0497	0,0138	0,0012
TRZ264	6,12	16,34	0,67	4,38	6,95	2,65	4,05	58,67	0,0500	0,0140	0,0015
TRZ265	5,88	15,32	0,64	4,77	11,32	2,07	4,38	55,45	0,0463	0,0116	0,0012
TRZ266	6,42	16,78	0,71	4,04	6,68	1,93	4,56	58,69	0,0670	0,0143	0,0014
TRZ267	5,68	15,22	0,64	4,32	8,27	1,39	3,95	60,35	0,0726	0,0119	0,0015
TRZ268	5,76	15,45	0,63	5,51	8,05	1,89	3,90	58,60	0,0751	0,0124	0,0013
TRZ269	6,16	16,39	0,65	3,77	8,37	1,86	4,33	58,31	0,0454	0,0132	0,0015
TRZ270	5,85	15,24	0,66	4,22	8,43	2,09	4,00	59,33	0,0663	0,0129	0,0012
TRZ271	5,76	15,41	0,63	5,34	7,43	2,89	4,00	58,37	0,0554	0,0127	0,0015
TRZ272	5,14	14,46	0,56	3,17	11,31	1,52	4,38	59,29	0,0558	0,0126	0,0012
TRZ273	6,16	16,38	0,69	5,04	5,96	1,81	4,12	59,65	0,0727	0,0137	0,0013
TRZ274	5,78	15,70	0,62	3,50	6,77	2,47	4,64	60,34	0,0559	0,0135	0,0016
TRZ275	5,76	15,17	0,66	3,44	10,77	1,44	3,19	59,41	0,0490	0,0128	0,0014
TRZ276	5,33	14,52	0,65	3,42	7,68	1,45	3,59	63,17	0,0813	0,0122	0,0014
TRZ277	6,55	17,04	0,69	4,60	7,22	1,30	3,74	58,67	0,0768	0,0145	0,0015
TRZ278	6,46	16,70	0,69	5,22	7,36	1,54	4,06	57,77	0,0848	0,0140	0,0014
TRZ279	5,44	14,84	0,61	3,37	9,63	2,31	4,18	59,44	0,0543	0,0118	0,0013
TRZ280	6,43	17,09	0,69	4,40	8,54	2,47	4,53	55,66	0,0609	0,0144	0,0017
TRZ281	5,85	15,25	0,67	4,04	9,97	3,25	4,60	56,15	0,0773	0,0129	0,0018
TRZ282	5,44	14,20	0,59	4,15	12,97	1,53	3,26	57,68	0,0530	0,0120	0,0014
TRZ283	6,24	16,43	0,67	3,86	9,47	1,97	3,15	58,05	0,0458	0,0125	0,0013
TRZ284	5,60	15,02	0,64	4,60	8,00	3,34	4,25	58,40	0,0494	0,0122	0,0015
TRZ285	6,03	15,46	0,68	6,83	6,51	2,26	4,39	57,66	0,0546	0,0127	0,0014
TRZ286	6,64	17,22	0,71	5,29	6,39	1,34	3,84	58,38	0,0773	0,0133	0,0015
TRZ287	6,38	16,92	0,66	3,78	9,38	1,80	3,70	57,22	0,0483	0,0142	0,0015
TRZ288	5,08	15,76	0,60	2,76	6,79	2,24	4,38	62,18	0,0767	0,0134	0,0013
TRZ289	6,04	16,80	0,70	3,15	7,25	1,41	4,23	60,22	0,0705	0,0143	0,0015
TRZ290	6,42	16,74	0,69	4,11	9,17	1,39	3,40	57,89	0,0590	0,0144	0,0014

Table 15: Normalised chemical composition of the analysed individuals for Zar Tepe

ID	Nb	Zr	Y	Sr	Ce	Ga	V	Zn	Cu	Ni	Cr
TRZ243	0,0014	0,0149	0,0024	0,0361	0,0052	0,0018	0,0098	0,0105	0,0031	0,0045	0,0073
TRZ244	0,0015	0,0145	0,0024	0,0732	0,0062	0,0017	0,0095	0,0108	0,0035	0,0046	0,0078
TRZ245	0,0015	0,0163	0,0024	0,0411	0,0056	0,0015	0,0086	0,0087	0,0027	0,0039	0,0077
TRZ246	0,0014	0,0140	0,0023	0,0416	0,0049	0,0017	0,0097	0,0094	0,0032	0,0044	0,0073
TRZ247	0,0014	0,0142	0,0023	0,0365	0,0070	0,0018	0,0093	0,0089	0,0027	0,0044	0,0076
TRZ248	0,0013	0,0140	0,0023	0,0326	0,0054	0,0017	0,0101	0,0100	0,0030	0,0041	0,0071
TRZ249	0,0014	0,0142	0,0023	0,0385	0,0056	0,0019	0,0102	0,0109	0,0032	0,0047	0,0078
TRZ250	0,0013	0,0147	0,0023	0,0436	0,0045	0,0017	0,0081	0,0094	0,0029	0,0040	0,0075
TRZ251	0,0015	0,0147	0,0024	0,0384	0,0058	0,0018	0,0115	0,0103	0,0034	0,0046	0,0079
TRZ252	0,0016	0,0145	0,0024	0,0415	0,0044	0,0017	0,0094	0,0103	0,0037	0,0049	0,0082
TRZ253	0,0014	0,0151	0,0024	0,0379	0,0062	0,0018	0,0100	0,0093	0,0028	0,0043	0,0072
TRZ254	0,0015	0,0158	0,0025	0,0369	0,0059	0,0019	0,0110	0,0108	0,0034	0,0051	0,0079
TRZ255	0,0016	0,0161	0,0025	0,0357	0,0064	0,0018	0,0113	0,0104	0,0024	0,0050	0,0085
TRZ256	0,0014	0,0146	0,0026	0,0617	0,0071	0,0018	0,0101	0,0101	0,0034	0,0050	0,0080
TRZ257	0,0014	0,0148	0,0025	0,0344	0,0076	0,0020	0,0116	0,0101	0,0031	0,0050	0,0078
TRZ258	0,0015	0,0154	0,0024	0,0388	0,0064	0,0017	0,0088	0,0101	0,0033	0,0043	0,0081
TRZ259	0,0014	0,0162	0,0024	0,0522	0,0061	0,0015	0,0081	0,0097	0,0031	0,0041	0,0072
TRZ260	0,0014	0,0173	0,0025	0,0368	0,0068	0,0015	0,0087	0,0088	0,0031	0,0040	0,0070
TRZ261	0,0015	0,0158	0,0023	0,0266	0,0059	0,0016	0,0093	0,0093	0,0029	0,0044	0,0077
TRZ262	0,0015	0,0151	0,0025	0,0445	0,0051	0,0017	0,0089	0,0109	0,0036	0,0049	0,0075
TRZ263	0,0014	0,0143	0,0023	0,0443	0,0070	0,0017	0,0098	0,0095	0,0030	0,0044	0,0073
TRZ264	0,0015	0,0147	0,0024	0,0383	0,0061	0,0018	0,0107	0,0088	0,0030	0,0045	0,0074
TRZ265	0,0015	0,0146	0,0022	0,0575	0,0061	0,0015	0,0093	0,0103	0,0029	0,0045	0,0072
TRZ266	0,0016	0,0156	0,0025	0,0407	0,0045	0,0018	0,0109	0,0097	0,0028	0,0050	0,0079
TRZ267	0,0015	0,0160	0,0024	0,0362	0,0052	0,0017	0,0099	0,0097	0,0024	0,0043	0,0069
TRZ268	0,0014	0,0142	0,0023	0,0501	0,0054	0,0017	0,0102	0,0103	0,0031	0,0047	0,0074
TRZ269	0,0014	0,0144	0,0024	0,0364	0,0054	0,0018	0,0101	0,0103	0,0030	0,0047	0,0073
TRZ270	0,0015	0,0165	0,0024	0,0398	0,0068	0,0017	0,0085	0,0099	0,0033	0,0044	0,0071
TRZ271	0,0014	0,0146	0,0024	0,0431	0,0044	0,0016	0,0096	0,0094	0,0031	0,0044	0,0077
TRZ272	0,0013	0,0146	0,0022	0,0434	0,0054	0,0015	0,0086	0,0088	0,0026	0,0037	0,0070
TRZ273	0,0015	0,0148	0,0023	0,0375	0,0048	0,0018	0,0113	0,0098	0,0030	0,0046	0,0079
TRZ274	0,0015	0,0148	0,0025	0,0334	0,0070	0,0018	0,0100	0,0091	0,0029	0,0047	0,0080
TRZ275	0,0015	0,0169	0,0026	0,0289	0,0064	0,0017	0,0096	0,0098	0,0028	0,0044	0,0093
TRZ276	0,0014	0,0163	0,0024	0,0337	0,0063	0,0016	0,0088	0,0086	0,0031	0,0040	0,0073
TRZ277	0,0015	0,0153	0,0025	0,0357	0,0055	0,0020	0,0114	0,0101	0,0038	0,0053	0,0080
TRZ278	0,0015	0,0148	0,0025	0,0367	0,0075	0,0020	0,0113	0,0113	0,0036	0,0050	0,0080
TRZ279	0,0015	0,0146	0,0023	0,0503	0,0061	0,0017	0,0090	0,0076	0,0026	0,0042	0,0068
TRZ280	0,0015	0,0142	0,0025	0,0591	0,0052	0,0020	0,0103	0,0103	0,0032	0,0053	0,0076
TRZ281	0,0014	0,0154	0,0025	0,0652	0,0052	0,0017	0,0103	0,0095	0,0027	0,0045	0,0073
TRZ282	0,0014	0,0151	0,0025	0,0455	0,0057	0,0017	0,0084	0,0100	0,0034	0,0045	0,0077
TRZ283	0,0014	0,0150	0,0025	0,0419	0,0067	0,0019	0,0101	0,0105	0,0032	0,0049	0,0076
TRZ284	0,0014	0,0155	0,0023	0,0394	0,0061	0,0017	0,0083	0,0101	0,0034	0,0044	0,0070
TRZ285	0,0015	0,0153	0,0025	0,0409	0,0054	0,0017	0,0104	0,0101	0,0030	0,0051	0,0071
TRZ286	0,0016	0,0151	0,0025	0,0348	0,0058	0,0020	0,0114	0,0105	0,0036	0,0053	0,0085
TRZ287	0,0014	0,0143	0,0024	0,0490	0,0061	0,0019	0,0099	0,0108	0,0034	0,0050	0,0077
TRZ288	0,0013	0,0134	0,0021	0,0601	0,0063	0,0017	0,0091	0,0078	0,0026	0,0037	0,0074
TRZ289	0,0015	0,0153	0,0024	0,0544	0,0063	0,0019	0,0106	0,0090	0,0029	0,0046	0,0078
TRZ290	0,0015	0,0158	0,0025	0,0419	0,0067	0,0019	0,0109	0,0106	0,0036	0,0051	0,0089

Table 15: Normalised chemical composition of the analysed individuals for Zar Tepe

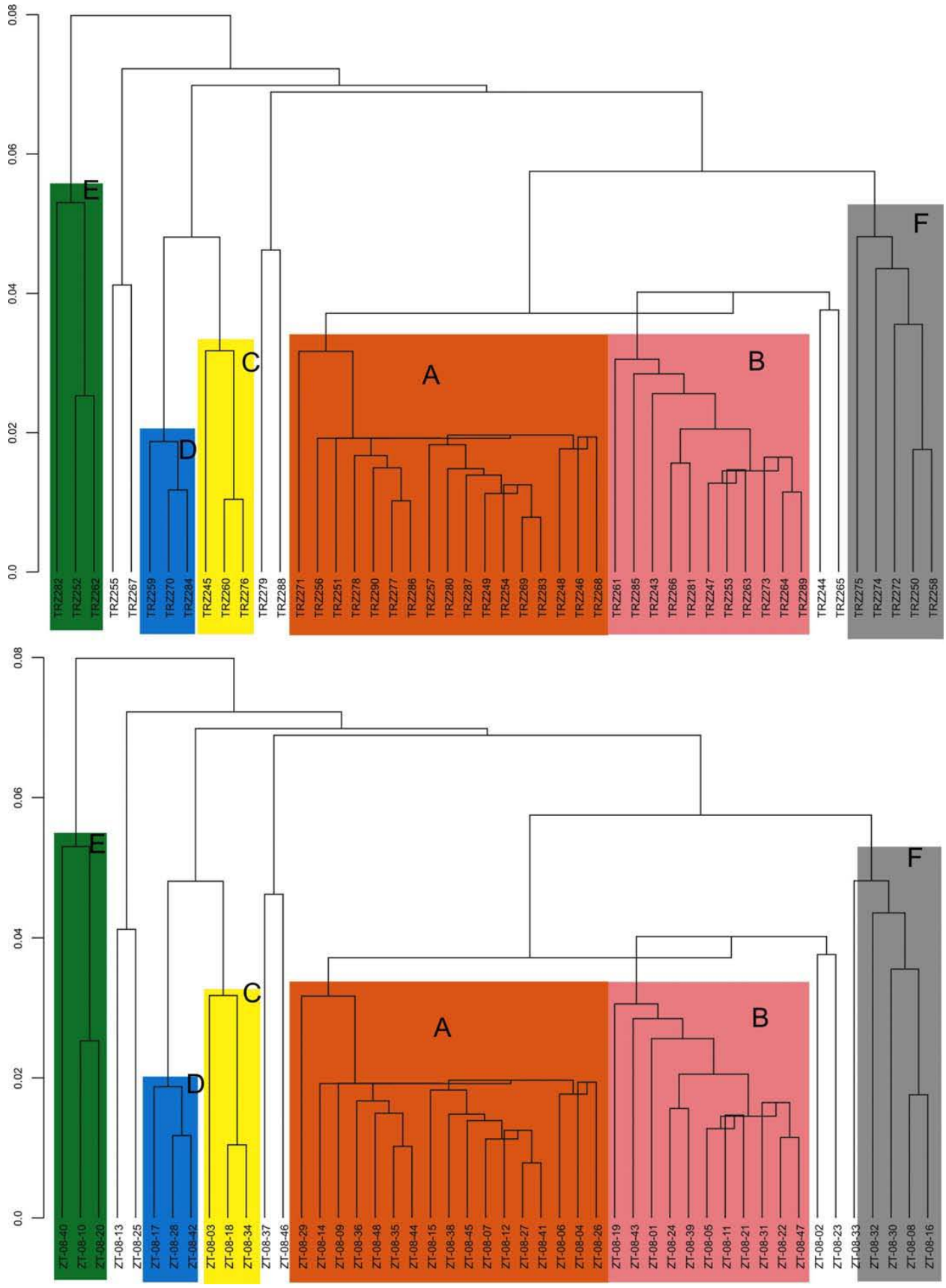

Figure 44: Dendrogram resulted from the cluster analysis performed on the subcomposition Fe_2O_3 Al_2O_3 SiO_2, Zr, Y, Ce, Ga, V, Nb, Zn, Cu, Ni and Cr using TiO_2 as divisor in the logratio transformation of the data of the 48 individuals of Zar Tepe using the Squared Euclidean distance and the centroid algorithm, performed by S-plus2000 (MathSoft, 1999)

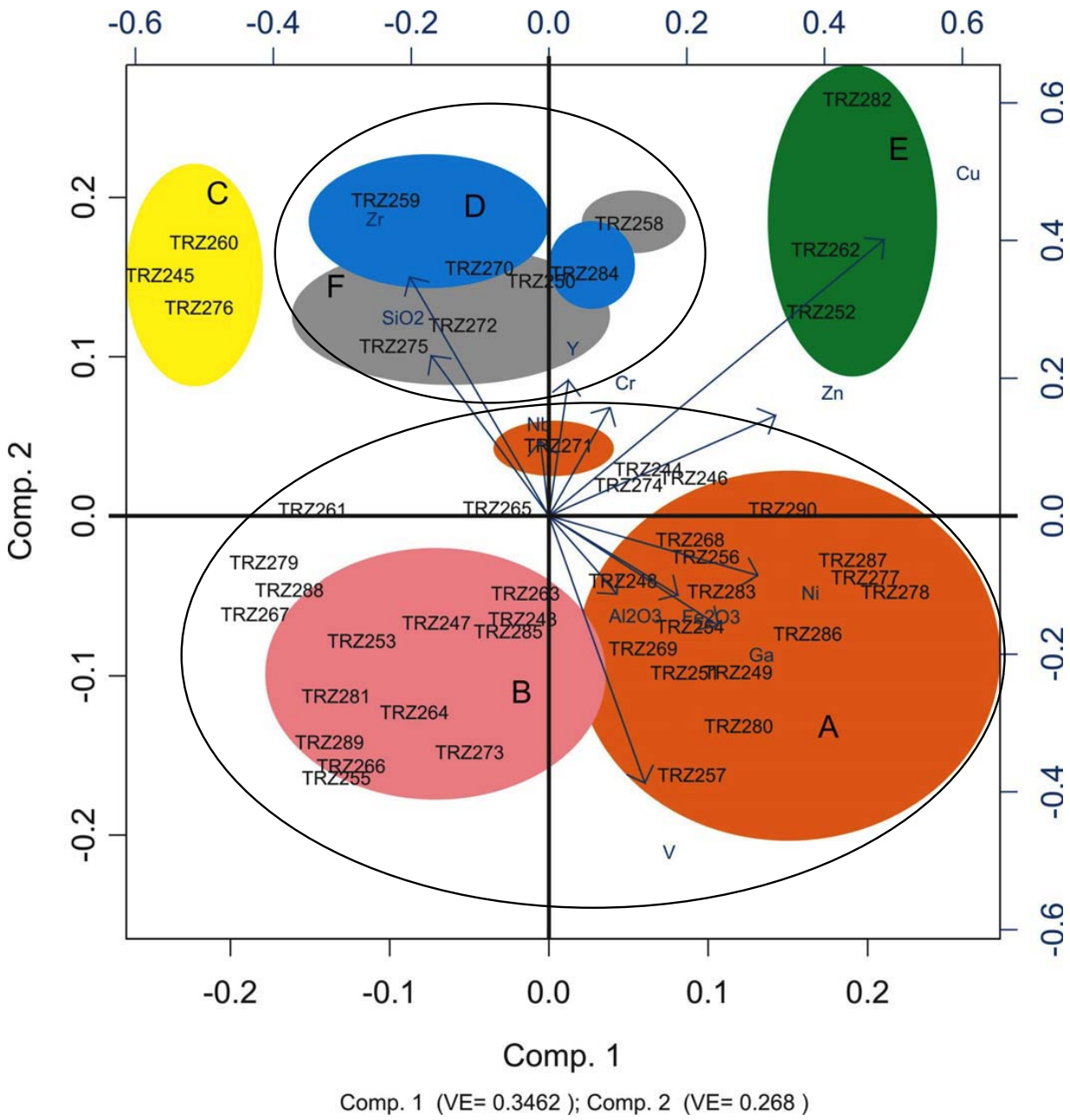

Figure 45: Biplot of the first two principal components, result of the principal component analysis applied upon the subcomposition Fe_2O_3 Al_2O_3 SiO_2, Zr, Y, Ce, Ga, V, Nb, Zn, Cu, Ni and Cr using TiO_2as divisor of the logratio transformation of the data of the 40 individuals of Zar Tepe

62% of the variability present in this data set. Crosschecking the raw chemical results with the results of this biplot is obvious that there are small differences mainly in the composition of trace elements between the subgroups which generally separate well in the biplot of the Figure 45. Even thought the groups D and F seem to be much more similar to each other than the other groups, by looking at the chemical data, small differences in the concentrations of Ga, V, Zn Cu, Ni and Cr can be observed. On the other hand, in the biplot can be observed that A and B are two subgroup with a very similar composition also beside small differences in Ni, Ga and V. Albeit the differences between the subgroups they are not sufficiently important to consider them as different productions thus they only indicate the existence of slightly different sub-productions in this archaeological site. These chemical differences according to DRX might be owed to small differences in the firing temperatures. The mean chemical composition and the standard deviation of the subgroups A, B and C is given in Table 16 and the mean chemical composition and the standard deviation of the subgroups D, E and F can be observed at Table 17. The typology of each subgroup is presented in Figures 46-51.

El.	A (n=17) Mean	Stand. Dev
Fe2O3%	6,10	0,34
Al2O3%	16,12	0,71
TiO2%	0,65	0,03
MgO%	4,20	0,61
CaO%	7,89	0,93
Na2O%	1,89	0,52
K2O%	3,76	0,37
SiO2%	56,05	1,35
Ba ppm	561	144
Rb ppm	132	11
Th ppm	14	1
Nb ppm	14	1
Zr ppm	142	6
Y ppm	24	1
Sr ppm	406	80
Ce ppm	58	9
Ga ppm	18	1
V ppm	102	7
Zn ppm	100	5
Cu ppm	32	3
Ni ppm	47	3
Cr ppm	75	4

El.	B (n=11) Mean	Stand. Dev
Fe2O3%	5,80	0,25
Al2O3%	15,46	0,76
TiO2%	0,64	0,02
MgO%	3,90	0,94
CaO%	6,82	1,01
Na2O%	2,27	0,70
K2O%	4,26	0,50
SiO2%	56,26	2,09
Ba ppm	536	120
Rb ppm	131	8
Th ppm	13	2
Nb ppm	14	1
Zr ppm	144	5
Y ppm	23	1
Sr ppm	398	94
Ce ppm	55	8
Ga ppm	17	1
V ppm	98	6
Zn ppm	91	5
Cu ppm	28	1
Ni ppm	44	2
Cr ppm	72	3

El.	C (n=3) Mean	Stand. Dev
Fe2O3%	5,06	0,01
Al2O3%	13,72	0,13
TiO2%	0,61	0,01
MgO%	3,79	0,60
CaO%	7,32	0,23
Na2O%	1,78	0,43
K2O%	3,53	0,20
SiO2%	58,65	1,39
Ba ppm	769	164
Rb ppm	113	3
Th ppm	12	1
Nb ppm	13	1
Zr ppm	157	4
Y ppm	23	0
Sr ppm	352	36
Ce ppm	59	6
Ga ppm	14	1
V ppm	83	1
Zn ppm	83	1
Cu ppm	28	2
Ni ppm	38	1
Cr ppm	69	4

Table 16: The mean chemical composition and the standard deviation of each element of the groups A, B and C of Zar Tepe

El.	D (n=3) Mean	Stand.Dev
Fe2O3%	5,30	0,23
Al2O3%	14,09	0,40
TiO2%	0,61	0,02
MgO%	4,10	0,23
CaO%	7,95	0,35
Na2O%	2,75	0,68
K2O%	4,06	0,29
SiO2%	55,17	0,97
Ba ppm	516	96
Rb ppm	118	4
Th ppm	12	2
Nb ppm	13	1
Zr ppm	151	5
Y ppm	22	1
Sr ppm	412	65
Ce ppm	60	4
Ga ppm	15	1
V ppm	78	2
Zn ppm	93	3
Cu ppm	31	2
Ni ppm	41	2
Cr ppm	67	1

El.	E (n=3) Mean	Stand.Dev
Fe2O3%	5,50	0,25
Al2O3%	14,19	0,51
TiO2%	0,60	0,03
MgO%	4,87	0,83
CaO%	10,80	1,48
Na2O%	1,88	0,78
K2O%	3,47	0,30
SiO2%	54,05	1,10
Ba ppm	525	99
Rb ppm	116	2
Th ppm	12	1
Nb ppm	14	1
Zr ppm	142	3
Y ppm	24	1
Sr ppm	418	18
Ce ppm	48	7
Ga ppm	16	0
V ppm	85	5
Zn ppm	99	4
Cu ppm	34	2
Ni ppm	45	2
Cr ppm	75	4

El.	F (n=3) Mean	Stand.Dev
Fe2O3%	5,32	0,37
Al2O3%	14,37	0,73
TiO2%	0,59	0,05
MgO%	3,69	0,69
CaO%	8,53	1,87
Na2O%	2,10	0,74
K2O%	3,98	0,54
SiO2%	56,97	1,56
Ba ppm	491	43
Rb ppm	122	6
Th ppm	13	1
Nb ppm	14	1
Zr ppm	147	12
Y ppm	23	2
Sr ppm	359	56
Ce ppm	57	10
Ga ppm	16	1
V ppm	86	9
Zn ppm	91	7
Cu ppm	28	2
Ni ppm	40	4
Cr ppm	77	10

Table 17: The mean chemical composition and the standard deviation of each element of the groups D, E and F of Zar Tepe

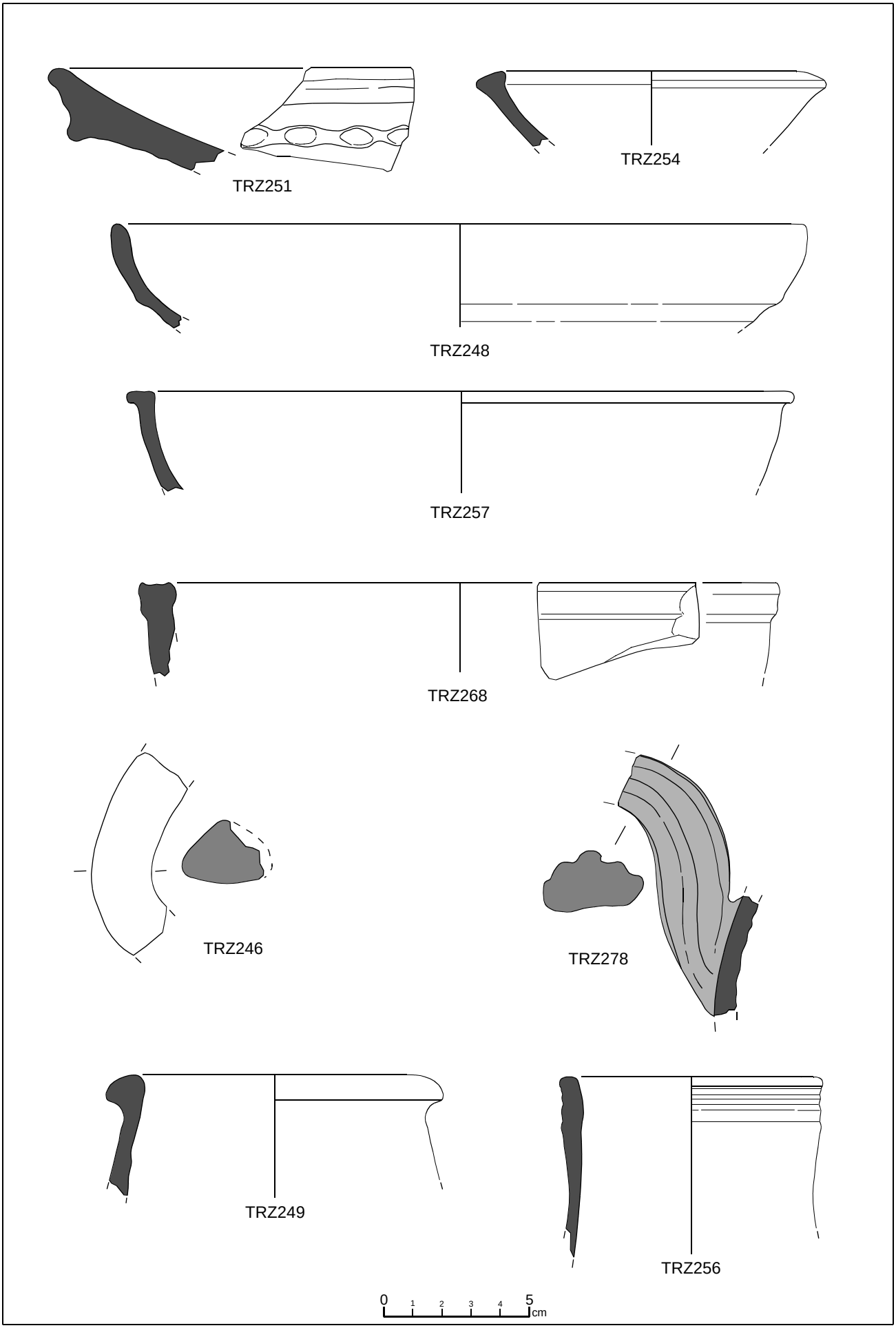

Figure 46: Typology of the subgroup A

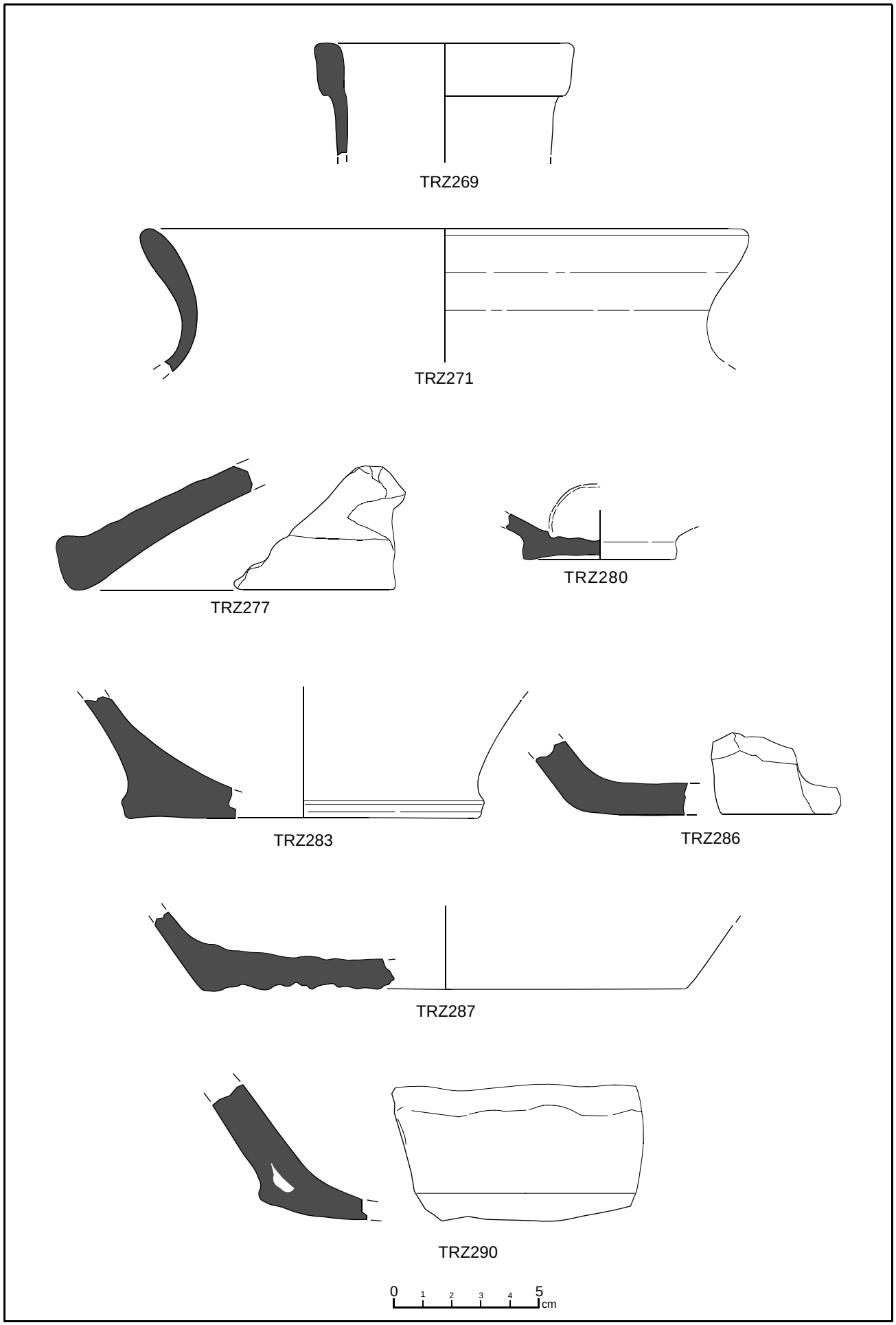

Figure 46: Typology of the subgroup A

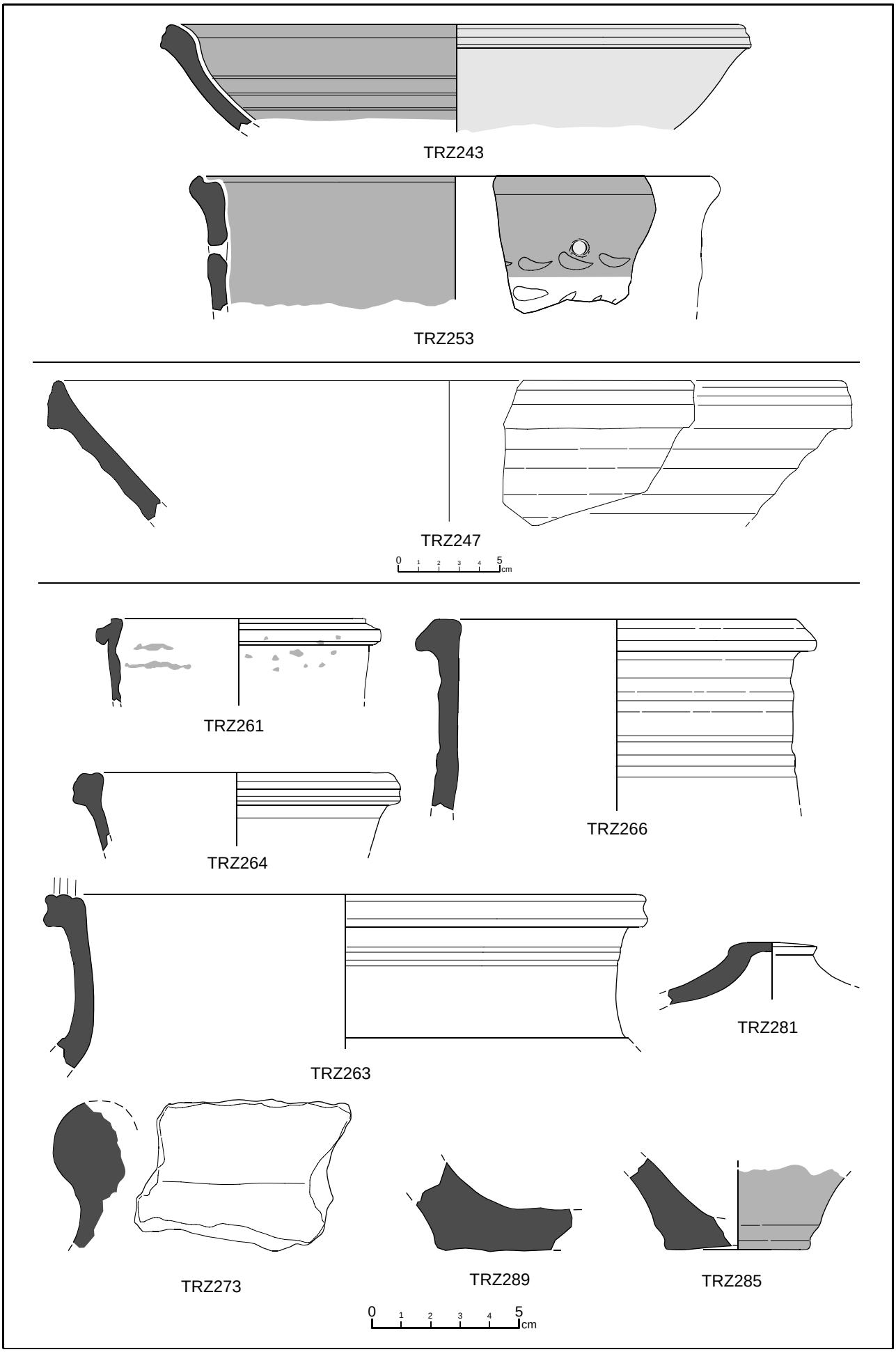

Figure 47: Typology of the subgroup B

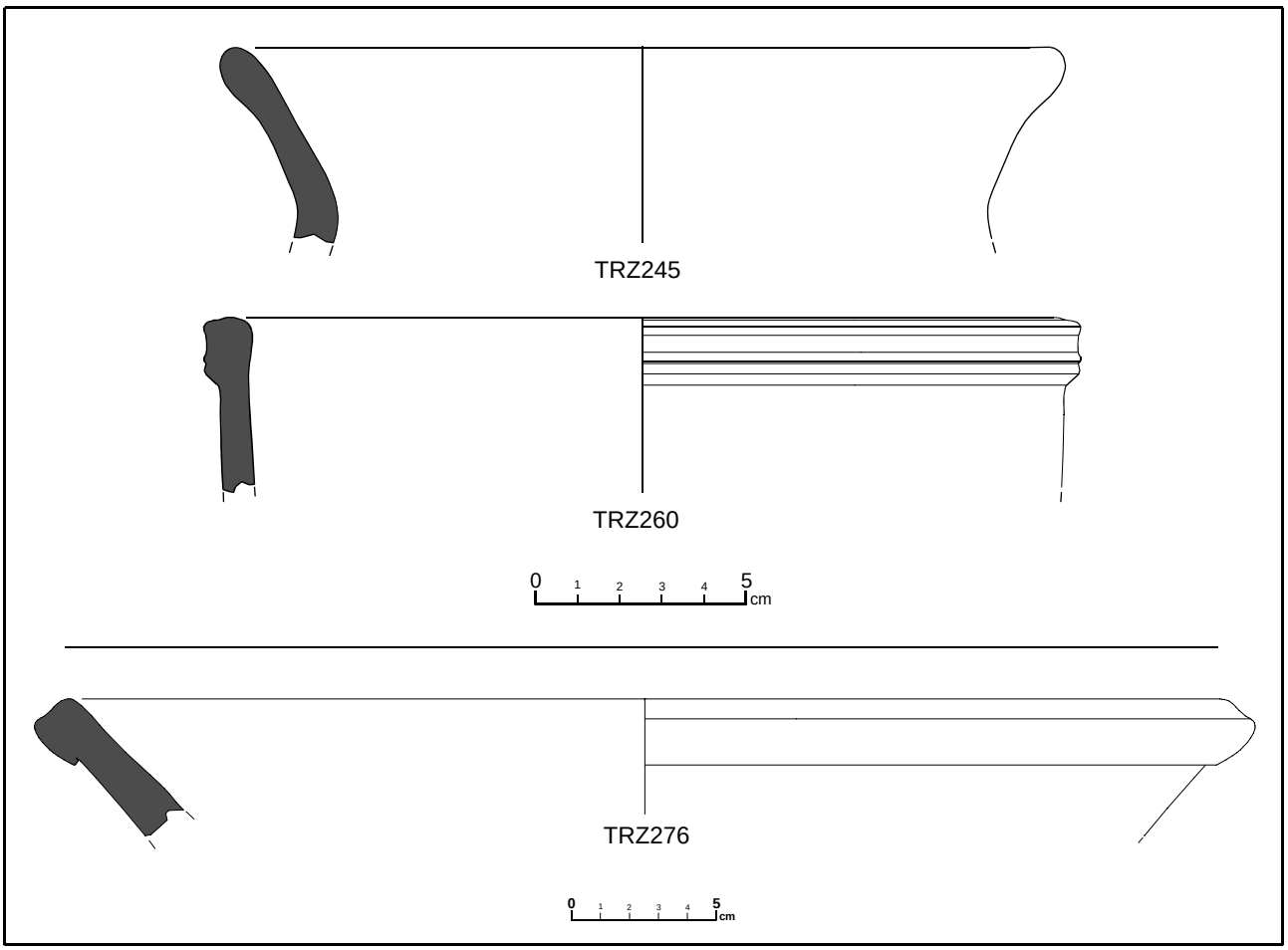

Figure 48: Typology of the subgroup C

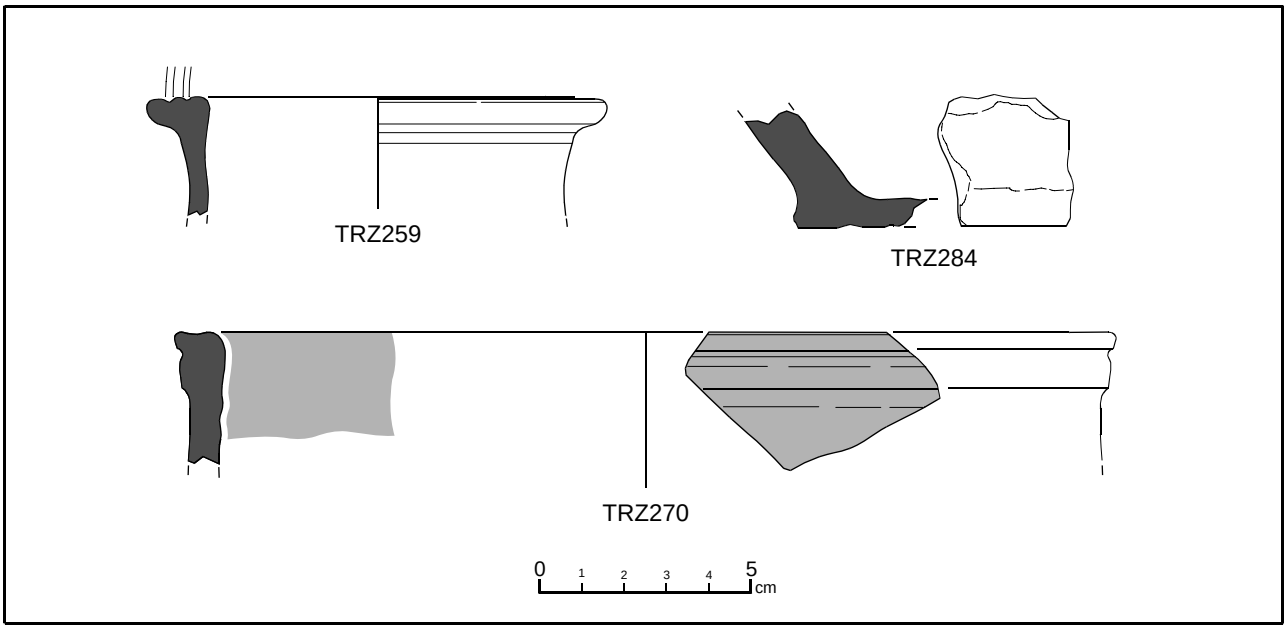

Figure 49: Typology of the subgroup D

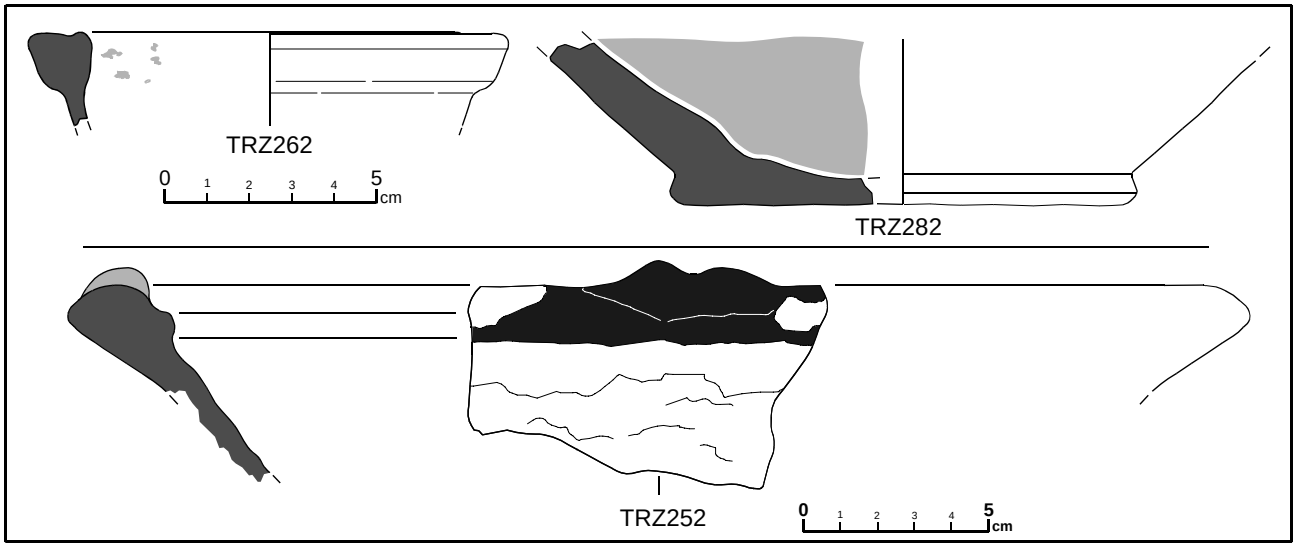

Figure 50: Typology of the subgroup D

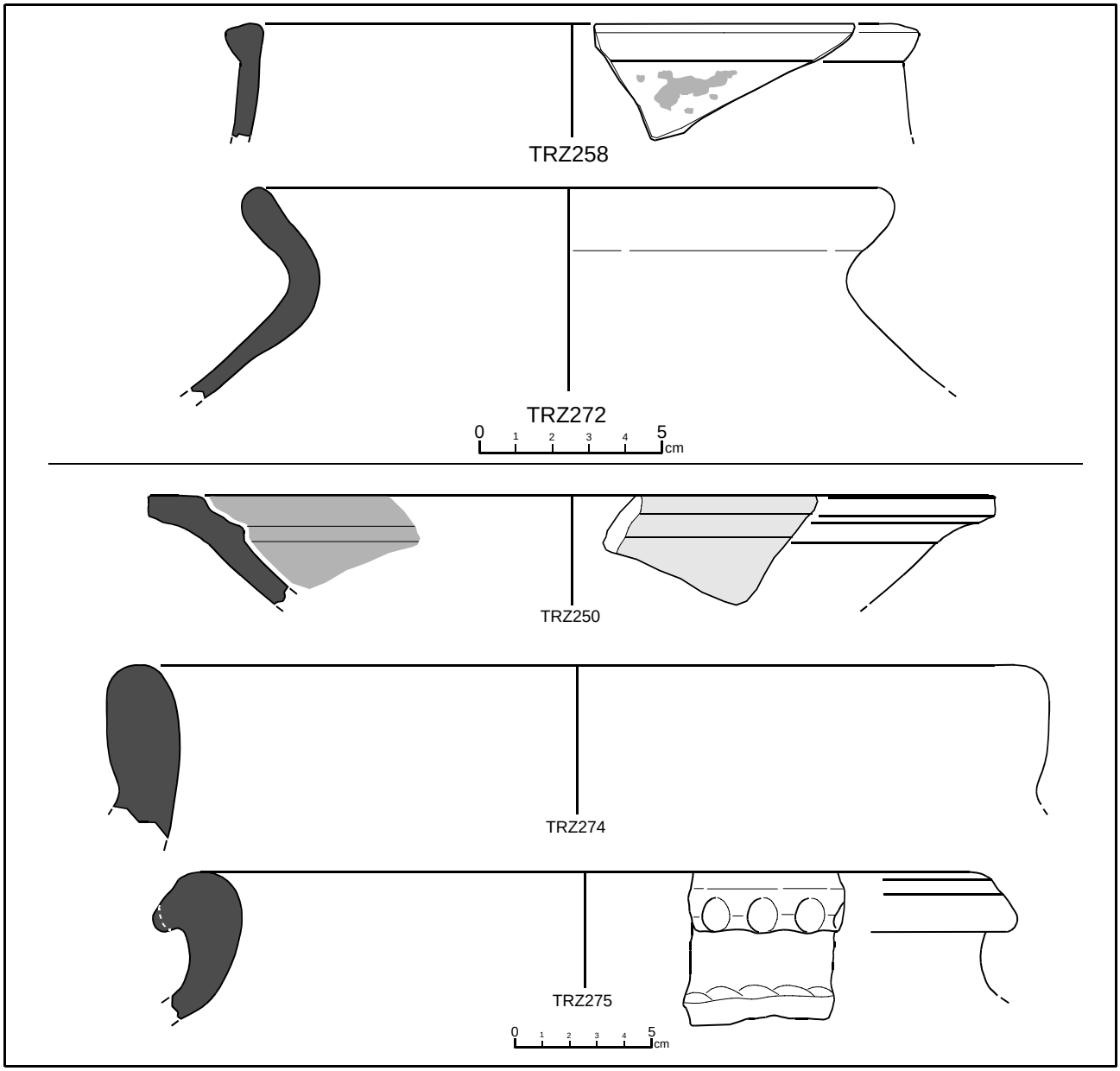

Figure 51: Typology of the subgroup E

Examination of the cooking pot TRZ272 from ***Zar Tepe*** using petrographic analysis (Figure 52) shows few differences in composition in relation to the pottery from ***Kampyr Tepe*** and ***Tchinguiz Tepe.*** Micromass of TRZ272 is reddish-brown under PPL, rich in iron oxides and homogeneous. Inclusions are frequent, equant, sub-rounded, single-spaced and they show a bimodal grain size distribution (Table 5). Predominant rocks are granitic fragments and crystals detached of these rocks (quartz, plagioclase, k-feldspars, amphiboles and mica-muscovite). Sedimentary rocks as sandstones are frequent together with micritic calcite concentrations whereas only few metamorphic rocks as quartzite and quartz-mica schist are present. Porosity is diverse, mainly formed by few mesovughs, macrovughs and meso-vesicles.

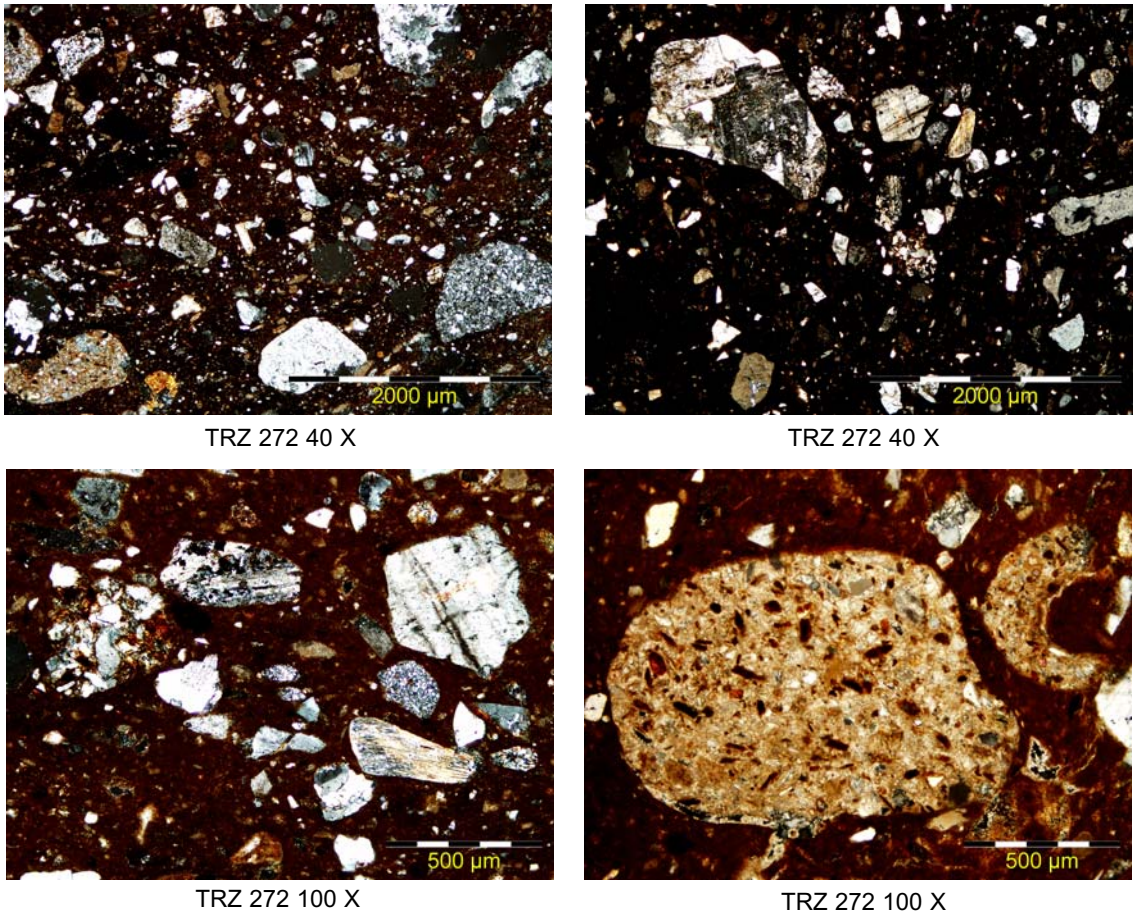

Figure 52: A microphotograph by crossed polars of the sample TRZ272 from Zar Tepe

Firing temperature and mineralogical aspects of ceramics from group A **of Zar Tepe:**

This subgroup is generally characterised by high to very high firing temperatures. Two mineralogical categories related to two different EFT-s can be established for this group. The first one corresponds to the rang of 950/1000ºC and is characterised by the presence of clear firing phases (gehlenite and pyroxenes) under advanced state of development, but the coexistence of illite-muscovite with these firing phases steel situates the temperature below 1050ºC. The individuals representing this fabric are: TRZ251 (Figure 53), TRZ257, TRZ268 and TRZ278. However, regarding the XRD spectrums of these individuals, their EFT must be closer to 1000ºC than to 950ºC. The second mineralogical category is characterised by the advanced decomposition of illite-muscovite and gehlenite and the total decomposition of calcite with the parallel clear increment of the pyroxenes that situate its EFT around 1050/1100ºC and it is represented by TRZ246, TRZ248 (Figure 53), TRZ249, TRZ254, TRZ256, TRZ269, TRZ271, TRZ277, TRZ280, TRZ283 (Figure 53), TRZ286, TRZ287 and TRZ290. Both TRZ246 and TRZ283 also present analcime in their difractograms.

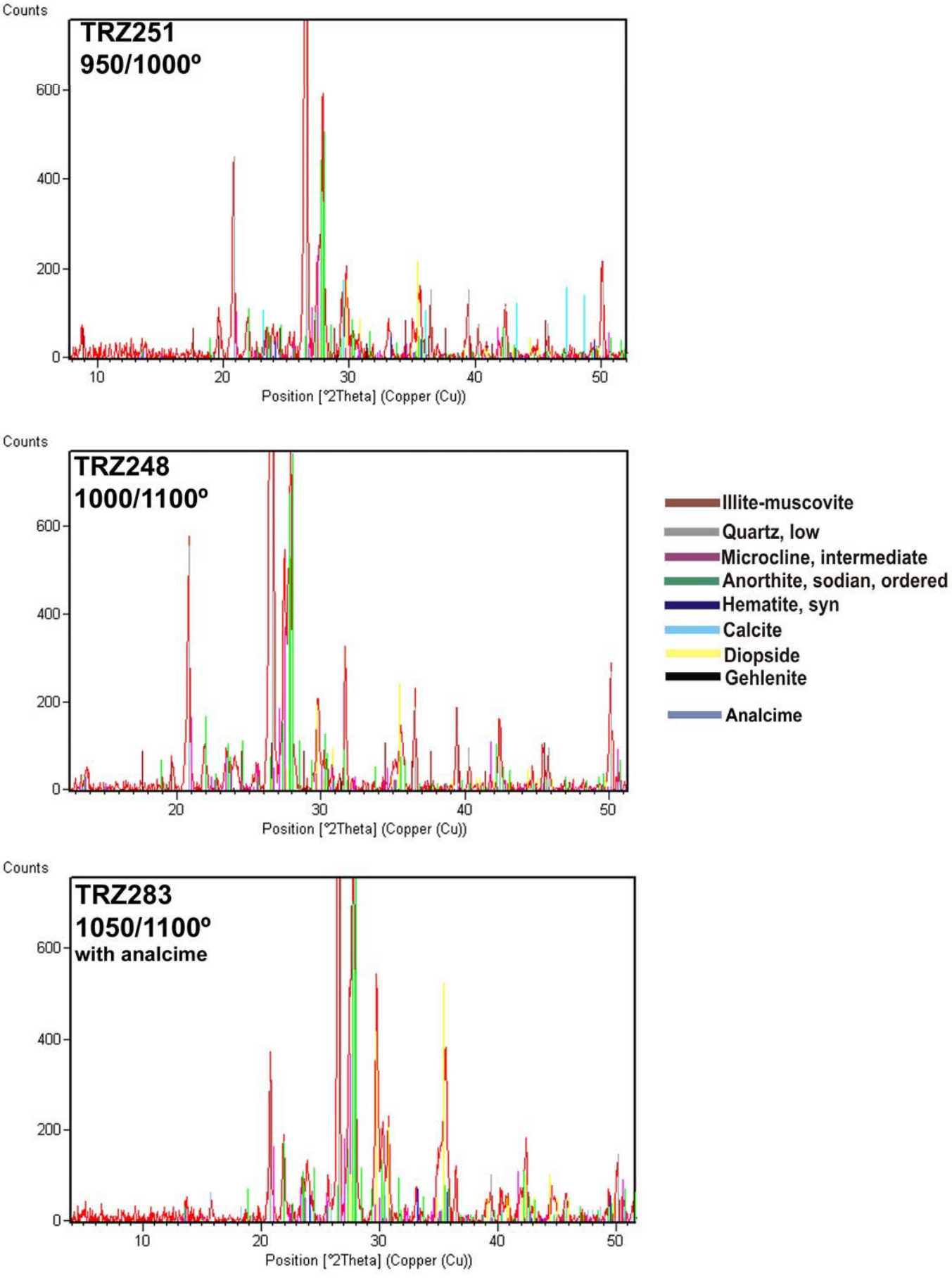

Figure 53: Difractograms of the individuals TRZ251, TRZ248 and TRZ283 (with analcime) representing the chemical group A of Zar Tepe

Firing temperature and mineralogical aspects of ceramics from group B **of Zar Tepe:**

The two mineralogical fabrics corresponding to the sub-production B represent lower temperatures. The first one only contains TRZ273 (Figure 54) and it matches with a range of 800/850ºC as in its difractogram can not be identified any clear firing phase. The second category represented by TRZ243, TRZ247, TRZ253, TRZ261, TRZ263, TRZ264, TRZ266 (Figure 54), TRZ281, TRZ285 and TRZ289 corresponds to a slightly higher temperature (950/1000ºC) due to the clear development of some firing phases (gehlenite, pyroxenes), the partial decomposition of gehlenite and total decomposition of calcite.

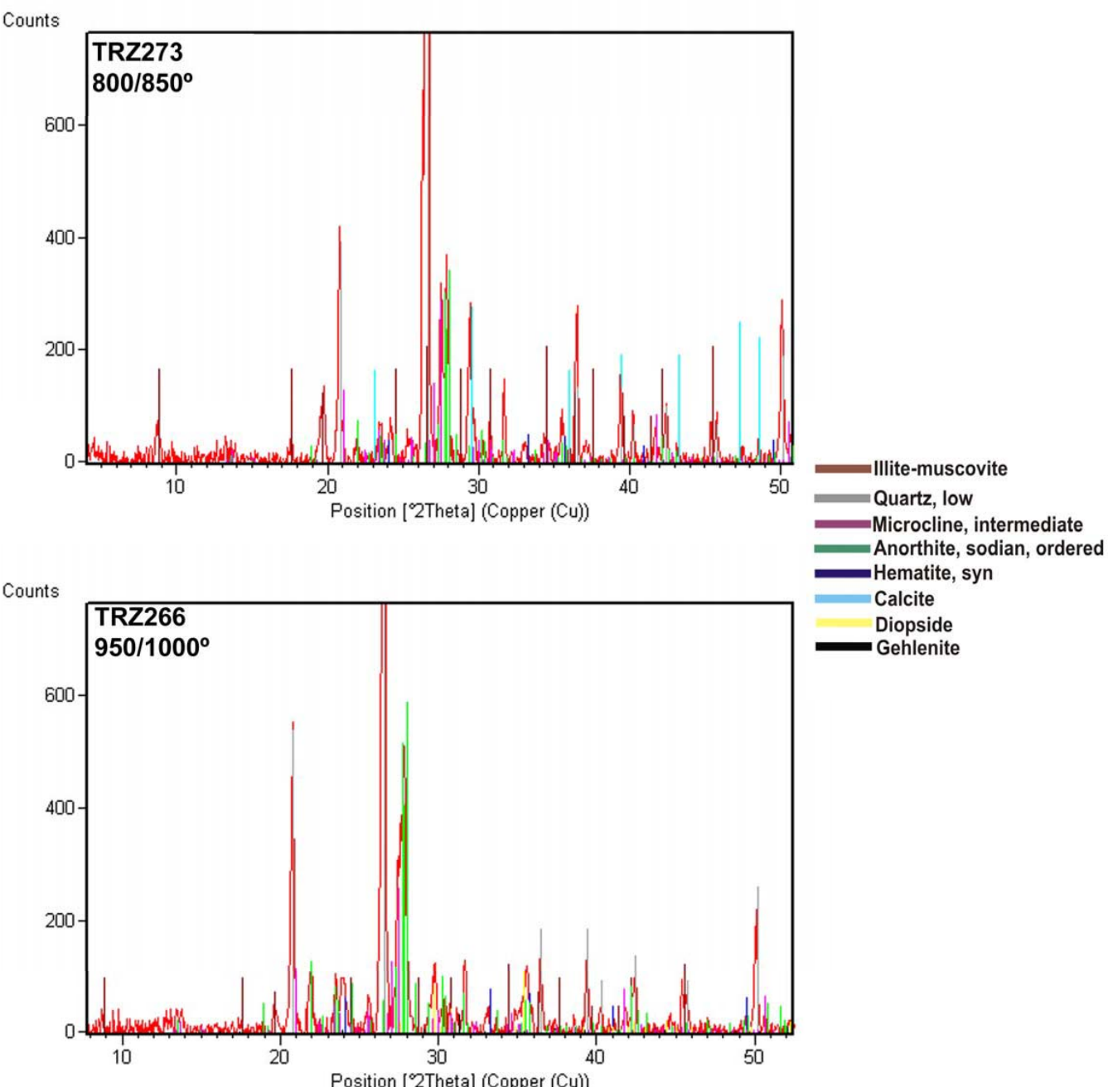

Figure 54: Difractograms of the individuals TRZ273 and TRZ266 representing the chemical group B of Zar Tepe.

Firing temperature and mineralogical aspects of ceramics from group C **of Zar Tepe:**

The EFT of this subgroup is very constant and it can be estimated around 950/1000ºC for all the individuals belong to it: TRZ245 (Figure 55), TRZ260 and TRZ276.

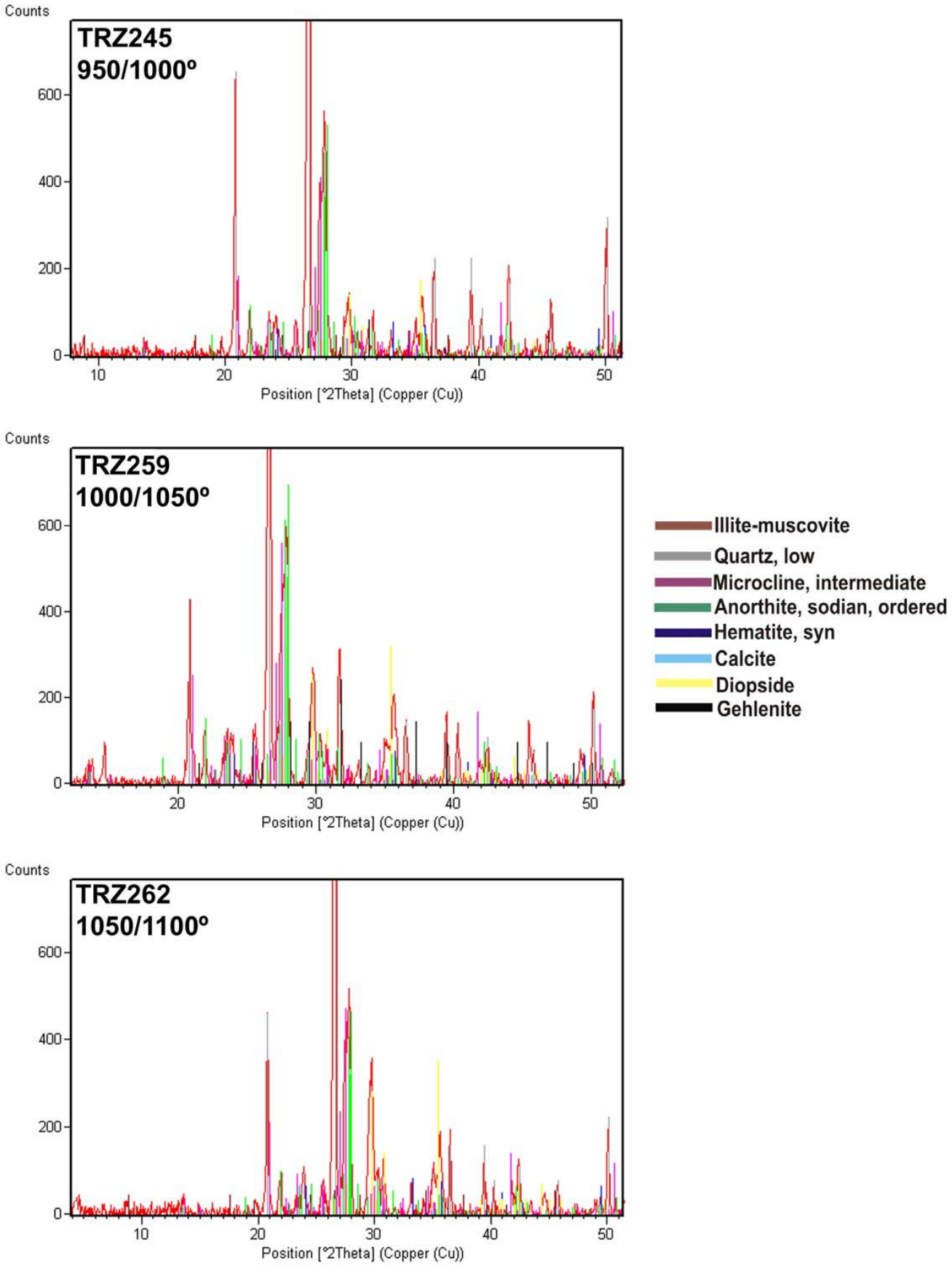

Figure 55: Difractograms of the individuals TRZ245, TRZ259 and TRZ262 representing the chemical groups C, D and E of Zar Tepe.

Firing temperature and mineralogical aspects of ceramics from group D of Zar Tepe:

The EFT of this subgroups (TRZ259 TRZ270 and TRZ284) is also constant and it is similar to C, although, due to a more advanced development of the firing phases must be estimated around 1000/1050ºC and not 950/1000ºC (Figure 55).

Firing temperature and mineralogical aspects of ceramics from group E of Zar Tepe:

This subgroup includes overfired ceramics all individuals (TRZ52, TRZ262 (Figure 50) and TRZ282) that must have been fired between 1050/1100ºC, because of the advanced decomposition of illite-muscovite and gehlenite and the total decomposition of calcite with the parallel clear increment of the pyroxenes. In this subgroup no existence of analcime could be observed.

Firing temperature and mineralogical aspects of ceramics from group F of Zar Tepe:

This is the most variable subgroup considering the mineralogical aspects. One individual TRZ272 (Figure 56) is low fired (800/850ºC) as in its difractogram no clear firing phases can be observed. Three individuals, TRZ274, TRZ250 and TRZ258 (Figure 56) are characterised by the coexistence of primary (illite-muscovire, alkaline feldspars) and firing phases (gehlenite and pyroxenes), thus their EFT approximates the range of 950/1000ºC. Finally, there is one overfired ceramic individual TRZ275 (Figure 56) which EFT must be around 1050/1100ºC because of the almost total absence of primary phases and the pronounced peaks of pyroxenes in its XRD spectra.

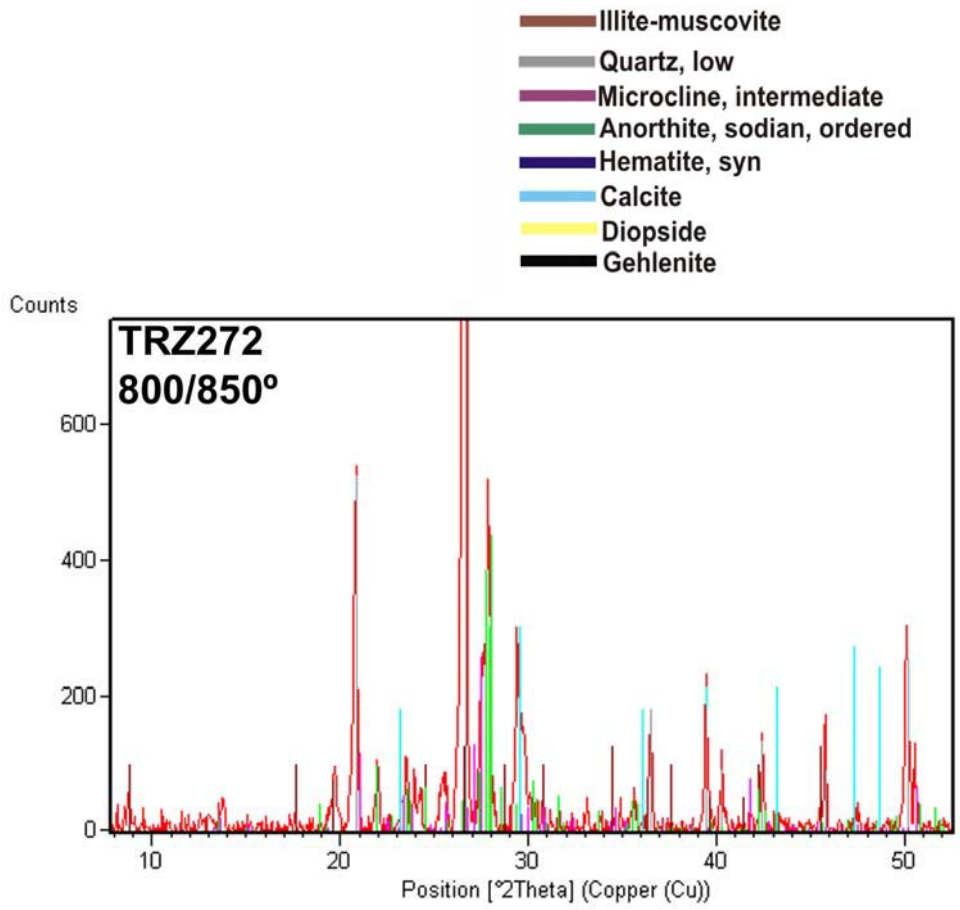

Figure 56: Difractograms of the individuals TRZ272, TRZ258 and TRZ275 representing the chemical group F of Zar Tepe

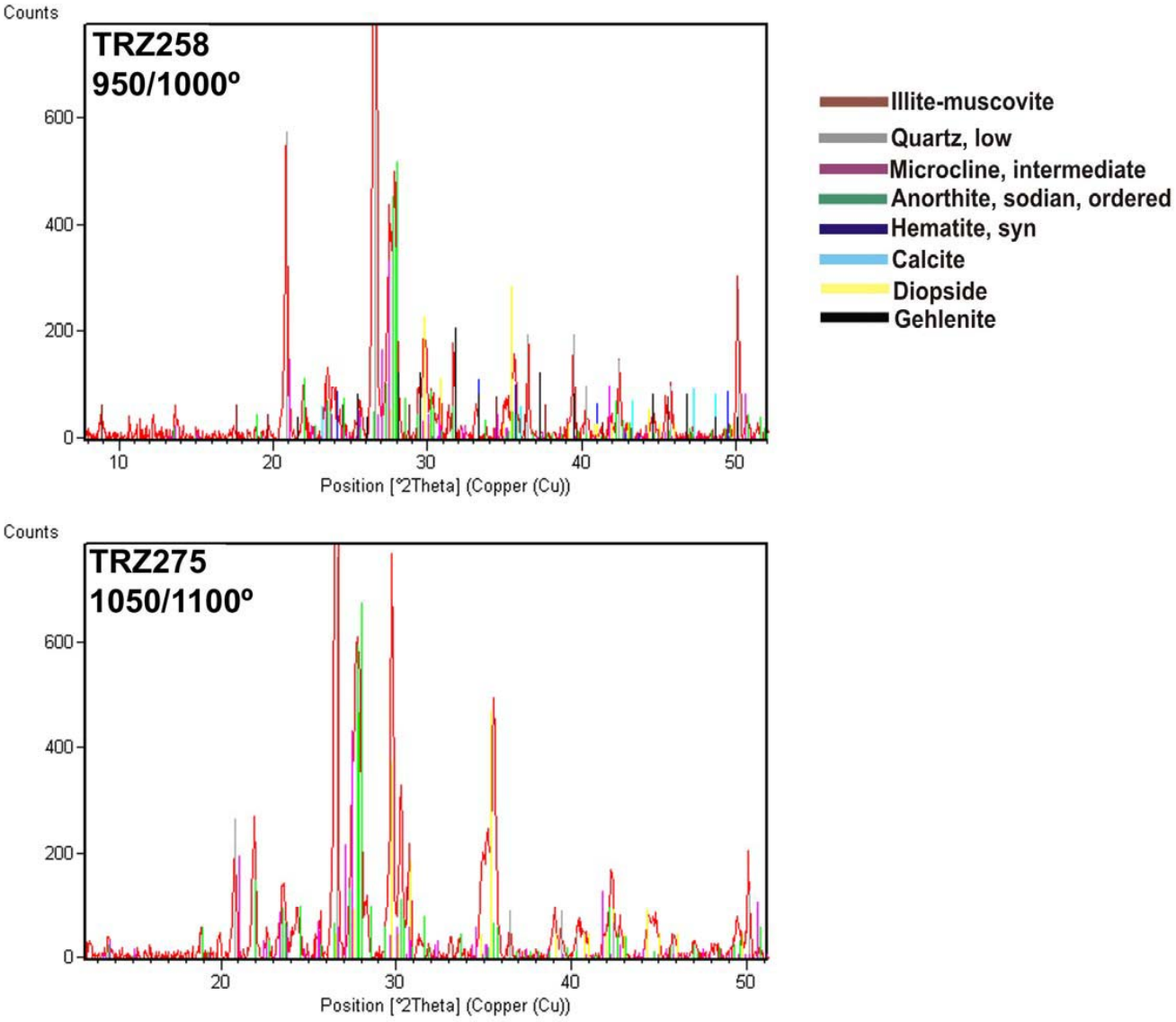

Figure 56: Difractograms of the individuals TRZ272, TRZ258 and TRZ275 representing the chemical group F of Zar Tepe

Integrated archaeometrical results

The total variation (Table 18) of the complete data set without considering the clear chemical outliers: TRZ163, TRZ170, TRZ172, TRZ182, TRZ187, TRZ162, TRZ171, TRZ104, TRZ084, TRZ161, TRZ189 and TRZ088 (267 indiniduals), and the following elements: Mo, Sn, Co, W, MnO, P_2O_5, Pb, Na_2O, K_2O, Rb and Ba for reasons that already have been explained a long this work, is equal to 0,1752 which is sufficiently low to indicate common geochemical origin. This reinforces the initial hypothesis that the raw materials used for the fabrication of majority of the analysed ceramic come from very similar clay deposits because of the limited adequate clay deposits in the area. The chemical elements which introduce more than the 50% of the variability according to the CVM of Table 18 maintained: CaO, MgO, Sr, Th, Ce and Cu. From which, CaO, MgO, Sr, Th and Ce are associated elements with high natural variability into the same or common calcareous raw material sources.

El.	Fe2O3	Al2O3	TiO2	MgO	CaO	SiO2	Th	Nb	Zr
Fe2O3	0,0000	0,0013	0,0025	0,0214	0,0344	0,0074	0,0137	0,0054	0,0115
Al2O3	0,0013	0,0000	0,0015	0,0204	0,0354	0,0038	0,0135	0,0041	0,0086
TiO2	0,0025	0,0015	0,0000	0,0233	0,0351	0,0031	0,0142	0,0034	0,0046
MgO	0,0214	0,0204	0,0233	0,0000	0,0475	0,0252	0,0350	0,0207	0,0317
CaO	0,0344	0,0354	0,0351	0,0475	0,0000	0,0361	0,0417	0,0268	0,0353
SiO2	0,0074	0,0038	0,0031	0,0252	0,0361	0,0000	0,0168	0,0051	0,0040
Th	0,0137	0,0135	0,0142	0,0350	0,0417	0,0168	0,0000	0,0160	0,0208
Nb	0,0054	0,0041	0,0034	0,0207	0,0268	0,0051	0,0160	0,0000	0,0055
Zr	0,0115	0,0086	0,0046	0,0317	0,0353	0,0040	0,0208	0,0055	0,0000
Y	0,0087	0,0073	0,0062	0,0221	0,0248	0,0081	0,0177	0,0025	0,0073
Sr	0,0409	0,0361	0,0359	0,0492	0,0488	0,0319	0,0479	0,0372	0,0364
Ce	0,0241	0,0223	0,0215	0,0481	0,0520	0,0224	0,0324	0,0224	0,0215
Ga	0,0107	0,0097	0,0122	0,0223	0,0324	0,0153	0,0147	0,0079	0,0189
V	0,0044	0,0037	0,0051	0,0244	0,0385	0,0084	0,0154	0,0073	0,0135
Zn	0,0089	0,0081	0,0089	0,0213	0,0267	0,0110	0,0190	0,0076	0,0128
Cu	0,0188	0,0218	0,0234	0,0361	0,0417	0,0293	0,0219	0,0239	0,0334
Ni	0,0065	0,0092	0,0116	0,0216	0,0349	0,0181	0,0137	0,0101	0,0222
Cr	0,0063	0,0051	0,0066	0,0205	0,0387	0,0082	0,0118	0,0069	0,0136
t.i	0,2268	0,2116	0,2190	0,4908	0,6306	0,2541	0,3661	0,2127	0,3016
vt/t.i	0,7722	0,8278	0,7996	0,3569	0,2778	0,6894	0,4784	0,8236	0,5808
r v,t	0,9814	0,9833	0,9744	0,9419	0,7934	0,9262	0,9488	0,9844	0,9022

El.	Y	Sr	Ce	Ga	V	Zn	Cu	Ni	Cr
Fe2O3	0,0087	0,0409	0,0241	0,0107	0,0044	0,0089	0,0188	0,0065	0,0063
Al2O3	0,0073	0,0361	0,0223	0,0097	0,0037	0,0081	0,0218	0,0092	0,0051
TiO2	0,0062	0,0359	0,0215	0,0122	0,0051	0,0089	0,0234	0,0116	0,0066
MgO	0,0221	0,0492	0,0481	0,0223	0,0244	0,0213	0,0361	0,0216	0,0205
CaO	0,0248	0,0488	0,0520	0,0324	0,0385	0,0267	0,0417	0,0349	0,0387
SiO2	0,0081	0,0319	0,0224	0,0153	0,0084	0,0110	0,0293	0,0181	0,0082
Th	0,0177	0,0479	0,0324	0,0147	0,0154	0,0190	0,0219	0,0137	0,0118
Nb	0,0025	0,0372	0,0224	0,0079	0,0073	0,0076	0,0239	0,0101	0,0069
Zr	0,0073	0,0364	0,0215	0,0189	0,0135	0,0128	0,0334	0,0222	0,0136
Y	0,0000	0,0401	0,0246	0,0057	0,0096	0,0082	0,0249	0,0130	0,0092
Sr	0,0401	0,0000	0,0561	0,0495	0,0412	0,0359	0,0636	0,0542	0,0434
Ce	0,0246	0,0561	0,0000	0,0308	0,0255	0,0253	0,0450	0,0315	0,0259
Ga	0,0057	0,0495	0,0308	0,0000	0,0108	0,0116	0,0214	0,0102	0,0088
V	0,0096	0,0412	0,0255	0,0108	0,0000	0,0099	0,0249	0,0116	0,0069
Zn	0,0082	0,0359	0,0253	0,0116	0,0099	0,0000	0,0257	0,0139	0,0117
Cu	0,0249	0,0636	0,0450	0,0214	0,0249	0,0257	0,0000	0,0164	0,0210
Ni	0,0130	0,0542	0,0315	0,0102	0,0116	0,0139	0,0164	0,0000	0,0081
Cr	0,0092	0,0434	0,0259	0,0088	0,0069	0,0117	0,0210	0,0081	0,0000
t.i	0,2401	0,7482	0,5314	0,2928	0,2610	0,2665	0,4931	0,3066	0,2526
vt/t.i	0,7294	0,2341	0,3296	0,5981	0,6710	0,6573	0,3552	0,5713	0,6933
r v,t	0,9638	0,7129	0,9670	0,9480	0,9893	0,9843	0,8960	0,9041	0,9743
vt	0,1752								

Table 18: Compositional Variation Matrix (CVM) calculated upon the complete data without considering TRZ163, TRZ170, TRZ172, TRZ182, TRZ187, TRZ162, TRZ171, TRZ104, TRZ084, TRZ161, TRZ189 and TRZ088 and upon the subcomposition: Fe_2O_3, Al_2O_3, TiO_2, MgO, CaO, SiO_2, Th, Nb, Zr, Y, Sr, Ce, Ga, V, Zn, Cu, Ni and Cr

The dedrogram of the 267 individuals resulting from the cluster analysis performed upon subcomposition: Fe_2O_3, TiO_2, SiO_2, Zr, Ce, Ga, V, Nb, Zn, Cu, Ni and Cr using Al_2O_3 as divisor in the logratio transformation and the Square Euclidean distance combined with the centroid algorithm is presented at Figure 57. In this dendrogram TRZ156 (TZ-08-AC-12.8) which is a cooking ware from the Antique Quartiles of ***Termez*** mark out from the rest of the material for its peculiar composition which already has been described. The rest of the material is rather similar chemically. However, different smaller subgroups can be observed. The subgroups identified for ***Termez*** are mainly the same. At the left site in this dedrogram the group **AC** is indicated with two more individuals incorporated from Termez: TRZ140 (TZ07-90/MON) and TRZ068 (TZ-5D-18/TCH-PRO), followed by the expanded **F2** group which is the ***Reference Group of Kiln 2 of Kara Tepe***, while at the right, the entire group **TRZ** is located. All individuals indicated in the rectangle marked around **F2** (Figure 57) must be variants of ***Kara Tepe's Kiln 2*** production. Regarding the sub-productions identified in the other two sites ***Kampyr Tepe*** and ***Zar Tepe***, it can be observed that they divided into smaller groups which also contain individuals from some sites of ***Termez***. Next to the extended group **F2** (Figure 57) there is a group of Kampyr Tepe indicated in the dendrogram that includes mainly individuals from the identified subgroups $\mathbf{KPT_{(A)}}$ and $\mathbf{KPT_{(B)}}$ integrating also two individuals from the ***Citadel*** : TRZ101 (TZ-07-4-51) and TRZ105 (TZ-07-4-55). This subgroup seems to be chemically related on one hand to the subgroup **C** identified for ***Zar Tepe*** and to a small subgroup formed by two individuals from ***Tchinguiz Tepe*** (Termez), one from the ***Monasteries*** (Termez), one from the ***Citadel*** (Termez) and two chemical outlayers from ***Zar Tepe***: TRZ054 (TZ-RC-10-4), TRZ118 (TZ07-68), TRZ255 (ZT-08-13), TRZ133 (TZ07-83), TRZ089 (TZ07-RB-5-39) and TRZ267 (ZT-08-25). All this subgroups of a similar chemical composition are limited by a rectangle called ***cluster Kampyr Tepe*** in this dendrogram (Figure 57). The next broader block marked in the dendrogram is the one of ***Tchinguiz Tepe*** (**TRZ** or **RC/RF**). In this block, a part from the group **TRZ**, associated to the archaeological site ***Tchinguiz Tepe*** (Termez), there are other subgroups chemically related to this group. Starting from the left there is a small subcluster including one individual from ***Kampyr Tepe*** (TRZ203=KPT-08IIIP/S-1) and two from the ***Citadel of Termez*** (TRZ109=TZ07-4-59 and TRZ110=TZ07-4-60), followed by a subgroup mainly formed by individuals identified into the groups **A** and **B** of **Zar Tepe**, three individuals from the ***Citadel of Termez*** (TRZ114=TZ07-4-64, TRZ098=TZ07-4-48 and TRZ095=TZ07-4-45) and two chemical outlayers from ***Kampyr Tepe*** (TRZ228=KPT-08-AC-1 and TRZ210=KPT-08-IP-2). Right next, at the left site of TRZ, the subgroup E of ***Zar Tepe*** is located that additionally incorporates now two individuals sampled at ***Tchinguiz Tepe*** (Termez): TRZ173 (TZ08-RC-18-1) and TRZ200 (TZ08-RF-27-2). Immediately at the right of **TRZ,** a small group formed by three individuals from ***Kampyr Tepe*** (TRZ204=KPT-08-IIIP-S-2, TRZ213=KPT-08-IN-1 and TRZ208=KPT-08-IIIP/S-6), one individual from ***Zar Tepe*** (TRZ238=ZT-08-39), three from the archaeological site of ***Tchinguiz Tepe of Termez*** (TRZ072=TZ07-5D-22, TRZ056=TZ-RC-10-6 and TRZ90=TZ07-RB-5-40), one from the **Monasteries of Termez** (TRZ143=TZ07-91) and one from the ***Citadel of Termez*** (TRZ117=TZ07-93). This set is followed by the last cluster chemically very similar to TRZ at the right side of the dendrogram which contains the subgroup D of Zar Tepe together with five individuals from ***Tchinguiz Tepe of Termez*** (TRZ070=TZ07-5D-21, TRZ067=TZ07-5D-17, TRZ072=TZ07-5D-22, TRZ092=TZ07-RB-5-42 and TRZ197=TZ07-RF-23-3, two from the ***Monasteries of Termez*** (TRZ141=TZ07-91 and TRZ142=TZ07-92) and one from the Citadel of Termez (TRZ108=TZ07-4-58). Finally at the right extreme of this dendrogram one small group formed by specific individuals of the group $\mathbf{KPT_{(B)}}$ of ***Kampyr Tepe*** is separated from the rest of the individuals due to small chemical differences in their composition.

The general conclusions that can be made by the archaeometrical study is that the ceramic material of the ***Kiln 2*** of the site of ***Kara Tepe*** of ***Termez*** always is founded somehow separated from the other productions related to the other two sites (***Kampyr Tepe*** and ***Zar Tepe***) and it is only composed by samples of this same kiln site and associable to individuals found at its close surroundings

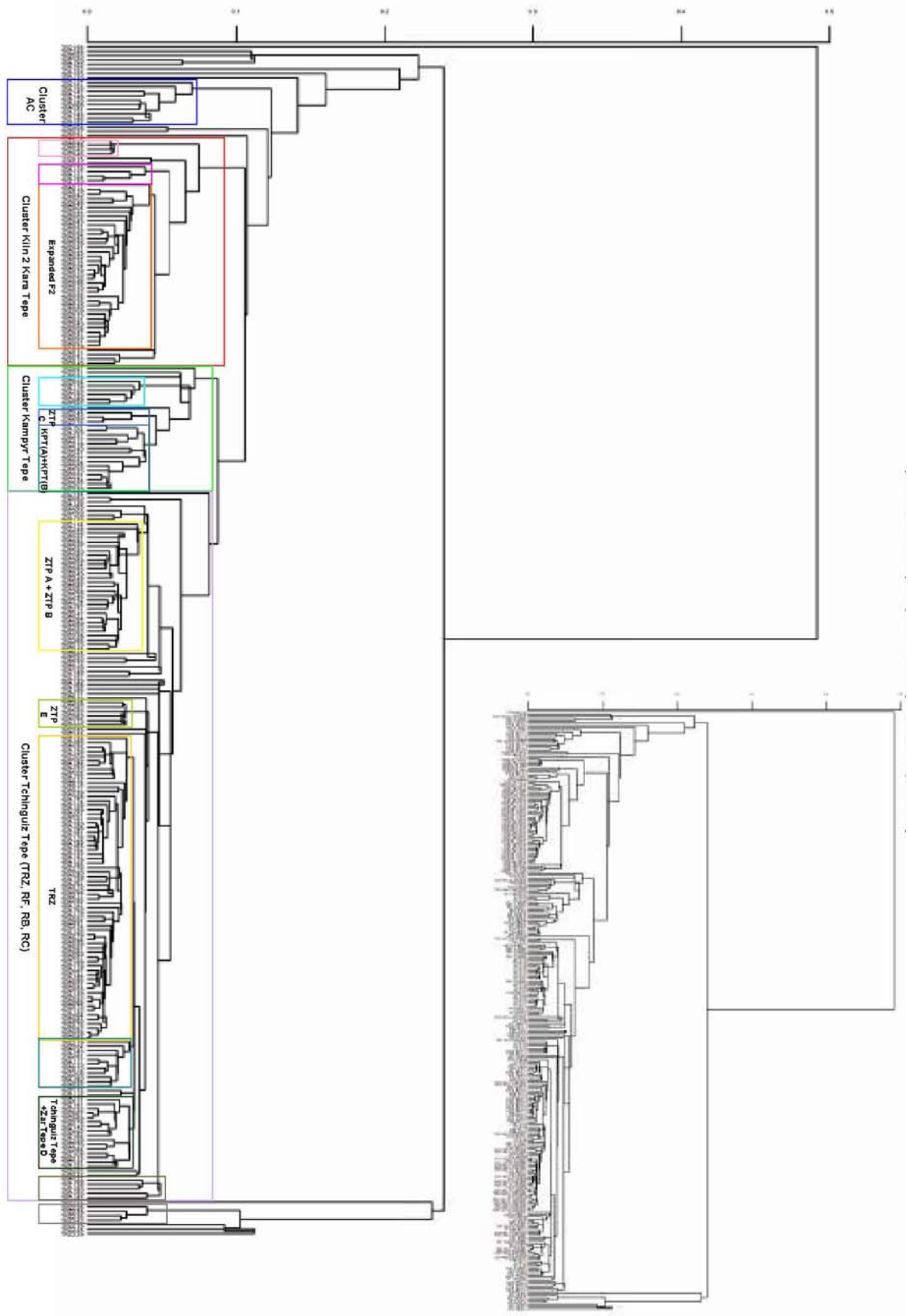

Figure 57: Dendrogram resulted from the cluster analysis performed on the subcomposition Fe_2O_3 TiO_2 SiO_2, Zr, Y, Ce, Ga, V, Nb, Zn, Cu, Ni and Cr using Al_2O_3as divisor in the logratio transformation of the data of the of the 267 individuals using the Square Euclidean distance and the centroid algorithm, performed by S-plus2000 (MathSoft, 1999).

(***Citadel or Monasteries***). It is also tends to be distinguished from the group **TRZ,** which is clearly associated to the subproductions of archaeological site of ***Tchinguiz Tepe*** at the broader area. On the other hand, the subproductions identified for **Tchinguiz Tepe** (Termez), after the integration of all the data, seem to be much more related to the production of both new sites included in this study (***Kampyr Tepe*** and ***Zar Tepe***). However, the subgroups **KPT$_{(A)}$** and **KPT$_{(B)}$** identified for ***Kampyr Tepe*** together with specific individuals from the ***Citadel*** (Termez) and the subgroup **C** of ***Zar Tepe*** together with some individuals from ***Tchinguiz Tepe*** (Termez), the ***Monasteries*** (Termez) and the ***Citadel*** (Termez), seem to be slightly different to both **F2** and **TRZ** indicating probably a slight difference in the ceramic manufacture of these specific groups.

Finally, despite of all the small differences between these subproductions, one hypothesis can be confirmed: the materials used for the fabrication of majority of the analysed ceramics, sampled at three different but located to a close distance sites, come from very similar or common clay deposits and the ceramic tradition follows a very similar or the same production patters for all the analysed material, that means the existence of a log lasting local/regional ceramic tradition in this geographical area.

The difficulties to be able to distinguish clearly between the different productions in an archaeometrical level front us to the essential complementation of already obtained results by a complete study of the possible raw material sources, in the near future, which might lead to a much better understanding of the production, distribution and consumption patters in this territory. On the other hand, the requirement to reinforce the typological and chronological study is obvious, as it will be a crucial to decide which one from the identified subgroups really correspond to different productions with possible chronological differences.

From a petrographical point of view, the two main categories of the studied pots, cooking wares and common wares, can be divided in several fabrics.

Cooking wares are represented by several typologies which can be correlated to different petrographic fabrics. From the 17 cooking wares analysed by XRF, XRD and thin section analysis from all sites of Surkhan Darya valley, 10 ceramics can be related to variety of pastes containing shell fragments and microfossils (**TRZ$_{(B)}$**, **TRZ$_{(D)}$**, **TRZ$_{(E)}$**, **TRZ1$_{(B)}$**, TRZ156 petrographic fabrics). All these ceramics share a basic technological aspect which is the addition of coarse shell fragments as main temper in rich iron oxide clay. However, differences in composition lead to distinguish between five petrographic fabrics, which can be attributed to different pottery productions. On the one hand, **TRZ$_{(B)}$** is similar to **TRZ$_{(E)}$** because the major temper is composed by shell fragments and clay-stone. On the other hand, **TRZ$_{(D)}$** share some characteristics with TRZ156 from **AC**, because in both cases, temper is formed by big fragments of shell and quartz-arenite. Finally, TRZ085 from **TRZ1$_{(B)}$** contains shell fragments but other rocks fragments are also frequents. All of them are compatibles with the petrographic composition identified in the common wares analysed from ***Termez***.

Following these results, is clear that potters have manipulated paste composition, adding coarse shell fragments into the fine iron rich clay paste, to obtain cooking wares with specific functional properties. Using this technological modification, potters made these pots more suitable for cooking, because coarse non plastic tempering offers high resistance to thermal stress and heat impact. Thermal stress appears when there is an inhomogeneous expansion of paste which occurs when components as added temper or other mineral inclusions have significantly grater expansion rates than the clay matrix. Shells are mainly consist of the mineral aragonite which, when heated up to about 500ºC, alters irreversibly to calcite. Calcite formed from shell-temper has a similar thermal expansion coefficient to that of the fired clay, thus when it is heated the amount of thermal stress within the pot is negligible. For this reason, shell-tempe-

ring raises the resistance to thermal stress (Rye, 1976; Steponaitis, 1984; Tite *et al*., 2001). Other studies have pointed out that limestone has a similar thermal expansion coefficient as shell and both help to reduce stresses and crack initiation and propagation during thermal shock (Hoard *et al.*, 1995).

Furthermore, in this pots shell particles tend to be coarse. Coarser they are bigger is the resistance to thermal-shock. Thermal shock is another kind of temperature-related stress. Thermal-shock occurs when a body is suddenly heated or cooled down. Generally, ceramics are relatively slow conductors of heat. When a cooking pot is placed over a fire, its external surface heats up more rapidly than the inner surface and the difference in thermal expansion between these two surfaces produces stress. The same process occurs when a heated pot is suddenly cooled down. The ability of a ceramic body to withstand thermal shock depends mainly on the size, shape, frequency and distribution of the pores and non plastic inclusions within the paste. Past studies showed as thermal-shock resistance is increased by adding temper as coarse as possible (Steponaitis, 1984). In our case, the shell-temper of these three individuals where it can be seen is quite coarse and oriented parallel to the vessel's surface. In that way, when failure appears, temper particles stop the crack propagation, leading to a high toughness.

On the contrary, 6 cooking wares correspond to fabrics without calcareous tempering (**$TRZ_{(A)}$**, **$TRZ1_{(C)}$**, **$TRZ1_{(D)}$**, **$KPT_{(A)}$** and **ZT**) and TRZ235 from Kampyr Tepe contains few microfossils being though similar to cooking wares without calcareous shell inclusions. From the above mentioned group, it is evident that **$TRZ_{(A)}$**, **$TRZ1_{(C)}$** , **$TRZ1_{(D)}$** and **$KPT_{(A)}$** fabrics are closely related in petrographical terms and differences among them are mainly related to the frequency and grain size on the inclusions. Between these fabrics we can observe than cooking wares from **$TRZ_{(A)}$** fabric are similar to the wares from **$TRZ1_{(D)}$**. Both contain few non plastic grains, generally sub-rounded, which grain size is always inferior to 500µm. The predominant inclusions are granitic rocks and crystals detached of these rocks, as quartz, plagioclase, k-feldspars, amphiboles and mica-muscovite. Metamorphic rock as quartz-mica schist is frequent whereas only few sandstone and chert have been identified. Other few isolated minerals are epidotes and opaques. Both coocking wares from ***Kampyr Tepe*** (TRZ233 from **$KPT_{(A)}$** and TRZ235, classified as a loner sample), present a similar mineralogical composition although frequent mica schist is also present. Furthermore, both cooking wares contain abundant rock fragment inclusions but their grain size is bigger in TRZ233. The non plastic inclusions found in fabric **$TRZ_{(C)}$** are compatible with the mineralogical composition of fabrics mentioned above. Nevertheless, grain size of non plastic inclusions is still bigger and quartz-mica schist grains become the main temper together with quartz, plagioclase and frequent mica-muscovite lames. Finally, the cooking ware TRZ272 from ***Zar Tepe*** exhibit clear differences in coarseness terms but temper seems to share the same local origin. In TRZ272, inclusions are more abundant and grain size arises 1.5mm. Granitic rocks and crystals detached become the predominant non plastic inclusions whereas sandstone and nodules of micritic calcite are frequent. Few grains of quartzite and quartz-mica schist are also present.

Common wares can be divided in three different sub-categories regarding the coarse fracture size. On the one hand, a medium coarse fabric is represented by the painted common ware TRZ084 from RC grid of ***Tchinguiz Tepe*** bellowing to **$TRZ_{(C)}$**, which shears some mineralogical characteristics with the cooking wares integrated in fabric **$TRZ_{(A)}$**. TRZ084 contains as predominant non plastic inclusions fragments of granitic rocks and crystals detached of these rocks as quartz, plagioclase, k-feldspars, amphiboles and mica-muscovite. Other frequent rocks are quartz-mica schist whereas sandstones and cherts appear as accessory rocks. Another medium coarse fabric is represented by the over-fired loner TZR067 from ***Tchinguiz Tepe***. However, firing process at very high temperature has altered the microstructure and the structure of rock fragments but frequents quartz and plagioclase grains can be observed together with few sandstones.

From the samples examined by thin section analysis, 19 common wares are represented by medium-fine fabric, which coarse fraction is charcterised by few inclusions with a grain size between 100-600µm (fabrics **KT-K2**, **TRZ1$_{(A)}$** and loners TRZ020, TRZ060, TRZ068, TRZ098, TRZ112, TRZ114, TRZ123 and TRZ142). All these wares are closely related in a petrographic point of view and differences are mainly related to the nature of the micromass and the presence/absence of microfossils on the clay. In this sense, from the 18 common wares, 8 present shell fragments or microfossils as part of the non plastic inclusions (fabric **KT-K2** and loners TRZ068, TRZ098, TRZ112 and TRZ114). Only in TRZ098 and TRZ114, the microfossils are frequents that indicates the use of marine sediments for paste preparation. In TRZ098 and the individuals included within **KT-K2** petrographic fabric, the process of clay mixing is evident and it appears as clots of calcareous clay mixed with red clay. However, the main non plastic inclusions are generally very similar to the ones identified by thin section in other fabrics of common wares.

The rest of the common wares corresponding to a medium-fine fabric don't contain any of these calcareous components. Seven of them (TRZ065, TRZ076, TRZ126, TRZ132, TRZ133, TRZ138 and TRZ143) are grouped in **TRZ1$_{(A)}$** fabric, characterised by a yellowish-brown micro-mass with granitic rocks and derived minerals as predominant non plastic inclusions. Quartz-mica schist fragments are also frequent together with few cherts and nodules of micritic calcite. Another common ware, from Kiln 2 of Kara Tepe (TRZ020), presents a similar mineralogical composition but chert grains are more frequent. Finally, quartz fragments and mica-muscovite lames are the most predominant inclusions in chemical out-layers such as TRZ123 from the ***Kiln 1 of Kara Tepe***, TRZ142 from the ***Monasterie*** and the TRZ060 from RC grid of ***Tchinguiz Tepe***. The micromass in all of them is richer in iron oxides and quartz-mica schist and plagioclase are frequent too. This medium-fine fabric is also represented by a chemical outlayer from ***Kiln 2 of Kara Tepe*** (TRZ041) which petrographic composition is very similar to the previously mentioned samples but it presents a major frequency of non plastic inclusions.

Finally, one common ware, TRZ127 from the ***Kiln 1 of Kara Tepe***, is characterised by a very fine fabric with few inclusions of a maximum 400µm long at axis dimension. Its micromass is heterogeneous, from yellowish to orange-brown which is an evidence of clay mixing, which appears as streaks or clots with clear boundaries of calcareous clay mixed with red clay. Non plastic inclusions are very rare and they are mainly quartz, plagioclase, mica-muscovite and opaques.

The non plastic inclusions identified in all thin-sections examined in this study are compatible with the range of geological deposits in the broader local area of Termez. Igneous rocks and some isolated minerals as quartz, plagioclase and k-feldspars are related to the hercinian basement together with metamorphic rocks as quartz-mica schist and mica schist. Other sedimentary rocks as quartz-arenite, siltstones and claystones are present in the geological filling of Surkhan Darya depression, formed during Mesozoic and Cenozoic. Finally, calcareous sedimentary rocks with shell fragments are characteristics from the Lower Cretaceous of this geological area.

With regard to technological aspects, the majority of the studied pots reflect a precision and sophistication in the choice, acquiring and manipulation of raw materials. Most of them are fabricated with local/regional raw materials. The addition of shell fragments in the case of the cooking wares is absolutely justified to optimize the functional utilities required in the use of these wears. At the same way, the use of medium-fine or fine pastes in the case of common wares and coarse or medium-coarse pastes in the case of cooking wares answer to the same principle of functional requirements.

References

ABDURAZAKOV, A. A., 1987, "Khimicheskie sostavy keramiki i glazurej arkhitekturnykh pamjatnikov, Uzbekistana", *IMKU* 21.

ABDURAZAKOV, A. A., 1988, "Khimicheskie sostavy rannesrednevekovykh stekol Srednej Azii", *IMKU* 22, pp. 205-211.

ABDURAZAKOV, A. A., 1996, "Khimicheskie sostavy srednevekovykh stekol Kara-tepe (X-nachalo XIII v.)" in : *Kara-tepe VI*, pp. 301-306.

ABDURAZAKOV, A. A., BEZBORODOV, M. A., ZADNEPROVSKIJ, JU. A., 1963, *Steklodelie Srednej Azii v drevnosti i srednevekov'e*, Tashkent, IAN UzSSR.

ABDOURAZAKOV, A., 2001, "La production artisanale en Bactriane-Tokharestan. Résultat des études chimiques et des restaurations", in : *La Bactriane au carrefour des routes et des civilisations de l'Asie centrale*, pp. 399-403.

ABDURAZAKOV, A. A., DZHALALOVA, S., 1986, "Issledovanie khimicheskikh sostavov drevnej bytovoj keramiki juga Uzbekistana", *IMKU* 20, pp. 205-210.

AITCHISON, J., 1986, *The Statistical Analysis of Compositional Data*, Chapman and Hall, London.

AITCHISON, J., 1992, On Criteria for Measures of Compositional Difference, *Mathematical Geology*, 24, pp. 365-379.

ARIÑO, E., SALA, R., LAFUENTE M., GURT, J.M., PIDAEV, SH., STRIDE, S., 2007, The ceramic kilns of Kara Tepe, in J.M. Gurt, Sh. Pidaev, A.M. Rauret and S. Stride (eds.), IPAEB 2006,*Preliminary Report of the First Season work of the International Pluridisciplinary Archaeological Expedition to Bactria*, vol. 1, pp. 13-44.

BUXEDA I GARRIGÓS, J., 1995, *La caracterització arqueomètrica de la ceràmica de Terra Sigillata Hispanica Avançada de la ciutat romana de Clunia i la seva contrastació amb la Terra Sigillata Hispanica d'un centre productor contemporani, el taller d'Abella*, Col·lecció de Tesis Doctorals Microfitxades, 2524, Universitat de Barcelona, Barcelona.

BUXEDA I GARRIGÓS, J. 1999b Problemas en torno a la variación composicional, en J. Capel Martínez (ed.), *Arqueometría y arqueología*, Monográfica de Arte y Arqueología, 47, Universidad de Granada. Granada. pp. 305-322.

BUXEDA I GARRIGÓS, J., CAU ONTIVEROS, M. A., 1997, Caracterización arqueométrica de las ánforas T-8.1.3.1del taller púnico FE-31 (Eivissa), in J. Ramon Torres (ed.), *FE-13*: *un taller alfarero de época púnica en Ses Figueretes (Eivissa)*, Treballs del Museu Arqueològic d'Eivissa i Formentera 39, Govern Balear, Conselleria d'Educació, Cultura i Esports, pp. 173-192.

BUXEDA I GARRIGÓS J., GURT ESPARRAGUERA, 1998, j., m., La caracterització arqueomètrica de les àmfores de Can Peixau (Badalona) i la seva aportació al coneixement de la producció Pascual 1 al territori de Baetulo, in *El Vi a l'Antiguitat, Economia, Producció i Comerç al Mediterrani Occidental (II Col·loqui d'Arqueologia Romana)*, Monografies Badalonines, 14, Museu de Badalona, Badalona, pp. 193-217.

BUXEDA I GARRIGÓS, J., KILIKOGLOU V., DAY P., M., 2001, Chemical and mineralogical alteration of ceramics from Late Bronze age kiln at Kommos, Crete: the effect on the formation of a Reference Group, *Archaeometry,* 43, pp. 349-371.

BUXEDA I GARRIGÓS, J., KILIKOGLOU, V., 2003, Total Variation as a Measure of Variability in Chemical Data Sets, in L. van Zelts (ed.), *Patterns and Process: a Festschrift in honour of Dr. Edward V. Sayre,* Smithsonian Center for Materials Research and Education, Suitland, Maryland, pp.185-198.

CAU ONTIVEROS, M. A., DAY, P. M., MONTANA, G., 2002, Secondary calcite in archaeological ceramics: evaluation of alteration and contamination processes by thin section study, in V. Kilikoglou, A. Hein and Y. Maniatis (eds.), *Modern trends in scientific studies on ancient ceramics,* BAR International Series 1011, Archaeopress, Oxford, pp. 9-18.

DAVIS, J.C., 1986, *Statistics and Data Analysis in Geology*, John Wiley & Sons, New York.

HEIN, A., TSOLAJIDOU,A., ILIOPOULOS, I., MONNSEN, H., BUXEDA I GARRIGÓS, J., MONTANA G, KILIKOGLOU, V., 2002, Standardisation of elemental analytical techniques applied to provenance studies of archaeolgoical ceramics an inter laboratory calibration study, *Analyst*, 127, pp. 542-553

HOARD, R.J., O'BRIEN, M.J., GHAZAVY KHORASGANY, M., GOPALARATNAM, V.S., 1995, "A materials-science approach to understanding limestone-tempered pottery from the Midwestern United States", *Journal of Archaeological Science*, 22, pp. 823-832.

LEMOINE C., MAILLE, E., POUPET P., BARRANDON, J. N. Y BORDERIE, B. 1981. Étude de quelques altérations de composition chimique des cerámiques en milieu marin et terrestre, *Revue d'Archéométrie,* Suppl. S, pp. 349-360.

MARTINEZ, V., TSANTINI E., GURT, J M., PIDAEV, S., 2008, Archaeometrical study of the ceramics coming from the archaeological site of Termez in Uzbekistan, in J.M. Gurt, S. Pidaev, A.M. Rauret and S. Stride (eds.), *IPAEB 2007, Preliminary Report of the work of the International Pluridisciplinary Archaeological Expedition to* Bactria, vol. 2, pp. 141-194.

MATHSOFT, 1999, *S-PLUS 2000. User's Guide*, Data Analysis Products Division, MathSoft, Seattle, Washington, USA.

PICON, M., 1973, *Introduction à l'étude tèchnique des céramiques sigillées de Lezoux,* Centre de Récherches sur les Téchniques Greco-Romaines, 2ª edició, Université de Dijon, Dijon.

PICON, M., 1984, Problèmes de détermination de l'origine des céramiques, in T. Hackens, M. Schvoerer (eds.), *Datation-caractérisation des céramiques anciennes Cours Intensif Européen (Bordeaux, Talence 1981), PACT Nº 10,* Paris, pp. 425-433.

RYE, O.S., 1976, "Keeping your temper under control", *Archaeology and Physical Anthropology in Oceania*, 11, pp. 106-137.

SEGEBADE, C. Y LUTZ, G. J. 1980. Photon activation analysis of ancient Roman pottery, in E. A. Slater and J. O. Tate (eds.), *Proceedings of the 16th International Symposium on Archaeometry and Archaeological Prospection (Edinburg, 1976)*, National Museum of Antiquities of Scotland, pp. 20-29.

SCHMITT, A. 1989. *Méthodes géochimiques, pétrographiques, et mineralogiques appliquées à la détermination de l'origine des céramiques archéologiques.* Thèse de Doctorat, Université de Bordeaux III, Bordeaux.

SCHWEDT, A., MOMMSEN, H., ZACHARIAS, N., BUXEDA, J., 2006, Analcime crystallization and compositional profiles-comparing approaches to detect post-depositional alterations in archaeological pottery, *Archaeometry*, 48, 2, pp. 237-251.

STRIDE, S., 2005, Géographie archéologique de la province du Surcan Darya (Ouzbékistan du sud/Bactriane du nord). Tesis Doctoral, Sorbonne, Paris.

TSANTINI, E., 2007*, Estudi de la producció i la distribució d'àmfores ibèriques en el NE peninsular a través de la seva caracterització arqueomètrica***,** Tesis Doctoral, Josep Maria Gurt i Esparraguera i Jaume Buxeda i Garrigós (Directors), Universitat de Barcelona, Barcelona.

Report on Radiocarbon Dating

Joan S. Mestres i Torres, Anna Maria Rauret

In order to proceed with the dating, the Radiocarbon Dating Laboratory of the University of Barcelona received one sample of material identified as wood and two samples of carbonaceous material from the archaeological fieldwork at the Termez site (Uzbekistan). Below is a report identifying the materials and their nature.

TCH-T 1	identified as wood
TCH-T 2	Carbonaceous material
TCH-T 3	Carbonaceous material

1. DESCRIPTION AND TREATMENT OF RECEIVED MATERIALS

The material identified as wood was composed of a powdery light-brown mass that contained friable clods and non-friable fibrous fragments. Clods and fragments presented the same colour as the overall mass and did not surpass a maximum of 12 mm in size. The identical colour of all the constituent materials would appear to indicate that the received material is the product of the disintegration of a single original material. The first sample of carbonaceous material included a fragment of rectangular charcoal measuring 14x8 mm and another triangular fragment with a base of 11 mm and a height of 13 cm. The fragments were accompanied by soil containing tiny fragments of charcoal. The two coal fragments were found covered by a chalky, earthen coating. The second carbonaceous sample was composed of charcoal fragments of varying sizes, which did not exceed a maximum of 28 mm, accompanied by carbonaceous soil. The amount of material received in each sample is indicated in the second column of Table I.

The materials for dating were subjected to a treatment that has two purposes. The first aim is to eliminate contamination by any foreign components produced by chemical compounds of indefinite age from the exterior environment, and to remove any potential contamination from its manipulation after extraction of the material. The second purpose is to isolate with the greatest possible integrity the constituent most representative of the age of the material to be dated.

The material identified as wood was passed through sieves of 2, 1 and 0.5 mm and the granulometric fraction less than 0.5 mm was discarded. The useful material that remained is indicated in the third column of Table I. Then the granulometric fraction greater than 2 mm (Fr/gr 1) was ground to a granulometry of less than 0.5 mm. In order to separate out the water-soluble fraction, the ground material was suspended in water and boiled for ten minutes. The material was then treated with hydrochloric acid at room temperature to eliminate the carbonates. Finally, the residue of the previous treatment was subjected to treatment with 1.2 m hydrochloric acid at 90ºC for twenty hours in order to eliminate resins and sugars. The residue of the acid treatment was then treated for a further 20 hours with 0.25 m sodium hydroxide at 50ºC in order to eliminate tannic acids and any other possible biogenic organic material acquired during the period in which the material served its function. Lastly, the residue of the alkaline treatment, which is composed basically of cellulose and lignin, was treated with sodium chloride in order to eliminate the lignin by oxidation and extract the cellulose from the wood. The final treatment failed to produce the expected cellulose. Instead, in its place, there was a light-grey residue that looked mineral. It did, however, contain a small proportion of organic matter. In order to increase the

amount of organic matter recovered, the granulometric fraction less than 2 mm and greater than 0.5 mm (Fr/gr II) was subjected to the same chemical treatment as the fraction of larger granulometry, but without extracting the cellulose. The combustion of the residue from the alkaline extraction (see Section 3) revealed that the carbon content of the fraction was still insufficient for an acceptably precise dating. In order to obtain more material for dating, use was made of the alkaline extractions from the two granulometric fractions recovered by acidification. The different fractions of purified material are shown in the fourth column of Table I.

Table I. Treatment of materials

Identification of material	Original material (g)	Cleaned material (g)	Purified material (g)	Yield of purified material (g)
TCH-T 1	488,3	Fr/gr I: 126,3 Fr/gr II: 130,1	Alkaline-extraction residues: 89,082 Alkaline extractions: 8,239	--
TCH-T 2	3,609	2,317	0,393	17,0
TCH-T 3	5,763	2,241	1,420	63,4

From the first sample of carbonaceous material, the two largest fragments were separated and the chalking coating was removed with a brush. The cleaned charcoal fragments were fragmented along their natural grain in order to find and eliminate any possible intrusions of foreign material in their interior. The remaining material was passed through sieves of 1 and 0.5 mm and the granulometric fraction less than 0.5 mm was discarded because it contained no charcoal. From the granulometric fractions Ø > 1 mm and 0.5 mm < Ø < 1 mm, the small fragments of charcoal were then manually separated out with the aid of tweezers and added to the large fragments. Lastly, the cleaned charcoal obtained—the weight is indicated in the fourth column of Table I—was ground into dust. .

The second sample of carbonaceous material was passed through a sieve of 0.5 mm and the lesser granulometric fraction was discarded because it contained no charcoal. Insofar as their size permitted, the fragments of charcoal in the greater granulometric fraction were cleaned on their surface with a fine brush. Then they were fragmented along their grains in order to find and eliminate the intrusion of any foreign elements in their interior. Lastly, the cleaned charcoal recovered—its weight is indicated in the fourth column of Table I—was ground into a dust.

The two samples of pulverized charcoal were treated with 2 m hydrochloric acid at 95ºC for twenty hours in order to eliminate carbonates from water circulation and/or soil and from the fraction of water-soluble material. In order to eliminate any possible humic acids from the soil's vegetation cover, the insoluble residues from the acid treatment were suspended in water and treated with successive additions of 1 m ammonia at room temperature until the suspension was high enough to ensure the complete elimination of acid substances. Lastly, the residues resulting from this treatment were boiled in 0.4 m hydrochloric acid in order to eliminate carbonates of atmospheric origin. In this way, we obtained a residue of purified charcoal containing no carbonates or humic acids, which would then be apt for dating. The weight of purified residue is indicated in the fourth column of Table I.

2. PREPARATION OF ACTIVITY MEASUREMENT: BENZENE SYNTHESIS

Because the radiocarbon content of cellulose cannot be measured directly, the cellulose is transformed into an adequate chemical compound to conduct the appropriate activity measurement at ^{14}C per liquid scintillation. The chemical procedure used to prepare the chemical compound involved, namely benzene, is described below.

The residue from the alkaline treatment of material identified as wood was burnt in a combustion tube under oxygen flow. As the amount of carbon dioxide obtained was insufficient for precise dating, the alkaline extraction was also burnt in a combustion pump under oxygen pressure. Then the carbon dioxide obtained from the different fractions was added together.

The amount of purified charcoal recovered from the first sample of carbonaceous material to too small to carry out the radiometric measurement of ^{14}C content with acceptable precision. As a result, it was sent to the National Accelerators Centre in Seville to carry out measurement of the sample using accelerator mass spectroscopy (AMS) with a particle accelerator.

The purified charcoal from the second sample of carbonaceous material was burnt in a combustion pump under oxygen pressure. The carbon dioxide from combustion, which was conveniently purified and dry, was set aside for three weeks to wait for the radioactive decay of any ^{222}Rn that might accompany it. At the conclusion of the three-week wait, measurements were taken of the material's isotopic abundance of ^{13}C using mass spectroscopy on a small sample of carbon dioxide. Then, the remaining carbon dioxide was reduced with metallic lithium to form lithium carbide, which was hydrolysed to acetylene using relatively tritium-poor water. Finally, the acetylene was catalytically trimerised to benzene (MESTRES et al., 1991).

3. RADIOMETRIC MEASUREMENTS

In order to measure the radioactivity of the benzene containing the carbon present in the material to be dated, the quantity obtained is—if less than 5.2 ml—diluted gravimetrically with inactive benzene of analytic reagent grade to 5.2 ml. With the mix or directly using the benzene obtained from synthesis, solutions are prepared to measure activity by weighing out 5,000 ml which are added to glass vials of low potassium content along with adequate amounts of the scintillators Bu-PBD and Bis-MSB in solid form and previously weighed.

Oxalic acid II, which was supplied by the National Institute of Standards and Technology (USA), served as the standard reference substance for the activity measurement. It was overfired in carbon dioxide with a potassium permanganate solution and then transformed into benzene in the same manner as the other samples (*loc. cit.*). The preparation of the solution for the initial measurement of activity was also conducted in the same manner as the other samples. .

The baseline value for each vial was determined by measuring two reference blanks prepared identically as the samples, but using inactive benzene for the measuring solution.

The sample, two standards of initial activity and two reference blanks for the baseline value were each counted over a fifty-hour period, divided into fifty-minute intervals, in a liquid scintillation counter LKB Wallace 1217 Rackbeta. The efficiency of the measurement for each interval was determined using an efficiency calibration curve as a function of extinction. The calibration curve had been previously established from activity standards prepared in our laboratory (*loc. cit.*).

4. RESULTS AND DISCUSSION

Table II shows the results from measuring the isotopic abundance of ^{13}C ($\delta^{13}C$) and the results from counting and measuring radioactivity, along with their uncertainty expressed as 1x the standard deviation (loc. cit). As can be seen, the measured value of the isotopic abundance of ^{13}C for the sample is the normal value for charcoal, between –23 and –27‰ (STUIVER AND POLACH, 1977).

TABLE II
Results from the radiometric measurements

Sample	($\delta^{13}C$)	Measured quantity of benzene	Count estimation	Background	Net count estimation	Count efficiency	Normalized count estimation of benzene, sample A_5N	Normalized Count Estimation of Benzé, standard A_0N
	(‰)	(g)	(cpm)	(cpm)	(cpm)	(%)	(cpm/g)	(cpm/g)
TCH-T1	-32,481	0,57032	5,044±0,054	2,966±0,043	2,078±0,069	72,880±0,018	5,08±0,17	10,632±0,028
TCH-T3	-24,026	0,64387	6,922±0,043	2,996±0,043	3,927±0,061	72,856±0,024	8,35±0,13	10,632±0,028

Calculation of the radiocarbon age is based on the experimental results shown in Table II, using the following equation:

$$R = \frac{T_{1/2}}{\ln 2} \times \ln \frac{D_{0N}}{D_{SN}} \qquad (T_{½} = 5568 \text{ years})$$

where D_{0N} and D_{SN} represent the initial and residual content, respectively, of ^{14}C in the dated material, corrected by isotopic fractionation of ^{14}C and measured radiometrically or using AMS.

Applying the equation above to the results of the measurement enables calculation of the radiocarbon date. The result of dating(1) and the date code, assigned by the Laboratory, are indicated below:

Termez	
TCH-T 1	**5940 ±270 BP**
TCH-T 2	**2130 ± 45 BP**
TCH-T 3	**1940 ±130 BP**

The present results can reliably pertain only to the received samples.

The sample of presumed wood has produced an exaggeratedly high result for the archaeological context under study. As a result, it suggests that the material or rather the chemical fraction of it to be dated is not representative of the archaeological event intended for dating. As the archaeological association lies beyond all doubt, the aberrant date obtained must arise from an error in synchrony. To explain the error, two hypotheses may be entertained: firstly, the construction of the fortification wall may have made use of material already ancient at that time; or, secondly, the conservation of the wood may have been so deteriorated as to have practically disappeared (the uniformity of the fortification wall material and the absence of cellulose support this hypothesis), with the consequence that the chemical treatment eliminated the sparse wood remains and that the material to be dated was, in reality, allochthonous organic matter associated with the brick or clay itself. Support for the second hypothesis arises in the abnormally low value of the $^{13}C/^{12}C$ isotopic ratio (see column **$\delta^{13}C$** in Table II). The value more closely resembles humus than wood, for which an approximate value of -25‰ should be expected. Given that the dating of the presumed wood is not representative of the archaeological context, the result is offered not as a common radiocarbon date, but only for informational purposes, as the outcome of a chemical and radiometric experimental process. For this reason, the usual UBAR code has not been assigned.

5. CALIBRATION OF THE RADIOCARBON DATA OBTAINED AND EVALUATION OF THE RESULT

Radiocarbon dating is based on a fundamental hypothesis which supposes that the specific radiocarbon content present in materials suitable for dating remains constant over time. This hypothesis is not entirely correct, because there have been fluctuations in the content. As a result, ages calculated on the basis of the hypothesis are conventional in nature. They deviate with respect to ages expressed on the solar time scale and they define what has been labelled the radiocarbon time scale. Measuring the radiocarbon age of tree rings whose age has been ascertained through dendrochronology, a curve has been established, which currently spans the last 12,400 years (REIMER *et al*., 2004). The curve, which is called the calibration curve, relates the conventional radiocarbon age to the age expressed on the solar time scale. It is not flat and it does not establish a one-to-one relation between the radiocarbon time scale and the solar time scale. In fact, more than one solar date may correspond to each radiocarbon date.

Because of the non-linear character and the complexity of the calibration curve, the probability distribution of the true calibrated date around the experimental calibrated date is not normal, as it is in the case of the probability distribution of the true radiocarbon date around the experimental radiocarbon date. The probability distribution of the true calibrated date is asymmetric and complex and it presents distinct modes around which one or more probability intervals can be defined. The sum of the intervals is equal to a probability of 68.3% or 95.4% (STUIVER AND REIMER, 1993). The two values are chosen by analogy to the probability distribution of the radiocarbon date and they correspond to the probability that the true radiocarbon date falls within an interval of time which, centring on the experimental radiocarbon date, has a width equivalent to two or fourth times the standard deviation, respectively.

Table III shows the results from calibrating the radiocarbon dates. Each column of the table is described in greater detail below:

Columns A and B: Sample reference and radiocarbon date code assigned by the Laboratory, respectively.

Column C: Radiocarbon date with uncertainty expressed in terms of standard deviation.

Column D: Calibrated experimental date(2) corresponding to the intersection of the experimental radiocarbon date and the calibration curve. It corresponds to the maximum mode of the probability distribution for the calibrated date.

Columns E and F: Intervals of calibrated date(2) looking at the modes of the probability distribution for the true calibrated date, corresponding to a total probability of 68.3% and probability, and the associated probability at each interval, respectively.

Columns G and H: Intervals of the calibrated date(2) looking at the modes of the probability distribution for the true calibrated date, corresponding to a total probability of 95.4%, and the associated probability at each interval, respectively.

TABLE III

Calibration of radiocarbon dates

A	B	C	D	E	F	G	H
TCH-T 2	UBAR-989 CNA366	2130± 45 BP	cal BC 174	cal BC 343−324 cal BC 205− 91 cal BC 67− 63	7,3% 59,6% 1,4%	cal BC 356−285 cal BC 255−249 cal BC 234− 44	17,8% 0,5% 77,1%
TCH-T 3	UBAR-990	1940±130 BP	cal AD 69	cal BC 90−75 cal BC 55−cal AD 235	2,2% 66,1%	cal BC 350−315 cal BC 210−cal AD 390	1,4% 94,0%

Figure 1 shows the portion of the calibration curve involved in the calibration of the radiocarbon dates. This portion of the curve makes it possible to see the dates involved and the possible distortions of the radiocarbon time scale in the specific chronological region. It also illustrates the calculation of the experimental calibrated dates as the intersection of the experimental radiocarbon dates with the calibration curve.

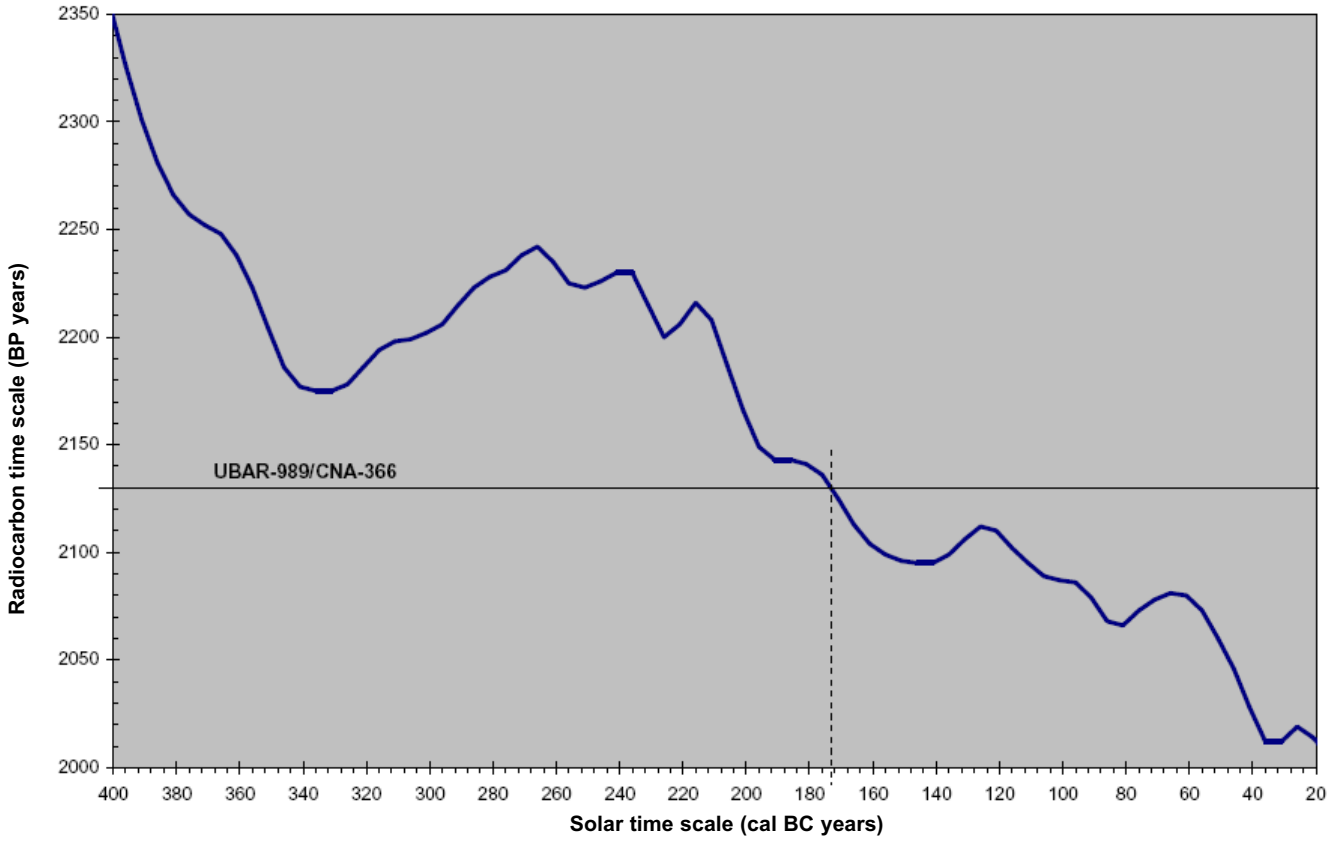

Figura 1A

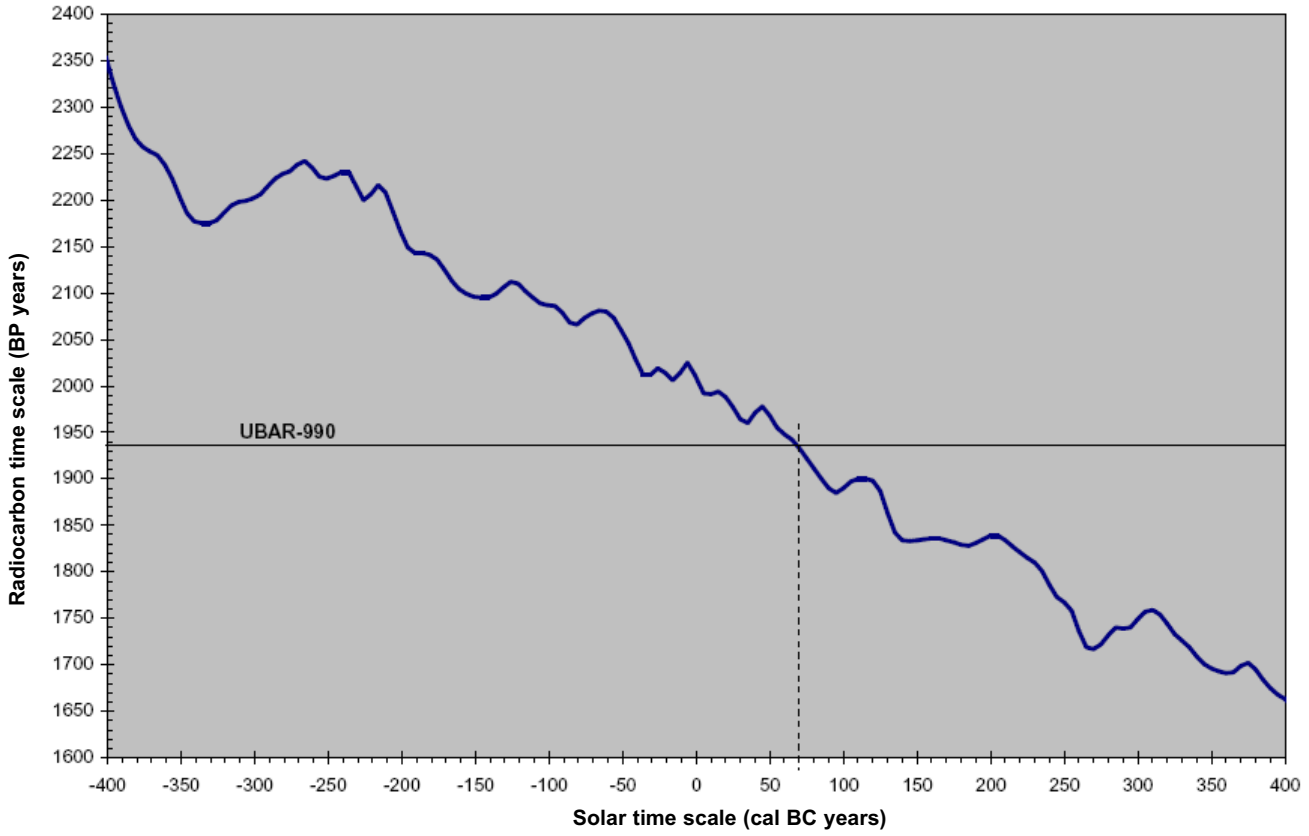

Figura 1B

Figure 2 shows the probability distribution of the true calibrated date and the intervals with the highest probability indicated in columns E and G of Table III.

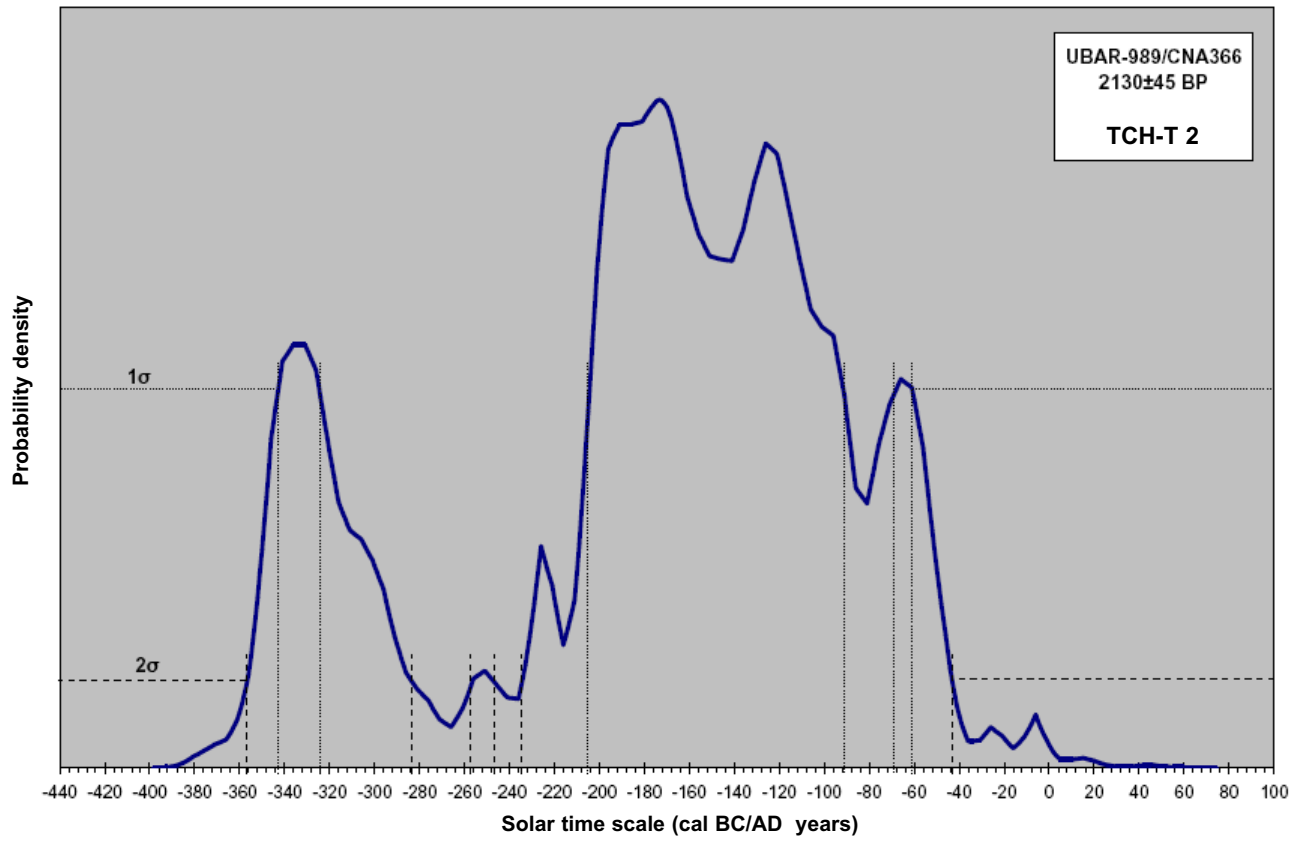

Figura 2A

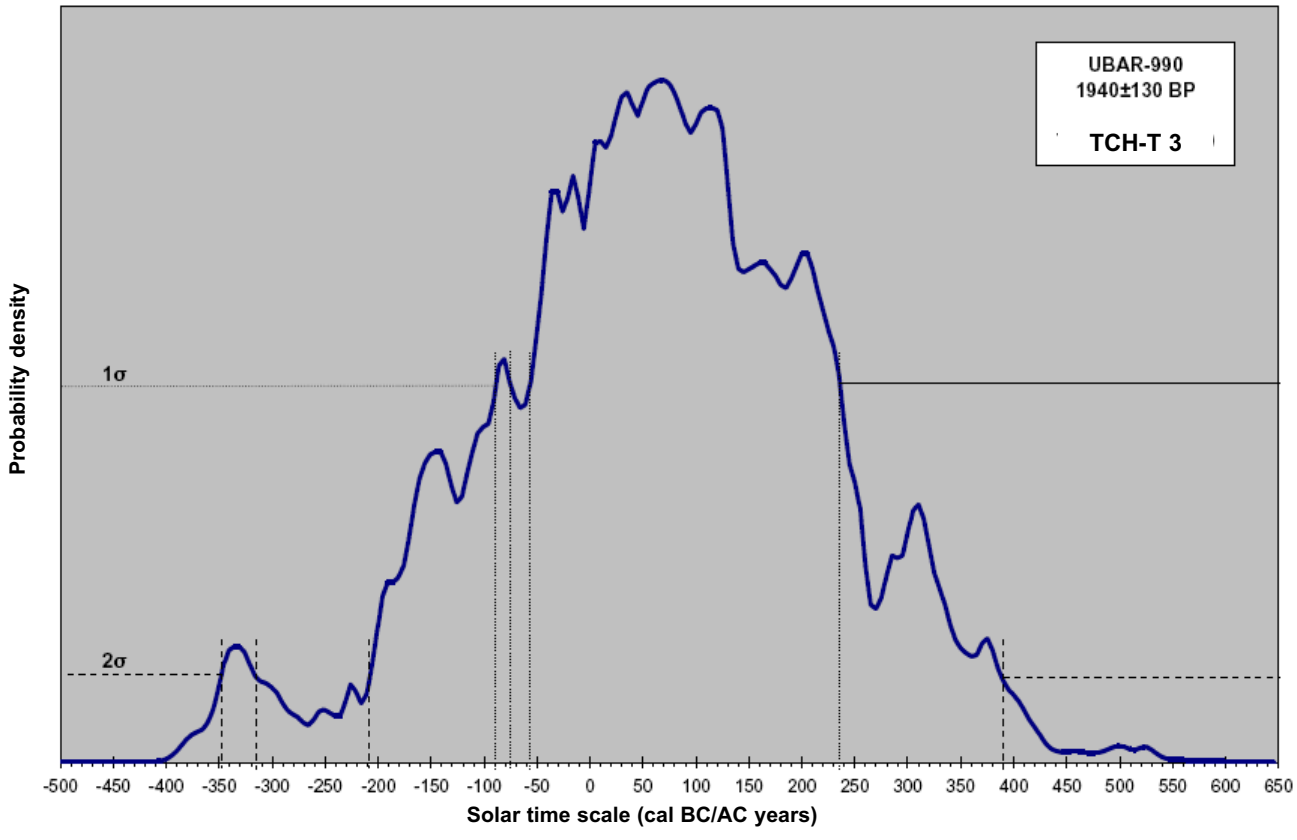

Figura 2B

Lastly, Figure 3 shows the curve of accumulated probability, enabling calculation of the probability that the true calibrated date is found in an interval of time as the difference between the corresponding coordinates at the interval end-points.

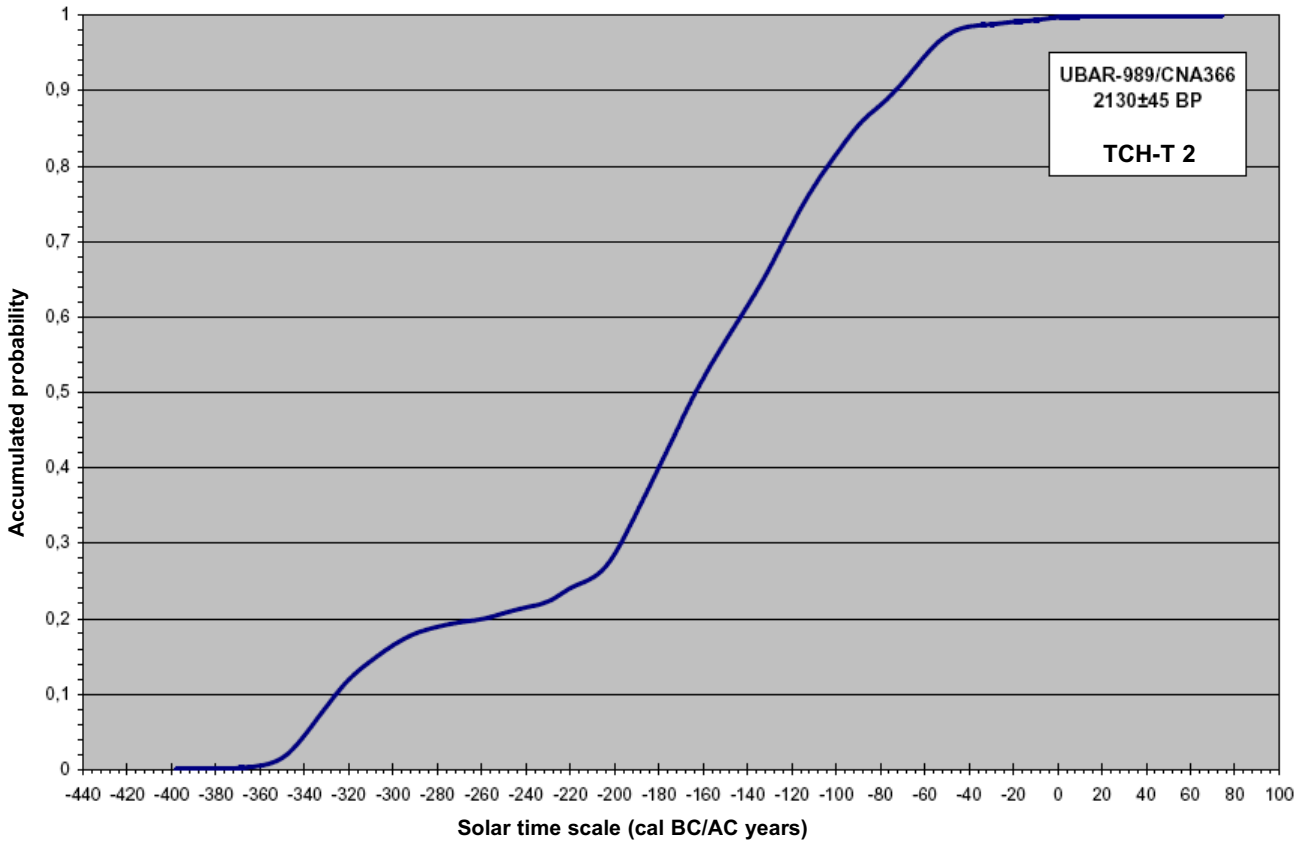

Figura 3A

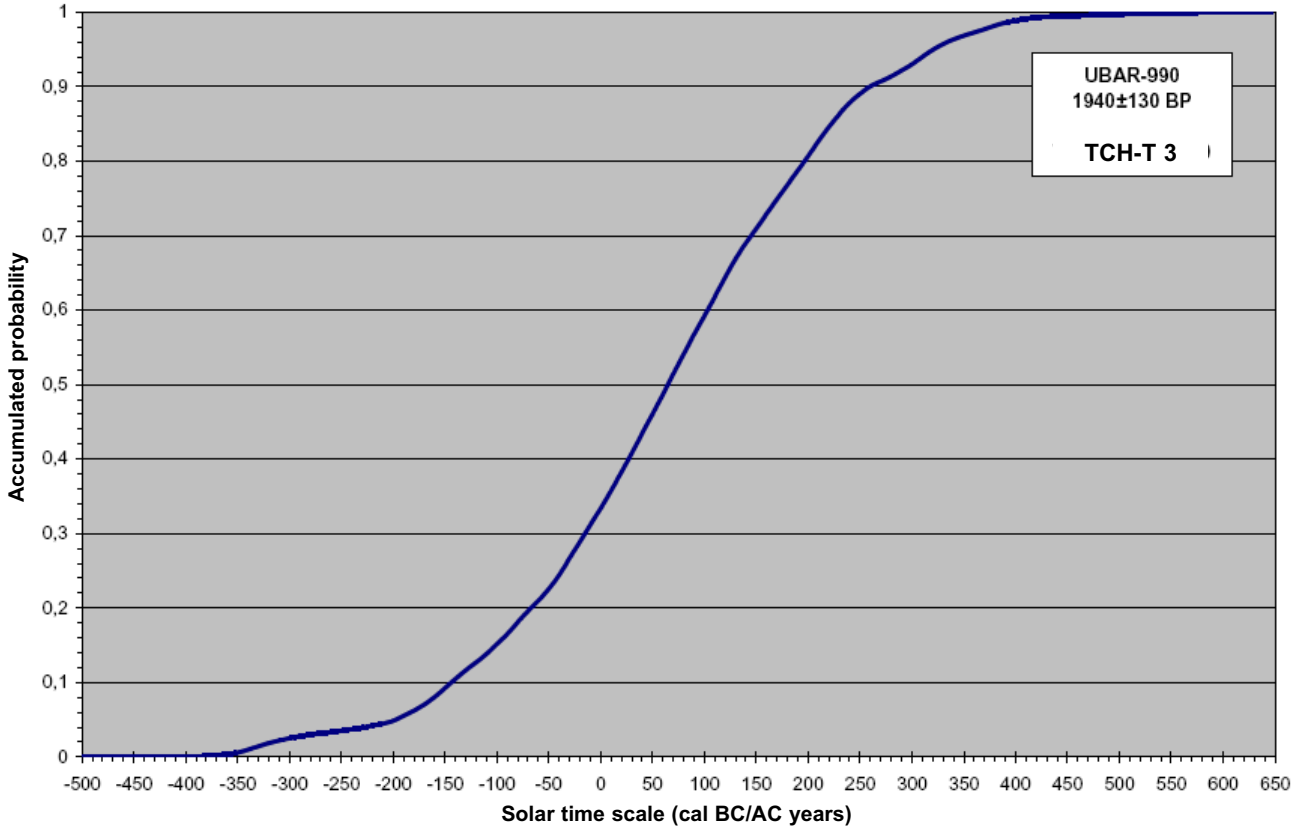

Figura 3B

6. DISCUSSION OF RESULTS

The Dating Laboratory would like to offer a reminder that radiocarbon dating by its very nature establishes the dates for the formation of materials and not the archaeological events in which the materials are used. A measured experimental date is an approximation to a physical date (MESTRES, 2000a, 2000b, 2003; MARTÍN AND MESTRES, 2002), which refers in the case of charcoal dating to the moment when the plant tissues were formed in the material later appearing as charcoal. In no case, however, does the physical date refer to an archaeological date, if by that is meant ascertaining the time when plant materials were transformed into charcoal or used in architectural structures or levels for which dating is desired. For the physical date to correspond to an archaeological date, recourse must be made to the requirements of association and synchrony (*loc. cit.*).

NOTES AND WORKS CITED

1. BP (before present): this is used to represent a date expressed on the radiocarbon time scale, taking the year 1950 AD as the starting point. It is always accompanied by an expression of uncertainty in terms of the standard deviation corresponding to the entire set of radiometric measurements.

2. The designation “cal years BC” (before Christ) is used to represent a calibrated date expressed in years BC, based on radiocarbon date.

3. The designation “cal years AD” (annus domini) is used to represent a calibrated date expressed in years AD, based on a radiocarbon date.

MARTÍN, A. I MESTRES, J.S., 2002: “Periodització des de la fi del Neolític fins a l’Edat del Bronze a la Catalunya Sudpirinenca. Cronologia relativa i absoluta”. Actes del XII Col·loqui Internacional d’Arqueologia de Puigcerdà: De la fin du Néolitique a l’Âge du Bronze entre l’Èbre et la Garonne, pp. 77-130. Puigcerdà, 2002.

MESTRES, J.S. (2000a): “La datació per Radiocarboni. Una visió actual” a *Tribuna d’Arqueologia* 1997-1998, pp. 195-239. Generalitat de Catalunya, Departament de Cultura. Barcelona.

MESTRES, J.S. (2000b): “Utilización inductiva y deductiva de las fechas radiocarbónicas. Ejemplo de aplicación a la prehistoria de la isla de Menorca (Baleares)” a *Contributos das Ciências e das Tecnologias para a Arqueologia da Península Ibérica*. Actas do 3º Congresso de Arqueologia Peninsular, Vol. IX, pp. 117-139. ADECAP, Porto (Portugal).

MESTRES, J.S., 2003: “La química i la cronologia: La datació per radiocarboni”. *Revista de la Societat Catalana de Química* 4, pp. 10-25.

MESTRES, J.S.; J.F. GARCÍA I G. RAURET, 1991: “The Radiocarbon Laboratory at the University of Barcelona”. *Radiocarbon* **31**(1), p. 23-34.

REIMER, P.J, G.L. BAILLIE, E. BARD, A. BAYLISS, J.W. BECK, C.J.H. BERTRAND, P.G. BLACKWELL, C.E. BUCK, G.S. BURR, K.B. CUTLER, P.E. DAMON, R.L. EDWARDS, R.G. FAIRBANKS, M. FRIEDERICH, T.P. GUILDERSON, A.G. HOGG, K.A. HUGHEN, B. KROMER, G. MCCORMAC, S. MANNING, C.B. RAMSEY, R.W. REIMER, S. REMMELE, J.R. SOUTHON, M. STUIVER, S. TALAMO, F.W. TAYLOR, J. VAN DER PLICHT I C.E. WEYHENMEYER. 2004: “IntCal04 Terrestrial Radiocarbon Age Calibration 0–26 cal kyr BP”. *Radiocarbon* **46**(3), pp. 1029-1058.

STUIVER, M. I H. POLACH, 1977: “Discussion: Reporting of ^{14}C Data”. *Radiocarbon* **19**(3), pp. 358

STUIVER, M. Y P. REIMER. 1993: “Extended Data Base and Revised CALIB 3.0 14C Age Calibration Program”. *Radiocarbon* **19**(1), pp 215-230.

Geomorphology of Tchinguiz Tepe and the valley of the Surkhan Darya (Uzbekistan)

Ana Sánchez del Corral

1.- INTRODUCTION

The archaeological site of Tchinguiz Tepe is located on the banks of the Amu Darya roughly eight km to the northwest of the city of Termez, near its confluence with the Surkhan Darya. Administratively, the valley is part of the province of the same name, which borders Tajikistan, Turkmenistan and Afghanistan. The Amu Darya serves as a natural frontier with Afghanistan. It is one of the great collectors of Central Asia and, along with the Syr Darya, one of the principal tributaries of the Aral Sea (fig. 1).

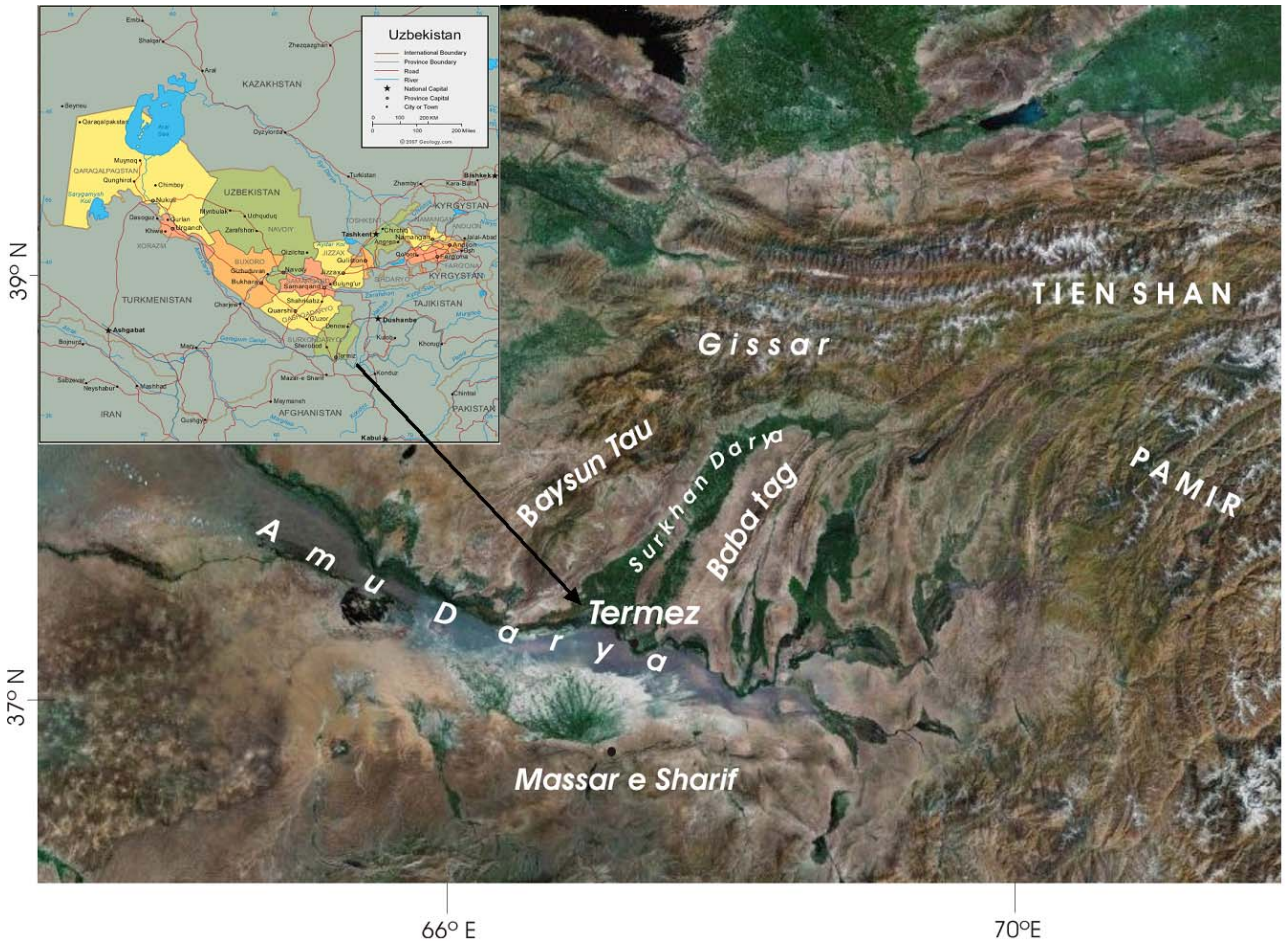

Fig. 1.- *Regional location of the work area. The satellite image (ACME) shows the valley of Surkhan Darya, which lies to the south of the Gissar range between the Baysun Tau and Baba Tag ranges. To the south of Amu Darya on the border with Afghanistan appears the alluvial megafan of Massar e Sharif.*

This paper is an initial contribution to the geomorphological analysis of arid environments in Central Asia in connection with geoarchaeology. The field work involved the general recognition of the terrain in order to provide data for the definition and interpretation of the units of relief in the archaeological zone and its surroundings (valley of the Surkhan Darya). The aim is to approximate the geomorphological context for the cultures whose remains are under investigation and to establish the erosion and sedimentary sequences that affect the site.

Use has been made of Soviet topographical cartography at various scales, including 1:100,000, 1:200,000, 1:500,000 and 1:1,000,000 (Gauss-Krüger projection, Pulkovo datum, Krassovskiy ellipsoid); maps at a scale of 1:250,000 produced by the Army Map Service (US Army 1952; Transverse Mercator Projection, European Datum, International Spheroid); and Russian geological maps at a scale of 1:200,000, J-4220 and J-4226.

The positioning of samples trenches, survey points and outline of the fortified enclosure of Tchinguiz Tepe was performed with a Garmin 300 GPS, which is precise to three metres.

The geographic location of the work area corresponds to an extreme continental climate. Average annual rainfall in Termez (310 m) is 140 mm, bringing the area into the FAO's category of arid land (rainfall< 200 mm/year). It can also be designated an arid desert (50/150 mm/year) with cold winters. Table 1 sets out the extreme nature of the temperatures in Termez.

Months	J	F	M	A	M	J	J	A	S	O	N	D
Ave.	4	6	11	18	25	29	30	28	22	16	10	6
High	11	12	17	26	33	38	40	38	32	25	19	12
Low	0	0	5	11	16	19	21	18	12	8	3	0
Rain	3	3	6	3	1	0	0	0	0	1	3	2
Snow	2	2	0	0	0	0	0	0	0	0	0	1

Table 1: *Temperature in Termez. Ave. = Average temperature; High = Average high temperature; Low = Average low temperature; Rain = Average number of days with rainfall; Snow= Average number of days with snowfall*

The wide range of annual and daily temperatures, which occurs as a result of the area's remoteness from large bodies of water, plays an important role in the area's geomorphological processes. Similarly, the duration of annual sunshine is high because of the area's latitude and scarcity of cloud cover. The Surkhan Darya region reflects sharp differences in altitude from the mountains to the alluvial plains, which translates into contrasting thermopluviometric systems. These systems constitute one of the topographical and climatic factors that influence the modelling of the valley's slopes.

The main pressure systems in these regions of Central Asia are the Mediterranean Low-pressure Cell and the Siberian High-pressure Cell, which control seasonal pressure and the swings in temperature and precipitation (Sorrel, 2006).

The general atmospheric circulation is affected by local climate boundaries: the Caucasus block the influence of low-pressure systems from the west or northwest and the high mountains ringing Central Asia to the south block the intrusion of southern air masses (India's monsoon system). According to Machallett et al (2008), summer is marked by a flow of high-altitude winds dominated by westerlies and thermal depressions producing turbulence all along the orographic barriers. In winter, low-pressure fronts are more common and act at the chief force driving aeolic transport force, which is predominant basically at high altitude to the extent that the sedimentation is a local and regional phenomenon.

This climate corresponds to a steppe biome, associated with flat areas that are marked by discontinuous plant cover and large areas where the substrate appears completely barren of vegetation.

2 THE VALLEY OF SURKHAN DARYA: GEOLOGY AND RELIEF

The valley of Surkhan Darya lies within the Afghan-Tajik depression. To the east rise the Pamir Mountains, separated from the valley by the Darwaz-Karabul fault zone. To the south stands the Hindu Kush, bounded by the Alburz faultline. The valley occupies a long structural depression running north-east to southwest at the foot of the Gissar-Zarafshanian mountain range (maximum altitude 4,425 m), broadly oriented from west to east and forming part the Tien Shan massif.

In this structural context, the Afghan-Tajik depression is organised in a series of blocks oriented NNE-SSW corresponding to a series of alternating depressions and mountain ranges. The large structures are normally defined by thrusts and asymmetric faulted folds with oblique-slip components that form a gradual arc northwards joining the Gissar Mountains (Thomas *et a*l. 1994) (fig. 2).

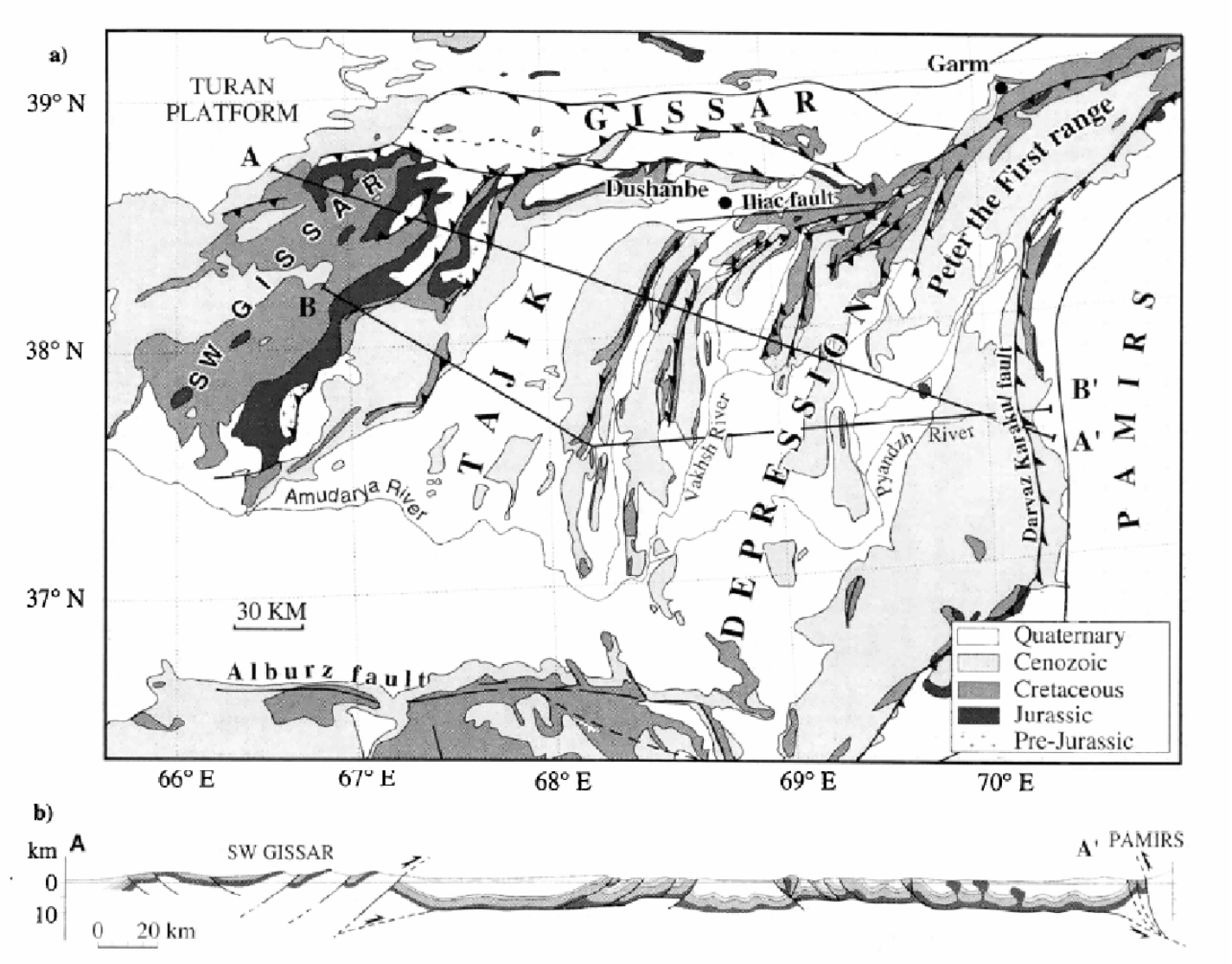

Figure 2. *Simplified geological diagram of the Tajik depression (Thomas at al. 1994)*

The structural mountain ranges (e.g., Baysun Tau and Baba Tag) are abruptly interrupted at the banks of the Amu Darya, which is the principal collector of the Afghan-Tajik Depression. In this stretch, the river runs generally west to east and flows through the southern sector of the depression, defined by the Alburz faultline. The Amu Darya continues its route to the Aral Sea through the Turanian platform, which serves regionally as the base surface of these vast orogenous structures.

The basin of the Surkhan Darya, the most westerly of the depressions, is considered a complex intramontane compression basin. Its Hercynian basement, reactivated during the Palaeogene and Neogene, is composed of metamorphic and crystalline rocks from the Baikal fold belt (Cambrian to Devonian) and can currently be found in the Gissar range, among other areas (Figs. 1 and 2).

The infill of the basin is formed by Mesozoic and Cenozoic sediments that underwent various deformations as a consequence of the indentation of the Pamir mountains into the Asian continent at the time of the collision between India and Asia (Coutand et al. 2002). Tectonic reactivations have been described at the edges of the depression during the Upper Miocene and Quaternary, giving rise to significant correlative sediments (Thomas et al. 1994). The cover, basically made up of sandstone, claystone and siltstone, is characterised by defined saline and anhydrite levels (Mesozoic-Cenozoic), related to halocynetic processes. (Yanbukhtin, 2008).

2.1 RELIEF AND LITHOSTRUCTURAL FACTORS

As indicated in figure 2, the Surkhan Darya valley is characterised by western mountains (*Baysun Tau*, 3,921 m), which are the chief concern of this paper; a central fluvial domain, and eastern mountains (*Baba Tag,* 2,290 m). The current course of the river lies somewhat off the valley's axis of symmetry, so that the fluvial domain on the right bank is twice as wide as the one on the left bank. The general lines of relief have a clear structural component, which is reflected in:

a) The organisation of the mountain systems into parallel ranges of decreasing altitude to the main river, coinciding broadly with anticlinal folds;

b) The outline of the drainage network, affected by transversal faults in the fold structures, derived from the observation of discontinuities and slips in the ranges and of the pattern of the drainage network exploiting these fractures; and

c) The disposition of a base surface or intramontane piedmont.

In the western mountains, the disposition of the relief enables differentiation of:

(1) An upper system in the highest areas of *Baysun Tau* and *Kugitantau*. It features outcroppings of Mesozoic materials from the Jurassic (Figs. 2 and 3). A wide synclinorium of Neogene sediments separates the system from the one immediately below.

(2) An intermediate system, immediately below, contains lithologies from the Cretaceous, Palaeogene and Neogene. The river *Sherabad* traverses the structure, passing through its periclinal closure (Figs. 3 and 4, section B-B'). Although it is of lesser height, it plays a key role in the control of alluvial fans.

(3) A lower system, which is more discontinuous and nearer the river, gives rise to several isolated relief structures on current fluvial and aeolic sediment. There are long hills such as *Gori Jaudag* (anticlinal structure of 553 m), *Gora Uch Kyzyl* (412 m) and *Tchinguiz Tepe* (325 m) (Figs. 3 and 4).

The three systems step down from the watershed to the river of the Surkhan Darya, gradually losing altitude towards the south. They end in the Amu Darya, to the south of which lies the northern desert of Afghanistan which reaches the Alburz faultline farther south.

According to the Soviet geological maps at a scale of 1:200.000 (numbers J-4220 and J-4226) and field observations, the lithostratigraphy of the area (table 2) can be differentiated as follows:

- Materials from the Upper Cretaceous, basically red and grey sandstone alternating with green-grey claystone and limestone with shells. Outcroppings arise from erosion of the higher series in the anticlinal structure to the north of Sherabad (*Krebet Kingata* and *Gori Besh Kyz*). The Upper Cretaceous contains claystone, sandstone, marlstone, siltstone, limestone and gypsum.
- The Palaeocene-Eocene contains sediments of marine phases. The lowest levels contain limestone, dolomite and gypsum, while the highest levels contain claystone, siltstone, sandstone, limestone and marlstone.
- In the Oligocene and Neogene, the phases become deltaic and alluvial (Bourgeois et al. 1997): greyish-blue and red sandstone, siltstone and claystone; red and ochre sandstone, reddish-brown

siltstone and claystone. Levels higher than the Neogene contain detritic rocks made up of thicker fragments. Sandstone becomes more common, always in the presence of siltstone and claystone. In the Pliocene, siltstone, claystone and sandstone are joined by conglomerates and gravels in sequences of considerable potential. This could be related to the reactivations at the mountain edges of the depression. Palaeogene and Neogene form asymmetrical outcroppings in the flanks of the anticlinal structures due to the tectonic deformations related to faults and thrusts (fig. 3 and fig. 4 section A-A' and B-B').

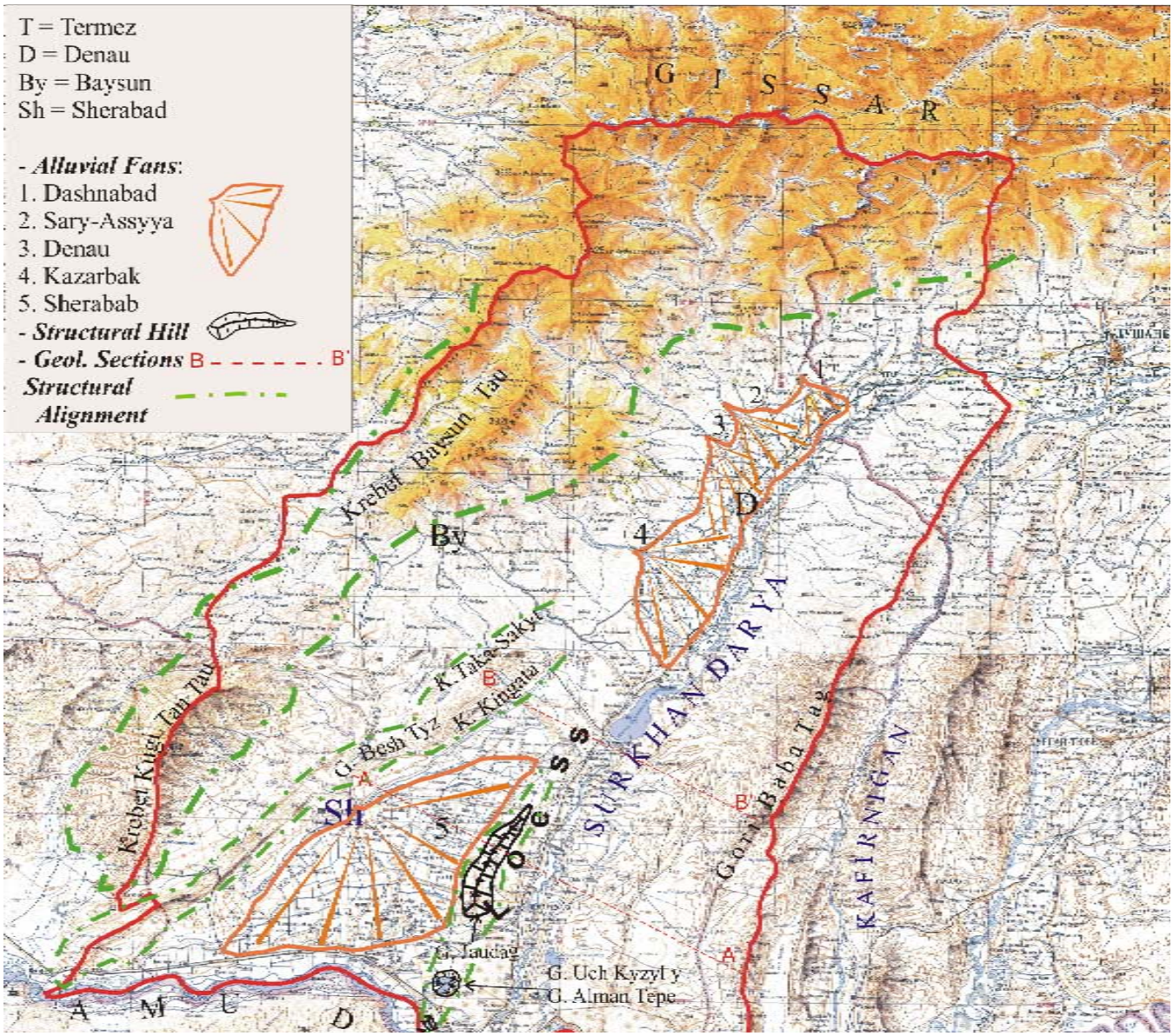

Figure 3: *Basin of the Surkhan Darya-Amu Darya, bounded by three structural mountain systems. The alluvial fans lie between the intermediate and lower systems, formed by structural hills. Tchinguiz Tepe is the farthest south of these hills. An area of loess spreads between the hills and the Surkhan Darya.*

				Formation	Abbr.	Thickness	Rocks Description
Cenozoic	Quaternary	Holocene		Amudarya Complex	$Q_{IV}ad$		gravel, sand, loam
		Pleistocene	Upper	Dushanbe Complex	$Q_{III}db$		gravel, sand, loam
			Middle	Ilyak Complex	$Q_{II}il$		loess-like loam, sand
			Lower	Vakhsh Complex Kulyak Complex	Q_Ikl+vh		conglomerate, gravel, sandstone, loam, clay and claystone
	Neogene	Pliocene	Gelasian Piacenzian Zanclean	Polisak Formation	N_2pl	800 - 900m	red-grey conglomerate, gravels sandstone, siltstone, claystone
				Karanak Formation	N_2kn	800 - 1500m	grey-brown siltstone, claystone, sandstone and conglomerate,
		Miocene	Messinian	Tavildarin Formation	N_1hn+td	500 - 1300m	grey and red-grey sandstone, brown-red siltstone and claystone
			Tortonian Seravallian	Khingou Formation			
			Langhian Burdigalian Aquitanian	Boldshuan Formation	$(Pg_3-N_1)bl$	440m	red and reddish brown sandstone, siltstone and claystone
	Paleogene	Oligocene	Chattian				
			Rupelian	Sumsar Formation	Pg_3sm	25 - 50m	greyish-blue and red sandstone, siltstone and claystone
		Eocene	Priabonian	Khanabad Formation	Pg_2al+hb	220 - 325m	claystone, siltstone, sandstone, limestone with shells, marlstone
				Isfarin Formation			
				Rishtan Formation			
				Turkestan Formation			
			Bartonian Lutetian	Alaj Formation			
			Ypresian	Suzak Formation	Pg_2sz	100 - 150m	claystone
		Palaeocene	Thanetian Seelandian	Bukhara Formation	Pg_1bh	110 - 230m	limestone, dolomite and gypsum
			Danian	Akdshar Formation	$Cr_2d?-Pg_1m$	0 - 80m	limestone, dolomite and gypsum
Mesozoic	Cretaceous	Upper	Senonian	Maastrichtian	Cr_2sn	240 - 580m	claystone, sandstone, limestone, gypsum and dolomite
				Campanian			claystone and limestone with shells
				Santonian			claystone, limestone with shells, gypsum
				Coniacian			claystone, marlstone and limestone with shell
			Turonian		Cr_2t	320m	claystone, siltstone, marlstone, sandstone and limestone with shells
			Cenomanian		Cr_2cm	280m	claystone, sandstone and limestone with shells
		Lower	Albian		Cr_1al	305m	claystone, sandstone and limestone
			Aptian Barremian		Cr_1b+ap	220m	reddish grey-brown and green-grey claystone, sandstone and limestone with shells
			Hauterivian Valanginian		Cr_1v+h	>140m	red and grey sandstone and claystone

Table 2: *Lithostratigraphic table corresponding to sheets J-4220 and J-4226a of the Soviet geological maps: the abbreviations are used in the legend of the maps and in the geological cross-sections of figure 4*

The southern part of the valley, where it gains in width, features other interesting Palaeogene and Neogene outcrops lying topographically on the Quaternary sediment of the Surkhan Darya-Amu Darya system: hills of *Gora Uch Kyzyl* (largely covered by a water reservoir) and *Gora Alman Tepe*. In the former we find materials from the Upper Oligocene, Miocene and Pliocene**,** and in the latter materials only from the Miocene and Pliocene. This detritic sediment shows intense colours from grey to yellow-ochre to red and it lies in parallel banks with slopes measured at 10 to 20 degrees west (fig. 4 section C-C').

Photo 1 shows the general aspect of the material in the outcroppings of *Gora Uch Kyzyl*. At this point, they have a visible potential of roughly 5 metres. They are formed by a sequence of alternative strata of sandstone (litharenite) and mudstone, which are red, grey and ochre. The formation contains layers of fine-grained sandstone with ripple marks related to the coastal marine sediment environments described in the area for the Palaeocene. Their structure is monoclinal with the strata in horizontal or subhorizontal position; in the vicinity of the reservoir they present a dip slope 10º west.

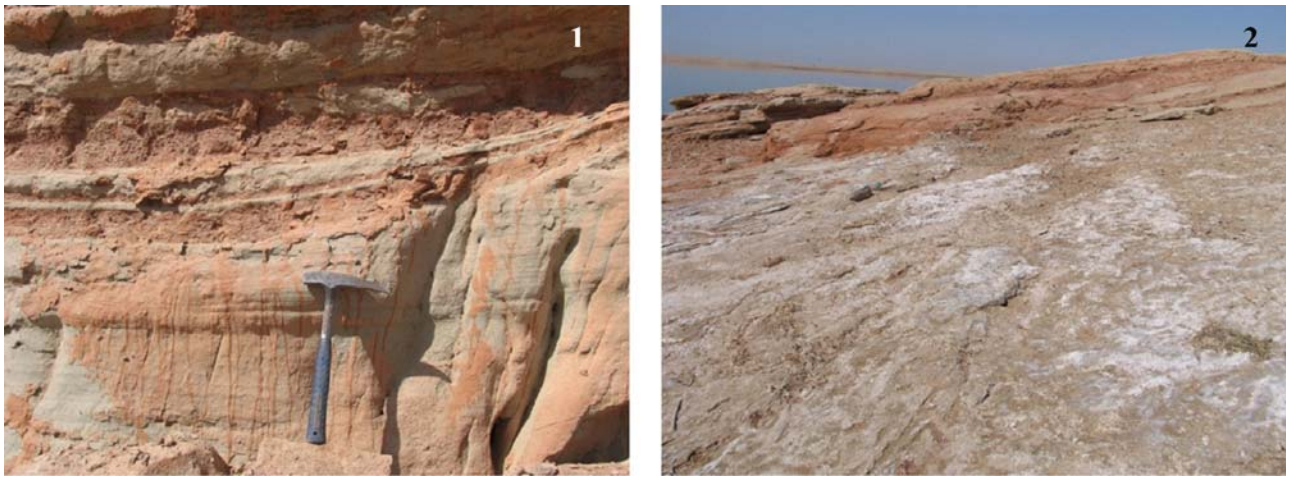

Photo 1: *Outcropping of Gora Uch Kyzyl. The sandstone shows significant oxide staining (1) and saline efflorescences (2)*

The eastern mountains on the left bank of the Surkhan Darya basin are the *Gory Baba Tag* range and other minor parallel ranges. The area features outcroppings from the Cenozoic, comprising the same materials described above, and the Cretaceous in the most internal parts of the structures, towards the parallel valley of *Kafirnigan* (fig. 3).

2.2 LARGE UNITS OF RELIEF RELATED TO MORPHODYNAMICS

The structural arrangement of the right walls of the Surkhan Darya valley, described in the previous section, offers a high-energy relief. Its areas of higher elevation are the source of a large portion of the products that have been mobilised and evacuated by gravitational processes and water. The large units of forms related morphogenetically to exogenous processes include: piedmonts, alluvial fans, areas of loess, deposits of sand and fluvial terraces.

2.2.1 Piedmonts and alluvial fans

The piedmonts in the basin show the notable influence of the large lines of structural relief, reflecting original features related to the convergence of several morphogenetic systems. The piedemont appears to be the basal unit that joins the mountain system with the fluvial terraces. In Surkhan Darya, however, we find a great morphostructure including the lower system and the bed of the Surkhan Darya in the northern two-thirds of the valley. In the southern third (approximately from the great reservoir downwards), the piedmont is located between the intermediate and the lower systems. Figure 3 offers a clear view of the importance of these circumstances in the organisation of the relief.

The basal surface, i.e. the surface of the piedmont, lies over rocks of ages ranging from the Cretaceous (Santonian) to the Pliocene, and it underpins a significant system of **alluvial fans**, which occur from the head of the valley to the Amu Darya. These alluvial fans are arid in type and arise in an area of tectonic instability, which has marked their origins and dynamics. Tectonic instability is also a control factor for a number of morphological parameters (Bull 1968), which are generated when channelled water and the materials it transports emerge from the mountains and their loads are deposited at the foot of these mountains as they lose speed and transport capacity.

Five main fans can be distinguished: 1) Sashnabab (apex height ± 800), 2) Sary-Assiya (apex height 700 m), 3) Denau (apex height 860 m), 4) Khazarbak (apex height 700 m) and 5) Sherabad (apex height 470 m). Between the third and fourth fans, two smaller fans are deposited, while two others, equally small in size, reach the banks of the Amu Darya (fig. 3). The fans are formed by sand, gravel and silt, which the Soviet maps date to the Middle Pleistocene and which constitute the Dushanbe complex (Q_{III}db in the cross-sections of figure 4 and table 2). The characteristics of the fans are set out below:

- Going down the valley, the fans increase to the valley's width, while their altitude, apex and slope tend to decrease in the same direction. The first and fourth fans are coalescent. The diffluence of drainage channels at the apex makes the surface drainage of the fans very dense.
- The distal area is located at a variable altitude ranging from between ± 440 and ± 500 m in the coalescent fans to ± 320 m in the *Sherabad* fan. The edge is difficult to determine because the distal area features an overlapping of fluvial and aeolic sediments. Some of the fans, such as *Khazarbak*, have a wavy border as a result of erosion from flooding water channels. In the distal areas, almost all of the fans converge with fluvial and/or aeolic formations.
- The *Sherabad* alluvial fan (fig. 3), the most southerly, is the largest. It also presents the most complex genetic and dynamic relationships with its surroundings. The fan collects water and sediment from a wide basin drained by the river Sherabab, which rises in the high peaks of Baysun Tau. The structural organisation of the massif is a determining factor in its size and shape. In this respect, the distal area is influenced by the structural relief of *Gori Jaudag* (556 m) and the *loess hills* that partially cover its eastern slope. This influence is also reflected in the outline of the fan's drainage network, which alters to adapt to the presence of the hills. All these characteristics, together with its position in an open zone near large rivers, have made and still make the space attractive for human settlement and exploitation. As can be seen in the Soviet map in figure 3, the Sherabab fan, for example, possesses a dense and complete network of artificial channels for irrigating crops that have high water demands, such as cotton.
- The alluvial fans play a critical role in surface drainage too, not only in the outline and morphometry of the complex drainage network, but in the hydrology. The channelled water descending from the peaks of *Baysun Tau* do not always reach the Surkhan Darya directly, because the main channel bifurcates at the apex of the fans. The water is distributed into multiple shifting channels that are largely lost to filtration. Channels with these characteristics are endorheic rivers that have undergone significant human intervention in order to make use of their water resources.

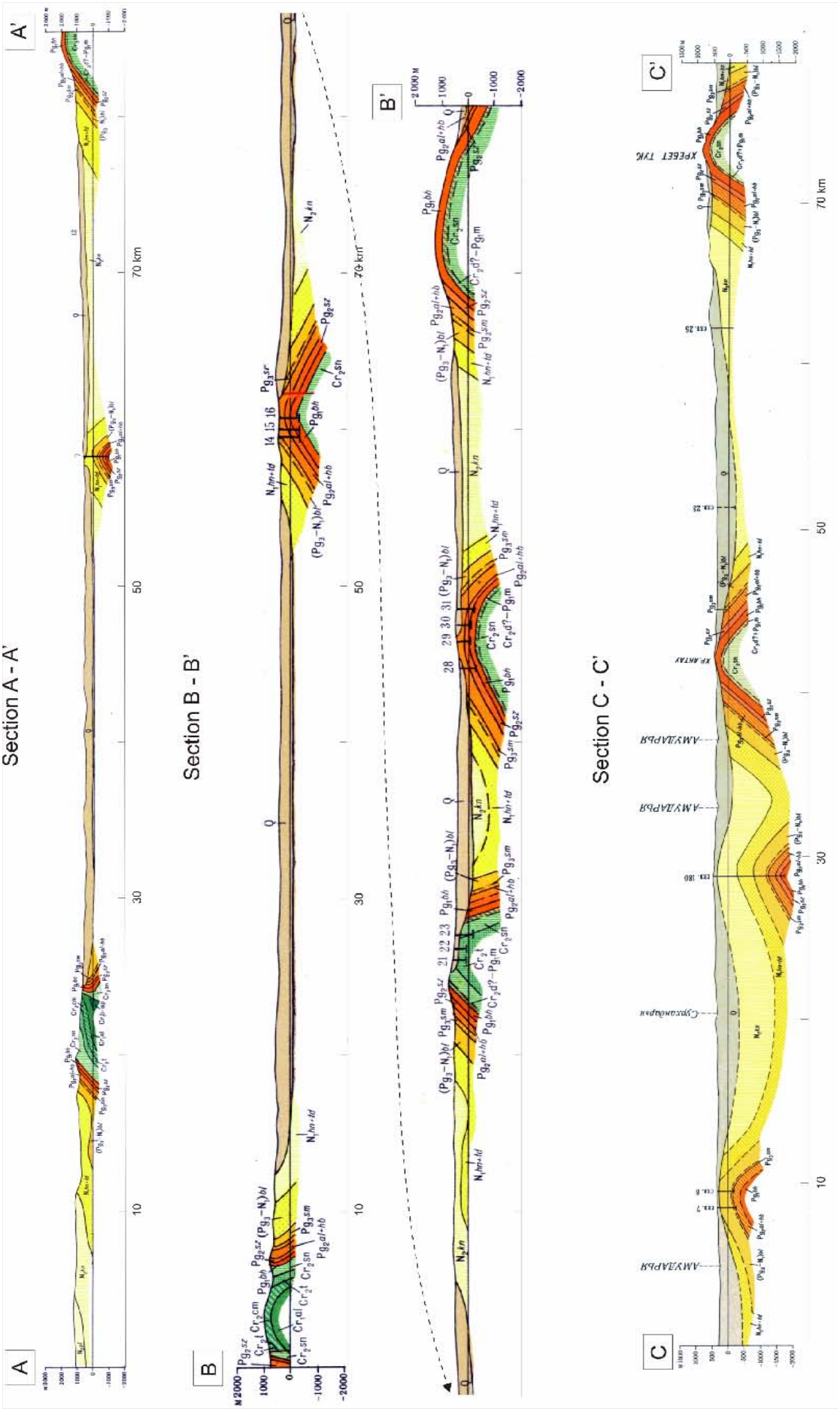

Figure 4: *Geological cross-sections from the Soviet geological maps J-4220 and J-4226. The location of the cross-sections is found in figure 3. Refer to table 2 for the lithostratigraphy abbreviations*

The fans are meaningful in two senses in the zone of study. Firstly, they behave as a form of accumulation. Secondly, they act as a source area of material that will be transported by the wind (mixing with *loess* deposits and sandy accumulations) and by surface runoff (joining the load carried by the large rivers). Basically, they work as a unit of sediment transit to other morphogenetic environments, which are aeolic or fluvial in nature. In addition, the erosion of cultivated soils under arid and semi-arid conditions provide a large part of modern windborne (aeolic) dust of grain-sizes smaller than loess (Tsoar & Pye, 1987).

2.2.2 Deposits of loess and sand

Loess deposits are one of the most interesting and complex recent types of sediment, because of the wealth of palaeoclimatic information they contain. Typical loess sediment is 20-60 μm (medium to thick silt) and has a mineralogical composition with a variable content of quartz, carbonate, feldspar, salts and clay minerals, depending on source area and post-sedimentary processes.

On the Eurasian continent, loess deposits extend more or less continuously from Central Europe to the Loess Plateau of China. Central Asia is one of the regions where such deposits are best represented, with sequences of up to 200 metres in thickness situated at the foot of hills bordering the great mountain changes of the region (Machalett, 2008). Their origin dates to the cold phases of the Pleistocene and their activity slowed after the last glacial advance, although short-term climate chains, such as the Medieval Warm Period (MWP) and the Little Ice Age (LIA) may have also marked phases of activity.

With respect to the formation of archaeological sites, the current activity of the loess deposits is quite low. The particles dispersed by dust storms measure less than 20 μm. This reflects the influence on the flow of aeolic dust from human activities related to the erosion of cultivated soils in semi-arid zones (Tsoar & Pye, 1987).

Theories on their genesis range widely as a result of the relative lack of shared knowledge between Soviet-Asian science on the one hand and western science on the other. With the opening-up of Russia and the independence of the former Soviet republics in Central Asia, a fruitful and interesting period of research and scientific exchange has begun. (For more information on the development of research on loess in the former Soviet republics, consult Jefferson et al. 2003). Soviet research took a great interest in edaphological and engineering issues, because the loess regions of Uzbekistan held potential as zones for irrigation and *loess soils* tend to subside and collapse due to their structure and characteristic texture (Smalley et al. 2002).

In Central Asia and in Uzbekistan, particularly, loess deposits can be explained by a theory of multiple causes, which Mavlyanov calls the "*Polygenetic Theory*". The theory offers several explanations of the deposition mechanisms of these and other loess-type sediments (Mavlyanov et al, 1987). The theory considers that (**i**) evacuation processes working on the loess fraction from the mountains are chiefly linked to water in its various modalities (*proluvial, diluvial*); (**ii**) sediment reaching the mountains' edges undergoes edaphogenetic processes (*eluvial/edaphogenetic theory*); (**iii**) wind action is undoubtedly at work in some cases and (**iv**) there is a variant of loess, which is "loess-like", and it is affected by diverse factors that modify its structure and composition (Smalley et al 2006).

In the abundant scientific literature generated by the subject, agreement seems to point to the high mountains as the source area from which fine particles emerge to be evacuated by torrents and melting glacier water. Later they undergo new transport processes and/or post-sedimentary processes that give rise to different types of loess. The literature has also pointed out that loess from the mountains is stored in nearby deserts serving as areas of intermediate storage. This loess is then taken up again as windborne dust/loess to be deposited in the perimontane zone, especially during glacial periods (Machalett et al 2006).

Loess accumulations in the Surkhan Darya valley take place in lowlands (between ± 480 and 300 metres of altitude) near the course of the river, and they assume the morphology of elongated hills. Their disposition along the main river is influenced by the local reliefs and alluvial fans. In the vicinity of *Dzhar Kurgan*, they are highly developed between the floodplain and the foot of the structural hills in the lower mountain system. Their distribution and evolution reflect the convergence of various morphogenetic systems. A significant change in climatic and energetic conditions occurs between the peaks and the low-

lands. Also of importance are the influence of the morphostructures and the topographical obstacles that affect the areas of deposit. They could correspond to the loess of the intermontane depressions of Mavlyanov et al (1987) where—according to the authors—loess of two kinds is found: “alluvial” and “diluvial” (deposited by torrential currents). The Soviet geological cartography at a scale of 1:200,000 (initials Q_{II}il, table 2) dates them to the Middle Pleistocene.

Between the loess hills and the sandy deposits, there is a band of transition or interphase that is difficult to interpret cartographically. It is an expression of the convergence of the processes at work in the area. The principal zone of **sand deposits** is the desert of *Pieski Kattakun,* which has a sand blanket and metric dunes that occupy the space between the Sherabab fan and the alluvial plan of the Surkhan Darya-Amu Darya. These dunes, however, are not as developed as the dunes that extend to the south of the Amu Darya, in Afghanistan. This can be explained by the configuration of the terrain, which is marked by topographical features such as the hill of Tchinguiz Tepe and vegetation that is sparse and discontinuous, but effective in controlling the deposition of windborne sand.

Based on their differing origin, age, mineralogical characteristics, granulometry and behaviour, it is useful to distinguish:

Loess

Aeolic sand

Aeolic dust

2.2.3 Fluvial terraces

The fluvial terraces linked to the Surkhan Darya show a high degree of human intervention, with multiple channels dissecting the surfaces and carrying water from one tributary to another, completely changing the pattern of surface drainage. Gravel and sand are predominant and they are very frequently covered in loess and sand.

In short, the geomorphology of the Surkhan Darya valley is complex, featuring a great variety of morphogenetic systems and types of morphostructures. Dynamic, it is an area that is tectonically active as well. It presents drainage systems which are fed by areas of high mountain and flow into base areas through an arid environment generating erosion and transport processes that are highly effective. In this context, the system of prevailing winds in the cold phases of the Quaternary is also an important control factor for the distribution of sand and loess, while the pattern of present-day winds generates significant mobility of windborne dust, causing a fine, always changing film to form over a large part of its surfaces.

3 THE HILL OF TCHINGUIZ TEPE

An initial study has examined the hill of Tchinguiz Tepe to establish the morphogenesis of the geological and morphological setting of the archaeological site. Its physiography is defined by a level area at around 300 m, in the geological context of an alluvial plain at the confluence of the Amu Darya and Surkhan Darya (see section 2).

The territory features small hills, some of which contain archaeological sites (e.g., Kara Tepe and Kampyr Tepe). Tchinguiz Tepe (325 m), another example, is highly representative from a geomorphological viewpoint, because it is an *inselberg* or highly visible and defined isolated hill on the banks of the river. At the crest of the hill, which measures 185 metres in length, stands the north face of the fortification wall. The construction of the other conserved wall—the eastern wall—takes advantage of jutting topography that bounds the inselberg on that side.

3.1 CHARACTERISTICS OF THE LITHOLOGY OF TCHINGUIZ TEPE

Structurally, the hill is defined as the most southerly outcropping of the lower mountain range (the least high of the three that make up the right-hand side of the Surkhan Darya depression) and it makes clear contact with the channel of the Amu Darya (see section 2.1). It is formed by detritic rocks (sandstone, siltstone and claystone) from the Miocene that are very similar to the rocks grouped regionally, according to the Soviet designation, as:

- *Boldshuan formation* (denoted as N_1hn+td in table 2), the lowest formation, corresponding to the Oligocene-Miocene, made up of reddish brown sandstone, siltstone and claystone (440 m of potential),
- *Khingou* and *Tavildarin formations* (denoted as $(Pg_3\text{-}N_1)bl$ in table 2), grouping series of red and reddish gray sandstone, siltstone and claystone with a variable potential of between 500 m and 1300 m, with the Upper Miocene defining most of the structure.

A similar nearby outcropping is the first anticlinal structure represented in the cross-section C-C' in figure 4.

Among these materials, fieldwork at Tchinguiz Tepe differentiates a covering of low potential, featuring discontinuous superficial formations that are aeolic, fluvio-aeolic, fluvial and slope-related in origin. As a function of this differentiation, the materials constituting Tchinguiz Tepe are grouped into two primary:

- **The coherent rocky substrate** refers to consolidated rock
- **Superficial formations (SFs)** do not conform to the coherent rock. They are principally detritic materials, which are unconsolidated although superficial crusts do fall within this category. They are fundamental for the interpretation of the site, because they constitute an important part of the material which is the object of archaeological intervention.

This phase of the work involved performing surveys of the coherent rocky substrate at: (1) Samples Trenches "RB", "RC" and "RT" (fig. 6); (2) other points of the outcropping along the hillside, namely "L" and "CF"; and (3) other outcroppings in the vicinity of the hill, namely "3CR" and "S-BAT". Surveys of the superficial formations examined different levels found in the profiles and, for Sample Trench RB, mineralogical and textural results were obtained.

The material most frequently found in the outcroppings or unearthed in the course of excavation beneath the SFs is sandstone which could be classified as litharenite with a carbonate cement. It appears in rock fragments of very diverse type and origin.

The examination of thin section indicates that some of the sandstone types show more traces of clay than others, containing plagioclase, microline, quartz, polycrystalline quartz and mica (muscovite), together with some clay. The contact of the clay with the sandstone is highly irregular in all samples. The quartz is quite angular and it contains areas of corrosion between Q and CO_3. There are also grains of slate. Together with mica, the slate is an indicator of highly varied source areas. The clay matrix contains some grains (the film that bounds the grains is the original matrix, because what grows in the most external space is CO_3). Sparite appears as cement, while grains of micrite and microsparite appear in the matrix.

Table 3 sets out the results of the mineralogical analysis of the total rock for the set of samples obtained from the substrate and superficial formations. The table and accompanying graph (fig. 5) show that the minerals that vary most in their proportion among the samples are the phyllosilicates.

In the clay zone of some substrate samples, the formation of caliche (+80% $CaCO_3$), or hardpan, is interpreted as a typical precipitation of carbonate in arid and semi-arid environments, caused by saturated water circulating through the soil. All these characteristics, together with patches of carbonate cement, or dispersed carbonate nodules, are indicative of palaeosoils typical of arid and semi-arid environments. Notable are the samples corresponding to the localised crust layer in Sample Trench RB, which has an average carbonate content of 34%, while the average for the rest of the superficial formations is 22% and it is only 15% for the coherent substrate (table 3, fig. 5).

SAMPLE	% Q	?% Carb.	? % Feld.	% Phyll.	% Calc.	% Dolom.	% FK	% Plag.	TYPE	
L-B	20	11	9	60	11	0	9	0	COHERENT ROCK	SUPERFICIAL FORMATION
L-A	36	13	18	32	10	3	9	10		
3-CR-2	27	**25**	13	35	20	4	13	0		
3-CR-1	25	22	13	40	19	3	13	0		
RB-S	36	9	18	37	9	0	18	0		
RT-B	37	13	**22**	28	11	1	12	10		
RT-A	**14**	**7**	9	**70**	5	1	9	0		
CF-C	16	22	**8**	54	22	0	8	0		
CF-B	19	21	9	50	21	0	3	6		
CF-A	23	15	18	44	15	0	11	7		
S-BAT-B	**38**	16	20	**26**	16	0	7	13		
S-BAT-A	26	7	12	55	7	0	3	8		
RB-E	29	14	**23**	34	14	0	11	12	Unconsolidated	
RB-C	28	**27**	**13**	32	24	3	5	8		
RB-B	24	32	17	27	32	0	17	0		
RB-A	35	18	18	30	15	3	5	13		
RB-D	**28**	22	15	**35**	19	4	15	0		
RB-I	**38**	**16**	22	**24**	16	0	8	15		
RB-H	**23**	19	10	49	19	0	10	0	Crust	
RB-F	**19**	36	8	37	36	0	8	0		
RB-G	20	**47**	10	24	44	2	10	0		

Table 3: *Mineralogy of the total rock of the substratum and superficial formations. Q = quartz; Carb = carbonate; Feld: = feldspar; Calc. = calcite; Dolom. = dolomite; FK = potassium feldspar.; Plag = plagioclase*

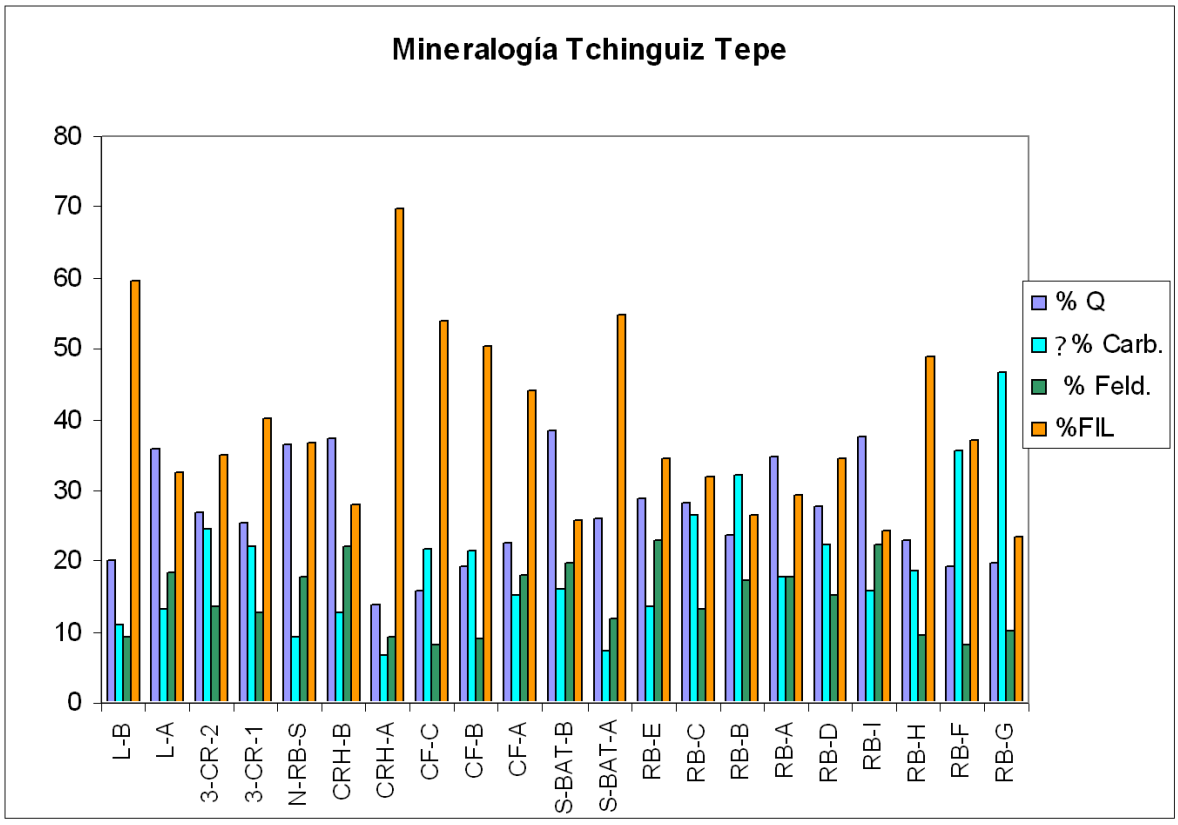

Figure 5: *Diagram of the mineralogy for the total rock from the samples taken of the substratum and the superficial formations*

The phyllosilicate content is high in most samples, both from the coherent rock and the superficial formations. The average quartz-phyllosilicate ratio in the substrate samples is 26/44, while it drops to 30/30 in unconsolidated SFs (table 4). Comparing the substrate and SF samples indicates a variation in content of quartz (26 to 30); carbonates (15 to 21) and phyllosilicates (44 to 30). Only carbonates are more plentiful in the superficial formations than in the substrate (table 4).

TYPE	Quartz	Carbonates	Feldspar	Phyllosilicates
1- S	26.5	15.1	14.1	44.3
2- SF	30.2	21.4	18.2	30.2
3- Crust	20.5	33.6	9.4	36.5
1 + 2	27.0	25.5	15.2	32.3

Table 4: *Average mineral content (%) in the simples by type: S = Substratum; SF = Superficial Formations*

The overall interpretation of the results obtained from mineralogical and textural analyses is that there are no significant differences between the samples of the coherent rock and the superficial formations. They appear to come largely from the vicinity of Tchinguiz Tepe itself or from areas of similar composition. The mineralogical variations indicated previously are explained by processes arising from the evolution of disaggregated and dragged materials, such as the slightly greater maturity in the superficial formations (higher proportion of quartz). The lower proportion of phyllosilicates in the SFs could be related to the lightness of these minerals, which are more easily carried by the wind. On the other hand, the proportion of carbonates in the SFs, particularly in the crust of Sample Trench RB (table 3), is more significant and has not yet been fully explained. The origin of the carbonates (predominately calcite over dolomite, see table 3) is attributable to the substrate itself and perhaps also to windborne dust.

As a whole, the sandstone shows signs of subaerial and edaphic change in addition to evidence of palaeosoils with biturbations, carbonate nodules, oxide staining, etc. The degree of alteration varies by zone. Normally the rock is quite friable and crumbles easily. Therefore, it is a potential source area of the superficial formations covering the hill slopes and of the sand evacuated by aeolic deflation to neighbouring areas.

As post-sedimentary processes in the superficial formations, saline efflorescences have been observed in places. They are neither as intense nor as frequent as those on *Gora Uch Kyzyil* (Section 2.1). However, they are indicative of current processes. They emerge from underlying levels, ascending by capillarity to a precipitation level of varying height. For this reason, the outcroppings appear on the surface in some places, but in others only appear in levels under excavation.

3.2 MORPHOLOGY, SLOPE DYNAMICS AND GEOSTRATIGRAPHY

A morphological analysis has been carried out on the slopes using a Digital Elevation Model (DEM). To conduct the analysis, digital images were taken of the level curves with the Arc-Info, Arc-View and Surfer programs. The resulting models, such as the shaded relief map, served as a basis for locating the walled enclosure with GPS. Serial topographical profiles were then generated with DEM to establish morphological and morphometric characteristics in combination with other procedures (e.g., field and map measurements of slopes and slope orientation).

The hill at Tchinguiz Tepe has a highly dissymmetric transversal profile. Its north slope is much steeper than its south slope. It reaches 288 metres in height, creating a wide space on which to site a walled enclosure, where our Samples Trenches are now under study (photo 2). The dissymmetry of the profile and the broad features of its relief have a morphostructural nature in relation to the geological structure of the lower mountain range. Tchinguiz Tepe may be considered an *inselberg* by durability and position, featuring topographical projects along its slope, which are associated with outcroppings of sandstone, siltstone and claystone (fig. 6).

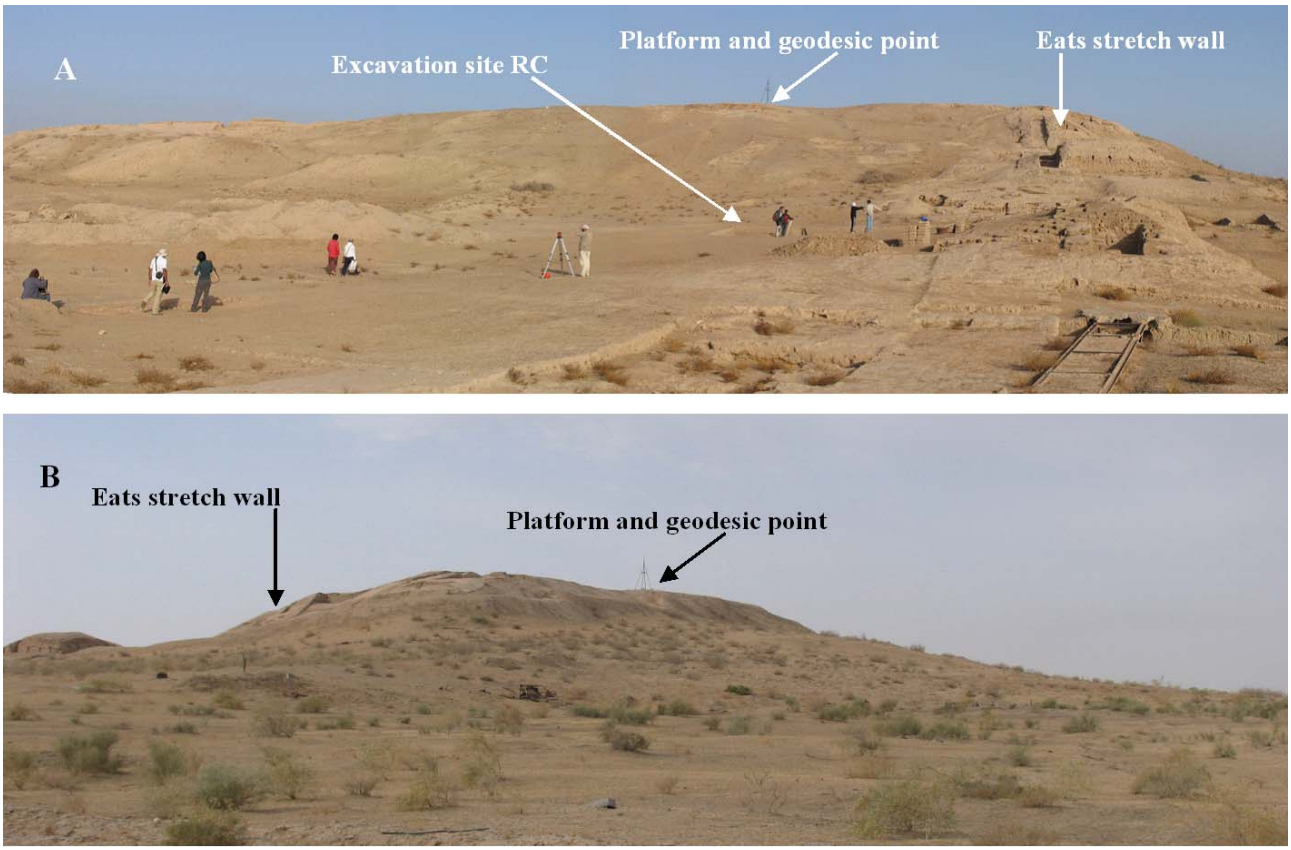

Photo 2: *(A) South slope of Tchinguiz Tepe showing the line of summits on which rest the northern face of the fortification wall, its eastern face and the topographical levels where excavation is occurring. (B) North slope, more precipitous, steeper than the south slope*

The south slope is not homogeneous across its entirety. The summit crest divides into two parts, with a concrete platform and, a few meters below, other ruptures and irregularities in the slope, which are related to the development of gullies (fig. 6 and fig. 7, sections B-B' and C-C'). These deep incisions could have been initially human in origin and subsequently accentuated by slope erosion-transport process (slope wash, rill wash…).

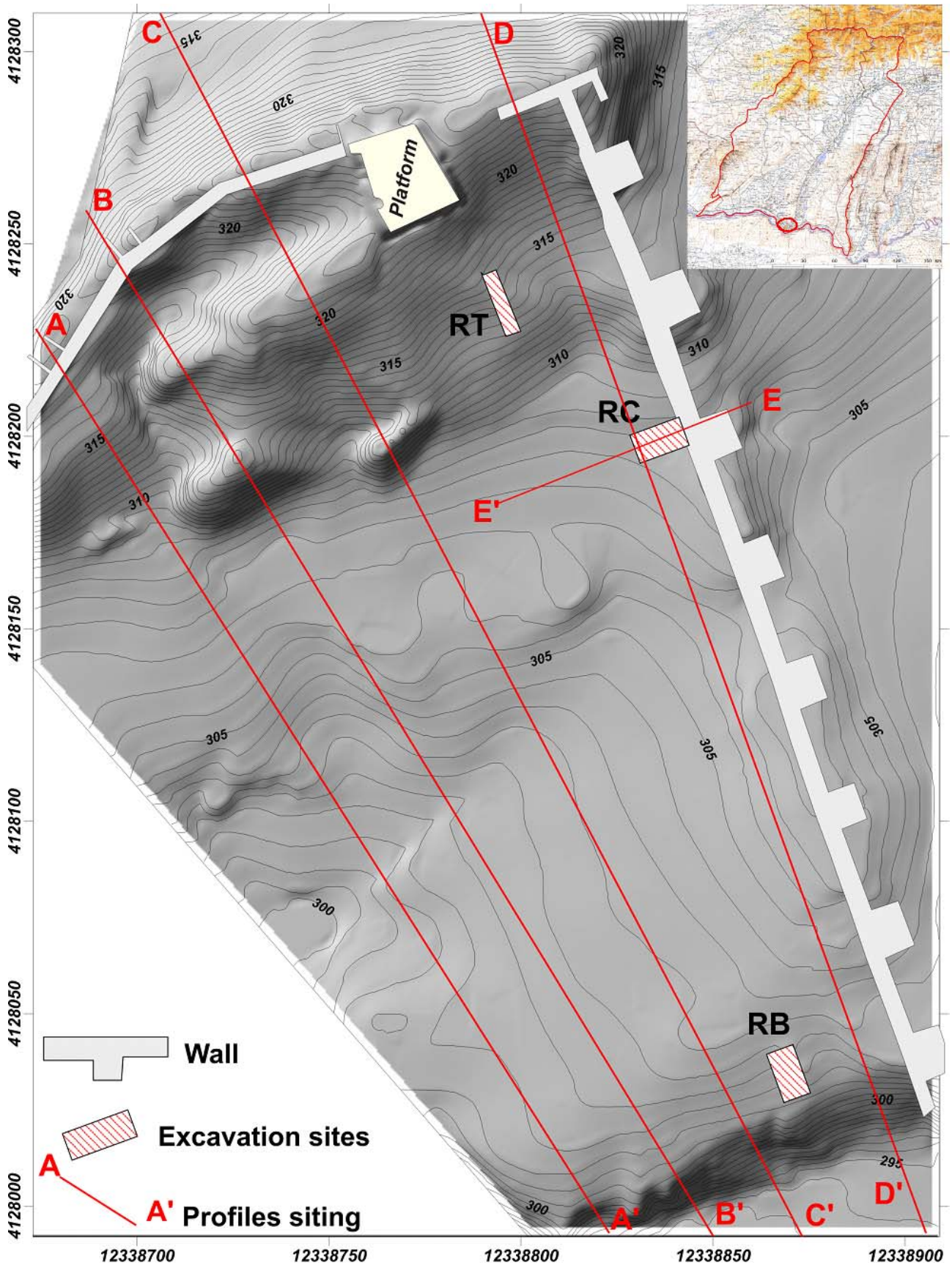

Figure 6: *Shaded relief map of the hill of Tchinguiz Tepe indicating the position of Samples Trenches RC, RT, RB and the topographical sections (profiles)*

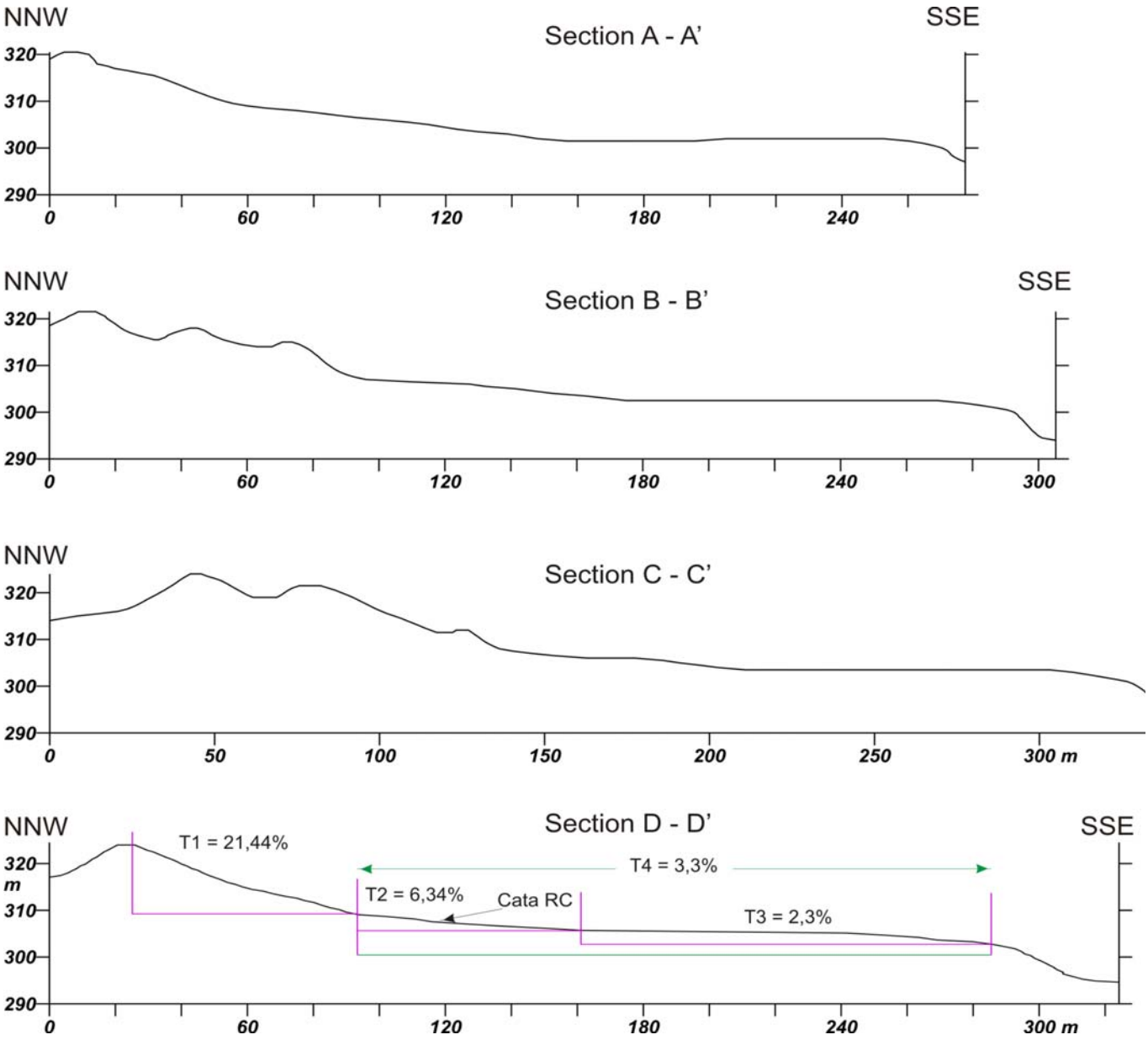

Figure 7: *Serial sections from the south slope of the hill of Tchinguiz Tepe with locations as shown in fig. 6*

Broadly, the eastern part of the hill features:

1. an upper segment, the steepest segment with frequent rocky outcroppings, corresponding to the hill's slope (T1);
2. an intermediate segment, which is less steep or forms a transition to the base or *transportational mildslope* (T2); and
3. a very flat, long segment of *footslope* (T3), which gives way to an escarpment of some 8 or 10 metres with outcroppings of the same materials making up the hill, highly altered but coherent. The structural origin of the escarpment may be related to the longitudinal lines of the Surkhan Darya valley as far as the Amu Darya, which affect the meanders of that river. At the base of the escarpment is a surface where two archaeological have been found: *Batiment A* and *Batiment B* (fig. 7).

The slopes gradient of these segments vary slightly from point to point, but they are generally 20-25% in the upper segment, 5-6% in the intermediate transition and approximately 2% in the lower segment, which is the largest and forms a pediment (fig. 7).

A detailed model was prepared of the geological structure, the foundation of the physiography of the hill, the sediments and superficial formations. The fundamentally sandy SFs are distributed with variable potentials and characteristics throughout the hill's profile in a given sequence from the upper segment to the distal zone. Their greatest width occurs in the intermediate segment and certain sections of the base surface. However, the notable human intervention, related to earth moving in the military training area and successive uses of the hill's soil, makes the distribution of SFs irregular by zones. As a result, they do not accord with the natural distribution model for SFs in arid environments. With this in mind, the geostratigraphic study of the cross-sections of the Samples Trenches has been conducted with reference to the position of the pits on the slope, that is, the toposequence that should have an influence on the potential of the SFs.

The description of the Samples Trenches' geostratigraphy, shown below, clearly demonstrates the control factors that stem from the slopes' morphology and the pits' position on the hillside.

3.2.1 Sample Trench RC

Sample Trench RC is located at an elevation of roughly 311 m, abutting the internal face of the fortification wall next to tower 4 (figure 6, 3D).

The location of the pit converges with:

a) a section of the foot of the hill, **T2**. The slope is 6.34% and it links the steepest segment **T1**, which has a slope of 21.44%, with the piedmont or **T3**, which is the broadest and flattest, with a slope of 2.3%. By considering **T2** and **T3** together, a general base segment **T4** can be obtained, with a gradient of 3.3%, as seen in figure 8, D-D',

b) and the level or topographical surface from which the eastern face of the fortification wall rises. It is broadly, but not exclusively, tied to dynamics of human activity (e.g., construction, abandonment, ruins, deposition) (figures 6 and 8, E-E').

From the geomorphological standpoint, the position of the slope partly controls the stratigraphic sequence tied to the present-day morphogenetic stage, and from the archaeological standpoint, part of the site's formation. In the context of slope dynamics, it behaves as an accumulation area for sediment dragged from the higher zones and for aeolic sand coming from the south.

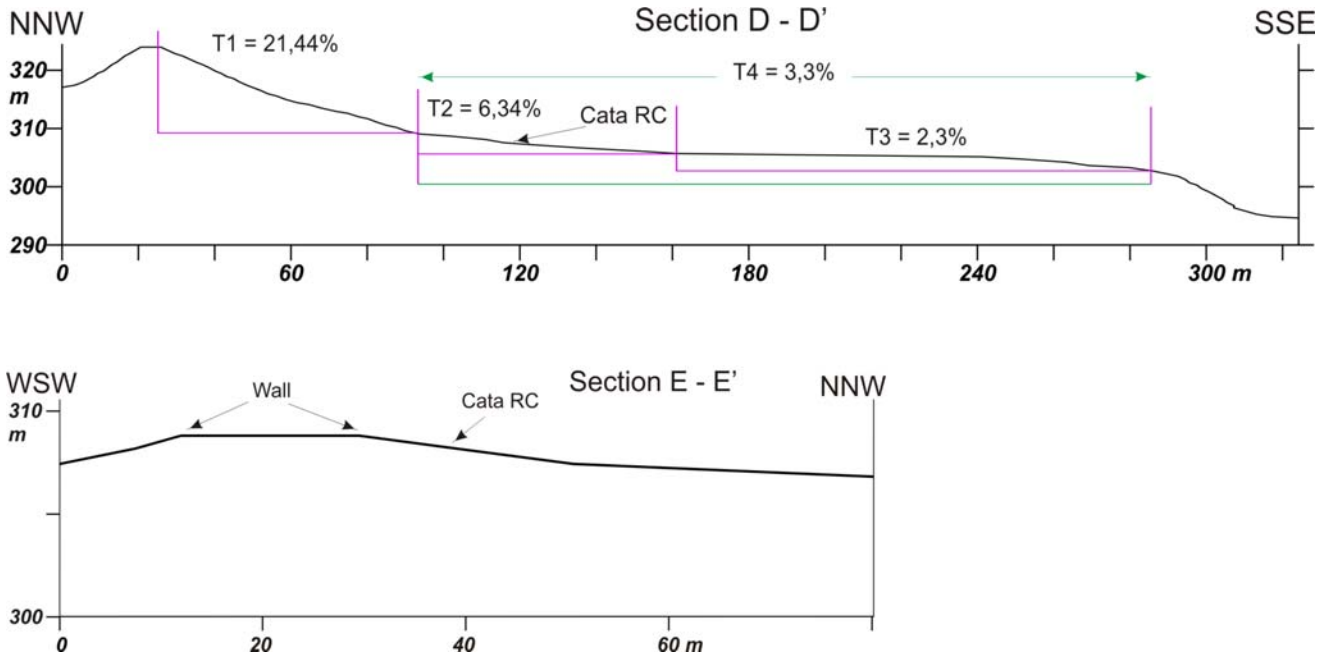

Figure 8: *Longitudinal section of the southern slope at the height of Sample Trench RC (profile D-D') and perpendicular to the pit and the fortification wall (profile E-E'). See fig. 6 for the position of the two profiles.*

Study of this sample trench is currently under way, but an early description of the stratigraphy of the western and northern cross-sections may serve as an example of the vertical stratigraphic sequences, lateral changes, etc. The observed levels appear in the stratigraphic column of figure 9. Its meaning is purely geological and valid for the geomorphological unit in which the column was taken, i.e., the base surface of the hill, which behaves differently from the distal zone or the hill's steep upper segment.

Stratigraphy in the western cross-section of Sample Trench RC Levels:

The total potential to the substrate is 196 cm, presenting a quite homogeneous ochre colour (between 10 YR 6/6 and 10 YR 7/4 in the Rock Colour Chart), except in levels with ash.

RC-a

This level is formed of fine to medium sand with sporadic pottery fragments. The surface shows *fine, black gravel, round and long in shape, and fine to medium sand*. Lithologically, they reflect quartzite and various igneous rocks and exogenous metamorphic rocks from the higher massifs, arising from fluvial transport. They form the present-day soil level.

At 22 cm, you can see a thin layer of fine sand, possibly related to a specific aeolic accumulation (sand sheet).

Potential of the cross-section of the Sample Trench (cm) = 28 – 35 – 30.

Contact between RC-a and RC-b is irregular and more accentuated in lower positions of the slope.

RC-b

This level has irregular contact with the preceding level, from which it is distinguished by being **sand of thicker granulometry**, massive in character, with little or no gravel and some charcoal and pottery fragments.

Potential of the cross-section of the Sample Trench (cm) = 32 – 26 – 20.

Equivalent archaeological level: **RC-a** and **RC-b** = **SU 1**.

RC-c

Fine to very fine sand, massive.

Potential of the cross-section of the Sample Trench (cm) = 30 – 27 – 37.

Contact between RC-c and RC-d is irregular.

RC-d

Very fine sand, which contains sporadic pottery in this cross-section.

Potential of the cross-section of the Sample Trench (cm) = 30 – 34 – 35.

Equivalent archaeological level: **RC-c** and **RC-d** = **SU 5**.

RC-e.

It is very similar to the previous level, but more compacted and richer in pottery and bone remains and limestone patches.

Potential of the cross-section of the Sample Trench (cm) = 16 – 18.

Equivalent archaeological level = **SU 6**.

RC-f ± 39 cm, fine undifferentiated sand, over the sandstone substrate. As in the previous level, it contains pottery remains, bone and limestone.

Equivalent archaeological level = **SU 10**, **SU 11.**

Stratigraphy in the northern cross-section of Sample Trench RC: Levels:

This cross-section lies perpendicular to the fortification wall and in the topographical layer from which the wall rises. The continuity of the levels described on the western side is lost in the direction of the wall, following a model similar to lateral phase change, representing variations in the characteristics in the sediment in this direction.

RC-a and **RC-b**

The top of the profile contains ***fine black gravel***, as in the previous cross-section of the surface cover, over ***fine to medium sand***.

Potential of the cross-section of the Sample Trench (cm) = 28 – 35 – 30.

In the northern cross-section of Sample Trench RC, the most superficial levels on the west side (**RC-a** and **RC-b**) grow progressively thinner until they disappear against the fortification wall (figure 9 B/). Laterally, they give way to human levels configuring a complex wedged and lenticular stratigraphy.

Equivalent archaeological level = **SU 1**.

RC-g

This stratum contains ***fine sand***. It forms a wedge containing adobe fragments embedded in a clay matrix. Towards the fortification wall, you can see highly numerous fallen adobe bricks and, on the south side, a great collapse. Because of their position in the stratum, these archaeological elements are considered a ruin arising almost exclusively caused by gravity. As a result, they have undergone minimal transport from their original position. They have not been dragged by water or wind, nor have they been intentionally moved to the current position. They are fully archaeological levels (figure 9 C). As these levels of fallen materials move away from the fortification well, they change and present pottery fragments that could originate from dragging.

Equivalent archaeological level = **SU 2**, which is described as a level of fallen adobe bricks.

RC-h

Grey sediment stratified with ash, very dark, almost black top; becoming clearer towards the wall, mixed with ash. The stratum contains abundant pottery in small fragments and particles of white limestone.

Potential = 20 cm to level reached by excavation.

Equivalent archaeological level = **SU 3**, covering SU18, circulation level on which the fortification wall stands.

Lower levels are all of purely human origin and all of them—except the most superficial layer of sand and gravel—appear to have a large human component.

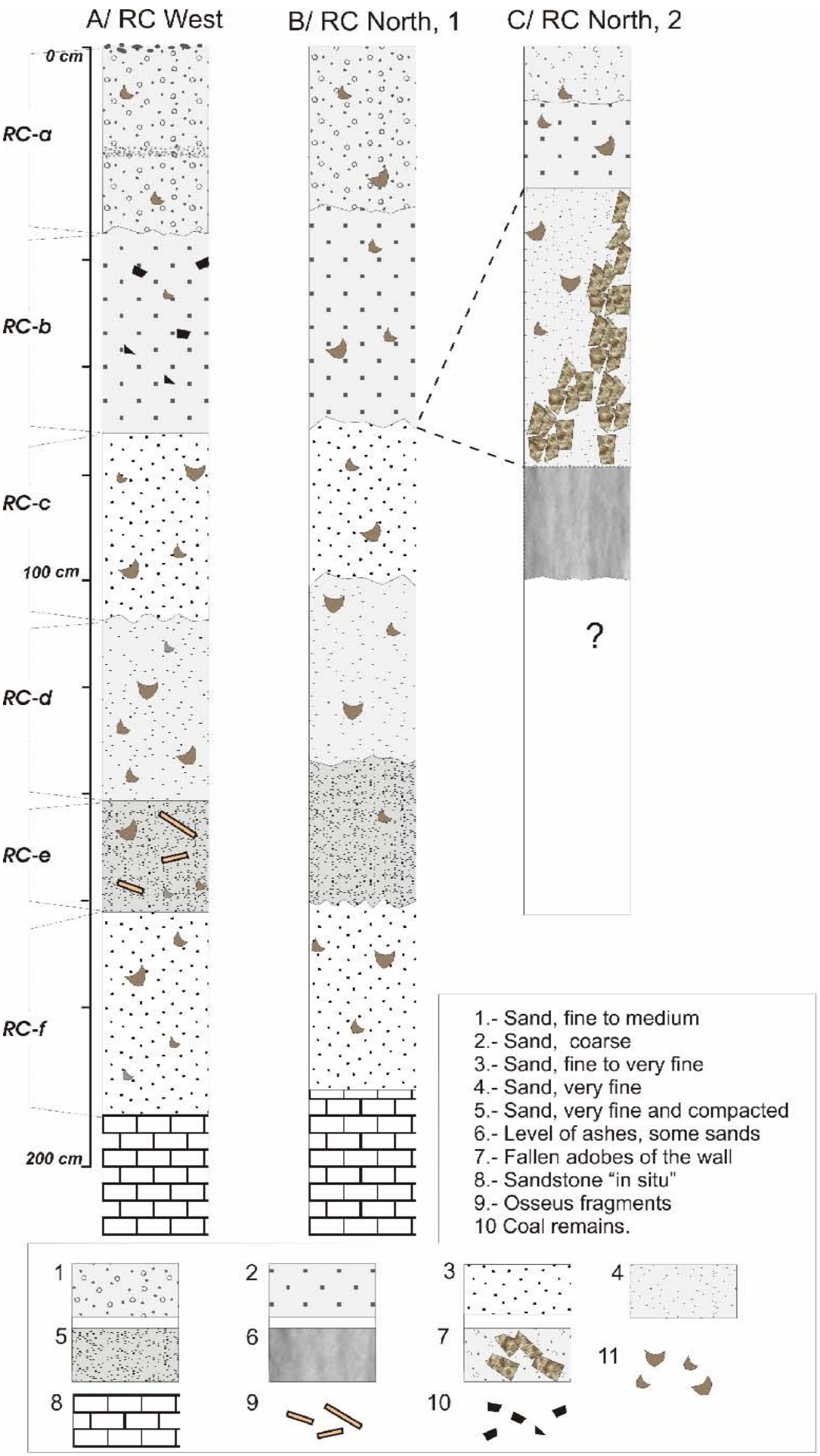

Figure 9: *Stratigraphic columns from Sample Trench RC, western and northern cross-sections*

Interpretation of Sample Trench RC:

● The western cross-section of the sample trench is the most distant from the fortification wall and it is associated with the surface of the hill's foot. For these reasons, the levels linked to erosion and natural transport agents are thicker. The disposition of the strata plainly reflects the natural agents that converged in its formation. The stratigraphic levels are sometimes irregular, but roughly parallel to one another and to the topographical surface of the slope, ruling out any intentionality in their arrangement.

● The northern cross-section may serve as an example of how the transition occurs from areas more heavily influenced by natural processes to the totally human area.

● The most superficial level, **RC-a**, associated with the current soil level, is a discontinuous covering of gravel and fine to medium sand. It behaves partly as a *surface sealing* by means of aggregation/compaction of clay particles, which cause a reduction in infiltration. For Poesen (1986), the effect of rocky fragments in the surface sealing is greater if they are partially encrusted in it, which occurs extensively across this surface. Finer particles are carried over it by overland flow in the scarce, but effective, event of rain. Superficial gravel, as with rock fragments in general, favour selective removal of fine materials by the wind (Baird, 1997). Wind action, for its part, plays two basic functions: (**a**) transporting sand from the neighbouring dunes of Afghanistan to the south of the Amu Darya, depositing it in part on the southern slope of the hill; and (**b**), removing sandy materials, leaving grain sizes too great for it, i.e. gravel and pebbles. In this way, the sand, which is still predominant, does not form wind-deposited sand blankets or any other type of significant accumulation.

● The stratigraphic levels including **RC-a** through **RC-d** are tied to normally natural transport and deposition processes, arising from surface runoff and the wind. Pottery remains, bone and limestone remains have been enclosed in a sandy matrix of variable granulometry according to level. Their behaviour resembles any clast of natural origin dragged across a slope. This set of strata is generated by natural agents and composed of natural and human materials**.** In the northern cross-section, they grow progressively thinner in the direction of the fortification wall and form wedges, giving way to levels of greater human or fully human composition.

● Level **RC-e** shows signs of corresponding to positions of human occupation *in situ* and it is covered by a level of fine sand with pottery, level **RC-f** (archaeological equivalent **SU 11**).

● Beneath, supporting the entire pocket of materials described above, the *in situ* substratum of grey sandstone appears. It is somewhat friable, although it does not crumble when handled. At this end of the Sample Trench, which is the farthest from the fortification wall, the sandstone is not carved or broken up. It shows no mark at all of human intervention. In the part closest to the fortification wall, a level of sandstone has been cut into steps. In all of these cases, the surface presents an alveolar texture, probably related to alveolar weathering process.

3.2.2 Sample Trench RB

The size of the Sample Trench is 10 x 14 m and it has an elevation of roughly 299 m. It is located at the distal edge of the base surface of Tchinguiz Tepe, where the southern face of the unconserved fortification wall would theoretically be located, near the escarpment on the southern face of the hill. The morphological surface in which the Sample Trench is excavated, at the base of the hill, has little slope (approximately 2%) (fig. 6). It has a thin, discontinuous covering. It is a complex text pit because of its variability and discontinuity of the superficial formations, for the fragments of sandstone and carbonate nodules, as well as for his notable degree of weathering to the substratum, who presents cemented levels.

Stratigraphy at the southern cross-section of the Sample Trench RB Levels:

RB-a

It has a discontinuous covering of sand and gravel of the same type noted in Sample Trench RC. The covering is observed in all the cross-sections of the sample trench and across the entire surface of the hill, with greater or lesser definition as a result of the discontinuous character of the formation. Scarce fragments of pottery appear.

Equivalent archaeological level = **SU 1.**

RB-b

At the southern edge, the potential of the level is 60 cm and it increases gradually to the north, reaching 92 cm at the midpoint of the cross-section and 124 cm at the other end of the excavated sample trench.

It is a massive formation of reddish sand embedding angular fragments of altered grey sandstone and ochre or orange mudstone. In the upper part, gravel and round, black pebbles appear. Dispersed carbonate nodules of between 1 and 3 cm also appear. The nodules and the mudstone fragments have a lithology that is similar to the underlying substrate and to those observed at *Gora Uch Kyzil*. The lower part of the level could correspond to the top of the profile of alteration for the highly developed substrate.

However, the presence of pottery gives rise to the notion that this level is of human origin or that the pottery remains have been incorporated in the natural level at some given point in time. This would have occurred as the result of intentional removal of the weathering profile in which the archaeological remains appear. One explanation would lie in preparatory work for the construction of the fortification wall's foundation in a substrate that is much more weathered and friable than the substrate in Sample Trench RC, in which only the surface supporting the first layer of foundation shows signs of carving.

Possible equivalent archaeological level **SU 6** is defined as "limestone and sandstone conglomerates in a sand matrix" (photo 3).

Two of the levels, **RB-a** and **RB-b**, have been observed with small variations on the western and eastern sides of the sample trench and in the western side of the extreme southern end.

Beneath appears the sandstone substrate *in situ.*

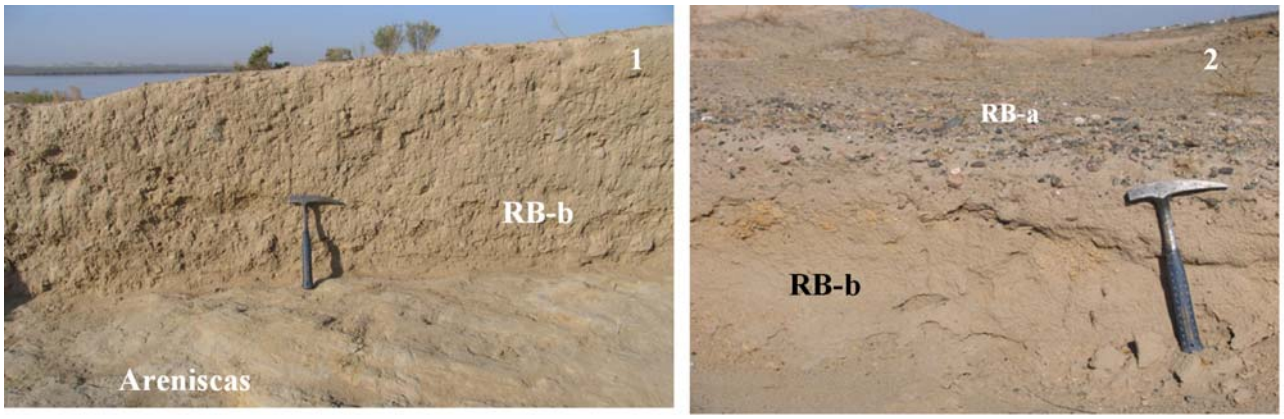

Photo 3: *Cross-section of the western side of RB: you can see the clasts and fragments of sandstone in lower levels of the profile. (2) You can see the most superficial covering of gravel and sand on the western side of the sample trench, equivalent to RB-b on this side.*

Here we did not observe the archaeological level **SU 5** ("level of compact reddish clay with pottery fragments from the 2on century BC"), which the archaeological planimetry indicates as covered by **SU 6** and covering **SU 11** = bedrock.

Beneath appears the sandstone substrate *in situ.*

Stratigraphy in the northern cross-section of Sample Trench RB Levels:

RB-a

The surface presents a superficial discontinuous covering of sand, gravel and small gravel. The gravel remains *in situ* while sand is carried by the wind. It is observed in all the cross- sections of the trial excavation and across the entire surface of the hill, in a more or less defined state.

RB-c

Sand and gravel with fragments of sandstone.

RB-e

This level has been detected only in this place. It contains complex material, based on their location and lithological features. It is very near the topographical surface and it can be observed in the northern cross-section and in the adjacent sides over the initial metres. It has the appearance of a cemented crust. It is composed of decimetric fragments of altered grey sandstone, with occasional orange and reddish staining, and pebbles and carbonate nodules, ochre in a sandy matrix. It contains no pottery. As indicated in the mineralogical analysis, the sample of the material shows a high content in carbonates and the percentage of feldspar is much lower than in the rest of the samples (photo 4). It is of natural origin. The presence - in the first moment of the excavation - of underlying levels with pottery, it complicated the interpretation. Finally there was reached the level of continuity of the formation that allowed to check his character of weathering rock in situ.

Potential 50 - 60 cm. *Possible equivalent archaeological level* = ***SU 1***

RB-f

Located beneath RB-c, it is a level of fine grey to ochre sand, with pebbles, round black gravel and scarce fragments of altered sandstone clasts. It contains pottery, which makes it difficult to interpret the overlying level as a natural formation. From an archaeological viewpoint, the interpretation is that it forms part of a foundation structure, alternating layers of compressed clay with layers of sandstone and carbonate rock (photo 4).

Equivalent archaeological level = ***SU 2.***

Beneath it lies the sandstone substrate. From north to south, it follows the slope of the hill, at 124, 92 and 60 cm from the topographical surface, indicating the potential of the superficial formation. The least altered areas are light grey in colour. Intense alteration has made the level highly friable and given it markings typical of palaeosoils, with staining in the form of reddish, orange and ochre circles tied to oxide migrations.

Photo 4. *North cross-section of Sample Trench RB showing the general aspect of the rocky sustrate, the underlying clay layer (RB-f), and one of the large fragments within it (RB-e)*

Interpretation of Sample Trench RB:

The position of the sample trench on the slope and its location with respect to the eastern face of the fortification wall lead to notable differences in its stratigraphy with respect to Sample Trench **RC**. Firstly, the total potential of the transported superficial formations is much lower in **RB**. This can be explained by its position on the slope, in the area of minimal sediment accumulation.

The frequency of pottery fragments and other human remains is similar in the two samples trenches. However, the relationships between the first clearly human stratum and the geological substrate are sharply different in **RC** and **RB.** This circumstance could be explained by the degree of the substrate's alteration (greater in **RB**), which would require some variations in the method for preparing it for the first construction.

4 OVERALL INTERPRETATION

Tchinguiz Tepe is an inselberg controlled by lithology and structure, presenting a covering of superficial formations (SFs) that are discontinuous but widespread and of variable thickness along the entire slope. The SFs contain various types of material:

Fine to medium grain sand from the weathering of the coherent rock (sandstone and mudstone), which has been dragged by water down the hill (overland flow and slope processes). The sand has been transported a short distance.

Fine to very fine sand and windborne dust, of exogenous origin. The sand and dust have been transported a longer distance and effected by the wind. Deposits appear across the entire slope.

Dark round gravel and pea gravel, mixed with sand, extends over the SFs across their entire surface, but discontinuously and with no prominent location.

The origin of the SFs is a matter of controversy. It is hard to explain by a single agent or process. In Tchinguiz Tepe, it appears to arise from the convergence of three great morphogenetic systems linked to arid environments:

Slopes, involving erosion and dragging of material from the coherent rocky substrate. A key role falls to superficial runoff of the Horton Overland Flow type, linked to environmental conditions in arid climates, where precipitation is scarce but intense, acting as a highly effective modelling agent.

Alluvial-colluvial, involving very round gravel and pea gravel from a distant igneous and metamorphic source area. It is linked to the Amu Daria-Surkhan Darya river system. This origin assumes to the gravels that appear in the immediate environment of the hill. But the origin of the gravels contained in the superficial formations of Tchinguiz Tepe hill, is yet in process of research.

Aeolic. Present-day wind activity is significant, with variable seasonal flows (Machalettt et al. 2008). At the local level, southwest winds carry sand and windborne (aeolioc) dust from the neighbouring Afghan desert. The source area of the desert's vast dunes is the alluvial megafans (Smalley, 2006), such as the Mazar e Sharif, located in the base platforms of the southern slopes of the Hindu Kush. These fans, in turn, are composed of sediment arising from the erosion of the great mountain range.

From a geomorphological perspective, the formation of the archaeological site in the geographic context of Tchinguiz Tepe is subject to wind action to a great extent. The wind acts as an unchanneled fluid, subject to turbulence, more mobile than water, and more frequent and constant. It can deposit its load among archaeological strata in formation and it can form wedges depending on the obstacles it encounters. In short, it is an agent that works more constantly over time and more extensively over space than water falling in the form of precipitation in this climate. Nonetheless, as noted earlier, water is also a powerful agent due to the nature of the rainfall and the high erodibility of the terrain.

The SFs are quite recent. Although no absolute dating is available yet, they can be linked to a historical epoch with total certainty. In this respect, the circulation surfaces established by the archaeology in the different samples trenches are a key piece of data. For example, the oldest circulation surfaces in Sample Trench RC lie between 0.30 and 0.12 cm from the coherent rocky substrate, indicating that only a thin and discontinuous film of sediment existed on the hill slope at that time. The width of material accumulating over this circulation surface is 1.43 m on the east side, 0.81 m in the centre and 0.82 m in the west side of the sample trench, offering values that give an idea of the intensity of sedimentation, irrespective of whether it is natural, human or mixed in character.

Most of the activity of the processes generating the SFs is doubtless related to climate variability over the last two thousand years. Climate changes in Central Asia, such as the Warm Medieval Period (MWP) and the Little Ice Age (LIA), have had an effect on temperatures and precipitation levels, which would be reflected in the variations in rates of erosion and sediment production (e.g., cf. Machallett, 2008, Yang et al, 2009, Boomer et al 2009). Present-day wind and slope activity is now at much slower rates, and the morphology of Tchinguiz Tepe and the area's morphogenetic context have been modified a great deal by recent human intervention.

Works cited:

Baird, A.J. (1997): Runoff generation and sediment mobilisation by water. In Thomas, D,S.G. (ed.): *Arid Zone Geomorphology*, Wiley, Chichester, 165-184.

Yang, B.; Wang, J.; Bräuning, A.; Dong Z. & Esper, J. (2009): Late Holocene climatic changes in arid central Asia. *Quaternary International*, 194, 68-78

Boomer, I.; Wünnemannn, B.; Mackay, A.W.; Austin, P.; Sorrel, P.; Reinhart, C.; Keyser, D.; Guichard, F. & Fontugne, M. (2009): Advances in understanding the late Holocene history of the Aral Sea region. *Quaternary International*, 194, 79-90.

Bull, W.B. (1968): Alluvial Fan, Cone. In Fairbridge, R.W. (ed.): *The Encyclopedia of Geomorphology*. Dowden, Hutchinson and Ross, Stroudsburg, PA (USA).

Coutand, I.; Strecker, M.R.; Arrowsmith, J.R.; Hilley, G.; Thiede, R.C.; Korjenkov, A. & Omuraliev, M. (2002): Late Cenozoic tectonic development of the intramontane Alai Valley, (Pamir-Tien Shan region, central Asia): An example of intracontinental deformation due to the Indo-Eurasia collision. *Tectonics*, 21, 6, 1053, doi: 1029/2002TC001358.

Jefferson, I.F.; Evstatiev, D.; Karastanev, D.; Mavlyanova, N.G. &. Smalley, I.J. (2003): engineering geology of loess-like deposits: a commentary on the Russian literature. *Engineering Geology*, 68, 333-351.

Machalett, B.; Frechen, M.; Hambach, U.; Oches, E.A.; Zöller, L. & Markovic, S.B. (2006): The loess from Remisowka (northern boundary of the Tien Shan Mountains, Kazakhstan)- Part I: Luminescence dating. *Quaternary International*, 152-153, 192-201.

Machalett, B.; Oches, E.A.; Frechen, M.; Zöller, L.; Hambach, U.; Mavlyanova, N.G.; Markovic, S.B. & Endlicher, W. (2008): Aeolian dust dynamics in central Asia during the Pleistocene: Driven by long-term migration, seasonality, and permanency of the Asiatic polar front. *Geochemistry Geophysics Geosystems*, vol. 9, Q08Q09, doi:10.1029/2007GC001938.

Mavlyanov, G.A.; Kasymov, S.M. & Shermatov, M.Sh. (1987): The Uzbekistan Loess, Genesis and Distribution. *Geojournal*, 15:2, 145-150.

Poesen, J. (1986): Surface sealing as influenced by slope angle and position of simulated stones in the top layer of loose sediments. *Earth Surface Processes and Landforms*, 11, 1, 1-10.

Smalley, I.J.; Mavlyanova, N.G.; Rakhmatullaev, Kh.L.; Shermatov, M.Sh.; Machalett, B.; O'Hara Dhand, K. & Jefferson, I.F. (2006): The formation of loess deposits in the Tashkent region and parts of Central Asia; and problems with hydrocollapse and soil erosion. *Quaternary International*, 152-153, 59-69.

Sorrel, Ph. (2006): The Aral Sea: *A palaeoclimatic archive*. Doctoral thesis. Institut für Geowissenschaften, Potsdam University, Germany. Laboratoire PEPS, UMR 5125, Université Claude Bernard-Lyon 1, France, pp. 109.

Thomas, J.C.; Chauvin, A.; Gapais, D.; Bazhenov, M.L.; Perroud, H.; Cobbold, P.R. & Burtman, S. (1994): Paleomagnetic evidence for Cenozoic block rotations in the Tajik depression (Central Asia). *Journal of Geophysical Research*, 99, B8, 15,141-15,160.

Tsoar, H. & Pye, K, (1987): Dust transport and the question of desert loess formation. *XVI INQUA Congress*, Paper 90-8.

Geoarchaeological Analysis in Arid Settings: the Case of Tchinguiz Tepe (Termez, Uzbekistan)

Enrique Ariño, Ana Sánchez del Corral

1. Introduction.

The hill of Tchinguiz Tepe is a structural *inselberg* of low elevation, which is more highly developed on its southern face than on its northern face. Outcroppings of ochre and red sandstone appear at the summit, on its slopes and at its base. The hill is elongated in shape and measures approximately 280 metres in length. It lies northwest-southeast in orientation and reaches an altitude of 325 metres above sea level.

The steep northern slope meets the base of the hill abruptly. The southern slope, where the most important archaeological remains are found, is longer and features a series of segments of varying slope. They can be distinguished on the central N-S axis as (1) an upper segment, which is the steepest (21.44%) and contains rocky outcroppings of great continuity; (2) a middle segment, which is less steep (6.34%) and transitions smoothly into (3) a very level segment (2.3%), which ends in an escarpment of roughly 8-10 metres in height.

The formation of the stratigraphy of Tchinguiz Tepe has been affected, as is usual, by natural and human agents and processes. The presence of sharp slopes made of easily eroded materials and a long human occupation of the site attach special importance to the geoarchaeological analysis of the deposits. The entire surface of the hill of Tchinguiz Tepe is covered by *superficial formations* of variable thickness, which have played a fundamental role throughout the investigation insofar as they are sediments that correlate to different processes, including human ones. In short, they are the expression of the processes of sedimentation-deposition that define the site. In addition, it is important to analyse how the site is related to its natural medium, because these relationships are fundamental in establishing absolute and relative dating and in obtaining environmental data on soil use and occupation in the area (Goldberg and Macphail, 2006).

The natural agents modelling the site have been functional before, during and since the cessation of human activity. These natural agents, typical of any morphogenetic system (i.e. processes, climate and relief, taken as a whole) are closely tied to environmental conditions. They can be functional now or in the past, appearing as inherited forms in the latter case. Over time, active processes or the intensity of activity may vary, but the modelling actions are permanent in one way or the other, because modelling is an open system. It is partly controlled by energy exchanges with other components of the natural system and with the sun, which acts as the ultimate driver of exogenous processes. In the area of Central Asia in which this work has been carried out, the present-day characteristics of the environment are tied to the fact that it lies in a continental land mass far removed from any large bodies of water. The conditions are likely to have remained similar during the period of time in which the stratigraphy of Tchinguiz Tepe has formed. However, climate variations combined with human activities may have caused significant changes in the region, if the findings of recent studies regarding the Aral Sea and a large part of arid Central Asia over the last 2000 years are representative (Sorrel, 2006; Yang *et al*, 2009; Boroffka *et al*, 2006; Oberhänsli *et al*, 2007; Chen *et al*, 2009). Well-known short-term climate variations, such as the Medieval Warm Period (MWP) or the Little Ice Age (LIA) (Machalett *et al*, 2008), may have affected the processes that produce and modify the superficial formations in the area of the site.

Human actions occur over a given period of time and, although they can be spaced out over time, they logically are especially active during the occupation of the site as an inhabited space. On the hill of Tchinguiz Tepe, we have documented human occupation from the 2nd-1st century BC, judging by the radiocarbon dating available from the excavation season of 2008. Although ancient Termez was destroyed by Genghis Khan in the winter of 1220-21 (Leriche, 2001: 82), the excavations and surveys of Tchinguiz Tepe have not yet uncovered any levels of occupation from the Islamic era. The date of Tchinguiz Tepe's abandonment as a place of habitation remains to be established with exactitude, but it does not appear to exceed the Kushan-Sassanian period (7th-8th centuries) (Leriche and Pidaev, 2007). However, a military base in the area has affected the topography of the site, although it has also contributed to the conservation of the site by limiting access and use of the land for other purposes. The surface of the site features military ditchs, as well as signs of earth moving by heavy machinery in some areas of the settlement, particularly at the southern end of the hill, which has probably been disturbed most severely. Disturbances of the original topographical surface by archaeological excavations should not be underestimated either. In this respect, the first excavations at Tchinguiz Tepe began in 1936 (Pougatchenkova, 2001). In addition, dumping from excavations in more recent periods has affected the original topography of the site.

2. Geomorphology, strata and superficial formations

In the case of the Tchinguiz Tepe site, the contribution of geomorphology takes into account the climatic context and the morphogenetic system of the site's surroundings, on the one hand, and it defines the physiography and the geomorphological units of space with respect to the site's location, on the other. The objective is to establish the causes and processes that have contributed to giving it its current form. To some extent, it tends to define and explain the evolution of a concrete space in which the units contain anthropic units as well.

2.1. Stratigraphic analysis

In geology, a *stratum* (*bed* or *layer)* is defined by its composition and texture. It is made up of a set of sedimentary materials that can be visually distinguished from others and may have highly varied dimensions. A stratum (or bed) is separated from underlying and overlying strata by stratification planes (top and botton respectively). These planes, whether they are in aqua-tic or subaerial media, are horizontal, sub-horizontal or sloped according to the sedimentary environment (slopes arise in fans, cones and deltas, for example.)

A series of strata implies a temporal sequence, which does not necessarily need to be vertical (stack of layers) in either natural or human settings. This is because the sedimentary process is not static, but can be displaced laterally like in deltas or during the transgressions (Anguita, 1988).

In the work zone, geological analysis marks as a stratum the set of materials—homogeneous in composition or texture—that have been carried intentionally or not from their original position or source area to another place. (This notion includes the collapse and subsidence of structures.) It is a body of sediments that are differentiated from adjacent sediments, although it is often difficult to observe the stratification planes.

The methodology of analysis followed has involved describing the vertical series of materials in the trial excavation sections. The observations were made at the point of greatest thickness and supplemented with observations at other key points, determined in each trial excavation according to its nature. The observed properties include lithology, granulometry, texture, colour and content of anthropic materials (basically pottery). This is reflected in a stratigraphic column that is significant only for the given point under observation. The most abundant sediment is sand and our interest lies in determining its origin in relation to wind action and slope dynamics. A magnifying glass was used in the field to estimate the morphoscopic characteristics and maturity of the sediment. The systematic survey of the levels will permit more precise analyses in the laboratory.

2.2. Slope analysis

On the hillsides of Tchinguiz Tepe—as at most archaeological sites—the sediments that cover and form are *superficial formations* with characteristics that differ from the geological substrate on which they rest. Among these characteristics are their cohesion, thickness and age. The sediments are more recent and usually unconsolidated, except in the case of crusts. Although a superficial formation may appear *in situ* (an weathering profile), account is only taken of transported formations in the context of this paper. In the deposition of the superficial formations, gradual variations and changes in composition (and origin) are observed in sediment quality such as colour, texture and granulometry, both vertically and horizontally. Such variations and changes have been very common in the area under investigation.

The slopes analysis has been fundamental in defining the geotopographic position of the excavated areas in the sloping segments in which they appear. In each trial excavation, varying processes predominate. For example, the middle zone acts as a transit area through which particles are dragged, while the base is more prone to deposition.

1) The study of trial excavation RC illustrates the way in which slope processes have affected the formation of the stratigraphy. To see this, it is important to bear in mind that RC is located where two topographical planes converge:

2) the first defines the foot of the hill (N-S orientation, slope ± 6.34 %), a zone prone to sediment accumulation, and

the second extends from the fortification wall in the interior of the enclosure (E-W orientation).

Consequently, the section of the trial excavation that is farthest from the fortification (western section) presents a series of sandy strata (SU 1, 5, 6, 19, 10 and 22) with a variable frequency of archaeological remains (e.g., pottery, charcoal, bones) of small size (centimetric), but packed in sediment that has been dragged by slope or wind conditions. The stratigraphy has been sharply affected by the topographical surface.

In addition, the sandy sediments varied laterally, forming wedges with levels arising from the collapse of the fortification (SU 2 and 4), anthropic levels deposited expressly by humans (SU 18) or levels of unknown origin, also probably man-made layers (SU 21 and 23) (Figure 1). In archaeological complexes, the sedimentary dynamic is not always obvious (i.e., geogenetic v. anthropogenetic causes). Analytic data are necessary to determine the complete history of a deposit in any stratigraphic sequence (Goldberg and Macphail, 2006: 37-38). However, the following sequence can be provisionally established for the lateral relationship of the part farthest from the face of the fortification wall (the western zone is the part most subjected to purely na tural forces) and the fortification itself (eastern zone), based on composition:

- The strata likely to be of *natural composition* (exclusively sandy matrix) in RC are parallel or subparallel to one another and to the topographical surface of the slope.
- The strata likely to be of *anthropic composition* (fundamentally clay matrix with fallen adobe bricks, occasional sand and ash, and plentiful pottery fragments) present a more variable geometry which is similar to the natural strata if a result of natural dragging, but random if intentional or a result of collapse.

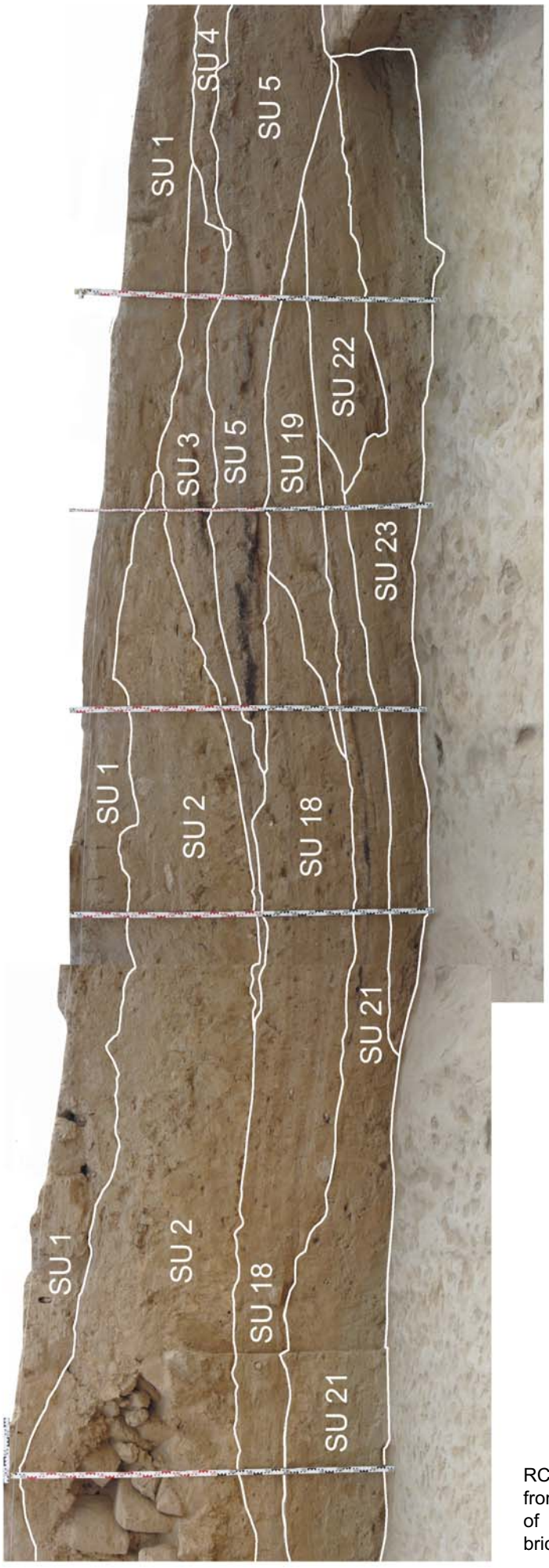

Figure 1: Southern cross-section of trial excavation RC showing the disposition and succession of materials from the most purely natural strata (sand, right-hand side of photo) to the most purely anthropic (fallen adobe bricks and clays, to the left)

3. Archaeological stratigraphy

According to the principles of stratigraphy established by Harris (1991), there are three types of archaeological SUs (Stratigraphic Units): layers, structures and interfaces. Most excavation records respect these categories. They reflect, for example, the approach used by the *Stratigraf* program, which was utilised by the University of Barcelona's mission to record the stratigraphy at Termez.

3.1. Identification of structures

One of the skills expected of an archaeologist is the ability to identify a *structure*. A structure is something that has been built, often using complex methods and generally composed of di-fferentiated parts, which should help in its identification during the process of excavation. Commonly, however, some structures such as adobe walls are hard to distinguish in the excavation of sediment generated by their destruction (Goldberg, 1979). In Termez, the use of *pakhsa* (structures of compressed clay or sand) poses an added difficulty, because we must base our differentiation of a *pakhsa* structure from a *layer* of sand or clay fundamentally on the degree of compression and its geometry. However, it is also necessary to assess the role of raw materials used in the construction of a *pakhsa* structure. The ratio of clay and sand may vary, affecting the degree of compression and, therefore, how perceptible the structure may be during excavation. Account must also be taken of the fact that a layer of sand or clay may be compressed or even cemented together by natural processes. As a result, it may acquire a consistency similar to *pakhsa* (for example, due to chemical precipitation of calcium carbonates). In addition, the disintegration of a *pakhsa* structure by natural agents yields a clay material that distorts the geometry of the original structure.

The problem is particularly serious when trying to differentiate *horizontal structures* (e.g. foundations built of *pakhsa*) in horizontal layers that may have become compacted due to other causes. Phenomena such as these can also lead to erroneous interpretations of georadar readings. For example, at Tchinguiz Tepe, in the excavation of trial excavation RT, a surface of compact clay was detected with pottery material and pebbles (Figure 2). It was interpreted as a stratum formed by sedimentation that sloped as a consequence of erosion acting on higher levels, but the doubt remains that it could be a *pakhsa* structure *in situ*, although demolished.

Figure 2: Detail of test pit RT showing a stratum of clay composition, with pottery and small black pebbles

In RC, SU 18 could be considered a structure since it is interpreted as fortification foundation. However, this interpretation is based less on the morphology or composition of the stratum than on its stratigraphic position: the first row of adobe bricks lies directly over SU 18. In excavation season of 2008, strata SU 21 and 22 were considered levels of the fortification foundation, similar to SU 18. They were located under SU 18, in a horizontal position, and rested on the sandstone substrate, which was carved by humans (Figure 3). However, the 2009 excavation rejected this interpretation: above SU 21 and under SU 18 a new sequence, including a dwelling structure, could be detected.

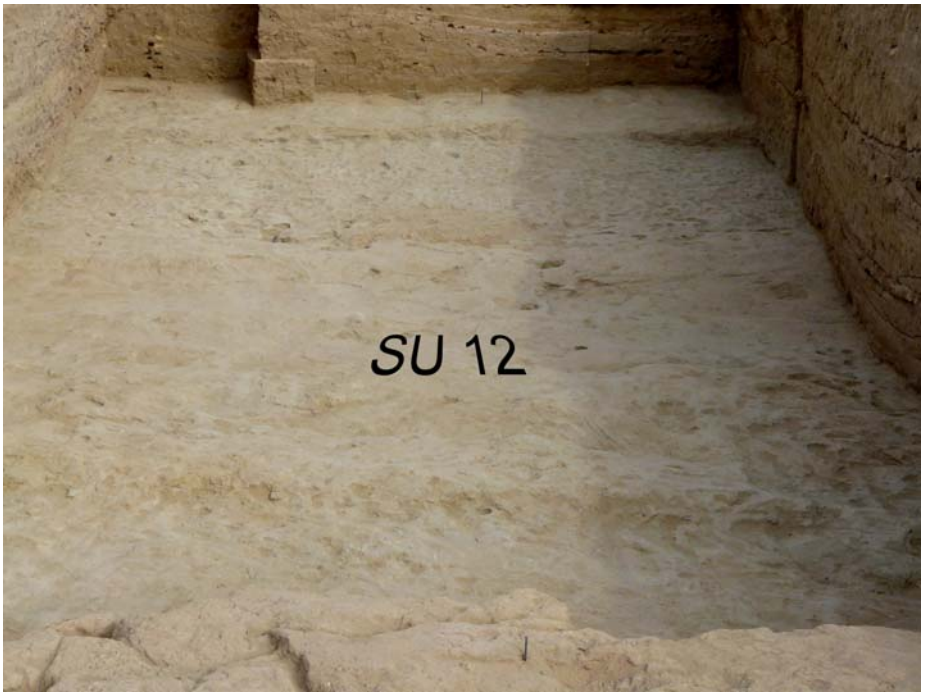

Figure 3: Detail of sandstone substrate (SU 12) in RC, showing marks struck in the substrate by human intervention

3.2. Identification of interfaces

We will set aside the problem of observing interfaces of separation between two SUs for when we treat the methodology for excavating strata, because the Harris system does not envisage the record of these interfaces independently. With respect to interfaces defined as *erosion surface of structures*, observation plays a role in the general interpretation of the site's taphonomy and it poses no great problems of perceptibility. By contract, the *erosión of strata* is usually undetectable in practice. But for specific indicators, it cannot be differentiated from an interface of contact between strata. With respect to holes or ditches perceptibility depends on any differences in colour, texture and composition that characterise the stratum which has silted into the stratum in which the hole has been excavated. In addition, the consistency of the stratum in which the interface is excavated affects how perceptible it is. A hole excavated in a compact stratum is easier to perceive than a hole in a less compact stratum, because the latter case contains interfaces with blurry lines. At Termez, most of the strata are basically sandy in composition and this face hampers the perception of holes or ditches. Similarly, the geometry of the hole is also a factor, because pits or holes are easier to perceive because than more regular geometric shapes. In the 2007 season, a hole (SU 9) defined in RB cut across a stratum with a clay matrix (SU 4). Later excavation of SU 4 revealed that remains still existed from the infill of the hole (SU 7) and a single fragment of Islamic pottery was recovered. The fact that SU 7 contained a clay infill—possibly from SU 4 itself—was the cause of the error.

3.3. Identification of strata

At Termez, the presence of sand as a basic ingredient of the sediments leads to the production of strata without compact tops. In other words, they are *open to a process of cumulative ongoing formation*. If the top of a sandy stratum is not sealed by the bottom of a stratum which has a different composition, then no interfaces appear. SUs 5, 19 and 22 in trial excavation RC offer an example of the problem. They can be differentiated by means of the intervening wedges of clay strata 18, 21 and 23, but the phenomena are observable only at the eastern edges of SU 5, 19 and 22 (Figure 4).

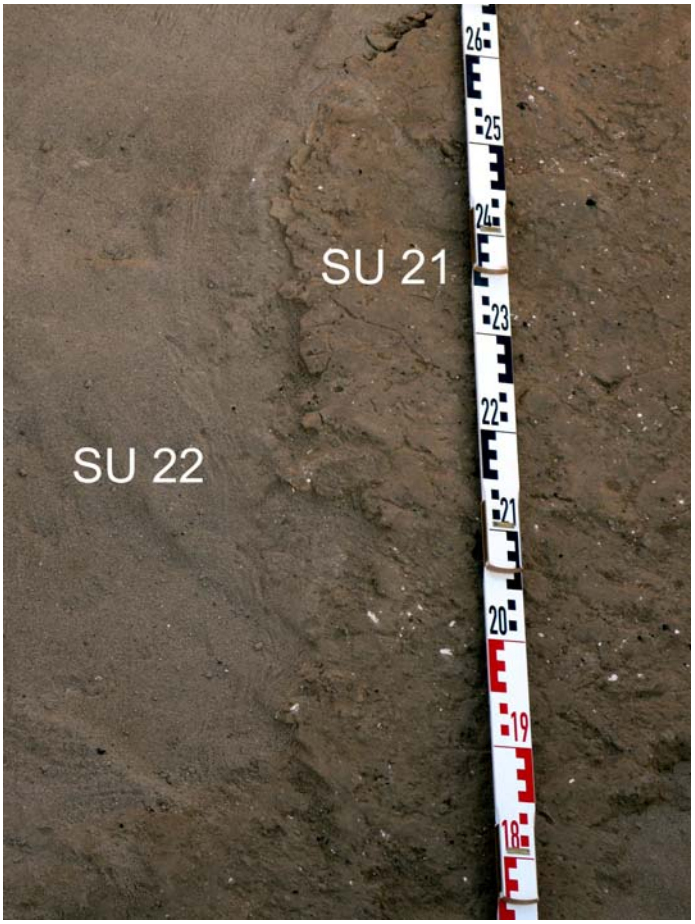

Figure 4: Trial excavation RC. Area where SU 21 (clay) comes into contact with SU 22 (sand)

4. Stratigraphic reading. Correlation between geological and archaeological levels at Tchinguiz Tepe. Experimental analysis of the trial excavations RB and RC

In general, there is a good correlation between the geological and archaeological stratigraphic levels. This is true in the sense that each stratum differentiated in the geological examination has a corresponding stratum described in similar terms in the archaeological examination, although the two readings were taken independently and with different methodologies. The *geological stratigraphy* summarised in Tables 2 and 3 arises solely from an examination of the walls of the excavated areas after the excavation was completed, while the archaeological stratigraphy was defined during excavation, as is common. In the case of trial excavation RC (Table 1), the observations have been made in the western section (the farthest from the fortification) and they have been supplemented by reading the stratigraphic profiles of the other sections in the excavated areas. In the case of trial excavation RB (Table 2), the observations have been made in its four sections and the central baulk left expressly for that purpose. Some differences appear in the order and grouping of levels. For example, as in RC (Table 1),

Geological stratigraphy	Correlating archaeological levels
RC-a = 35 cm. Discontinuous appearance of fine black round or elongated gravel particles with medium to fine sand is observed on the surface. Constitutes sealing surface. Highly scarce gravel eventually disappears. Medium to fine sand. At 22 cm, there is a level of fine sand with low potential. Contact with RC-b is irregular. Dispersed pottery. **RC-b** = 32 cm. Thick, homogeneous sand, no gravel. Charcoal.	**RC-a + b** = **SU 1** = 65 cm. Sand of brown-grey colour. Top presents hardened level of smooth black gravel, small in size (< 5 cm in diameter). Contains pottery. Formation: possible natural origin. Pottery appears in stratum due to dispersion from sites of original deposition by unspecified causes. Potential 15-65 cm.
RC-c = 37 cm. Fine to very fine sand, massive. Possibly aeolic sand based on the good selection of the sand's granulometry Sporadic pottery. ---------- **RC-d** = 35 cm. Very fine sand, sporadic pottery.	**RC-c + d** = **SU 5** = 70 cm. Level of brown-grey sand, loose, with occasional ashes. Contains pottery (24 brick fragments and a fragment of limestone used in architectural decoration). Formation: Possible natural origin, aeolic sand. Pottery fragments probably appear due to frequent use of site at the time of the deposit's formation. Potential 2-70 cm.
Note.-. The levels perceived between **N-RC-a** and **N-RC-d** are tied to processes of transport and deposition that are normally natural (e.g. superficial runoff and wind). This group of strata constitutes a formation produced by natural agents and made up of natural and human materials. The human materials have been packed by a sandy matrix of moderately variable granulometry, depending on the level. The disposition of the strata is typical of the natural agents acting in its formation; the contact surfaces, while sometimes irregular, are roughly parallel to one another and to the surface of the slope. That would appear to rule out intentionality in their location.	
RC-e = 18 cm. Very similar to previous level, but more compact and richer in pottery. No red clay is detected in the cross-section where the profile was viewed.	**SU 6 =** 15 cm. Level of sand with human contributions, dark brown colour, compact. At some points, the top presents a thin hard crust of compact red clay with white patches (limestone?) .
RC-f = ± 39 cm. Fine sand on a sandstone substrate. Pottery remains and bones.	**SU 10** = Sand. Serving as a foundation for dwellings. The upper part shows a thin cracked crust that could be a floor or surface of use.
Rocky sandstone substrate. Profile of alteration appears irregular based on variations uncovered.	**SU 11 and 12** = Rocky sandstone substrate.

Table 1. Correlation between geological and archaelogical levels in trial excation RC

the geological examination frequently distinguishes two levels where the archaeological examination only finds one. That occurs on two occasions (RC-a + b = SU 1; RC-c + d = SU 5). In the case of RC-a + b = SU 1, the phenomenon can be explained by the fact that they are two levels basically formed by natural agents. Where the geology distinguishes the most superficial gravel covering from the solid sandy mass which it covers, the archaeology only indicates “aeolic sand”, treating the gravel covering it as a phase within SU 1.

Geological stratigraphy	Correlating archaeological levels
N-RB-a = Discontinuous superficial covering of dark, very smooth pebbles and gravel. The gravel remains *in situ* while sand is carried by the wind. It is observed in all the cross- sections of the trial excavation and across the entire surface of the hill, in a more or less defined state. **N-RB-c** = Sand and gravel of 2-3 cm, fragments of sandstone.	**SU 1** = Current ground, subjected to wind action, and supporting vegetation cover typical of steppes. Pottery appears in the stratum, dispersed from its original place of deposition by unspecified causes.
N-RB-d = 40 cm of very fine sand, with some very round gravel that is less numerous than above. Contains some pottery remains. Fragments of altered sandstone.	
N-RB- e = This designation encompasses a complex formation near the topographical surface. It is composed of decimetric fragments of highly altered grey sandstone with some orange and red staining from iron oxides; pebbles and round nodular blocks. Ochre in colour. Lithological character to be determined. Centimetric nodules are distributed sporadically throughout the formation. Could be related to a paleosoil in origin. Sandy matrix.	**SU 3** = Blocks of sandstone and limestone conglomerates. No pottery.
N-RB- f = Level of fine sand, ochre to grey in colour, located below the preceding formation. Containing pottery.	**SU 2** = Level of sand. Level of infill covering a ditch (SU 8) open to a level of clay (SU 4).
N-RB-b = Massive formation of red sand packing angular fragments of grey sandstone (highly altered) and ochre or grey lutites (?) and nodules, >1 < 3 cm. Nodules and lutite fragments are similar to those appearing in the underlying substrate here. Similar lithology has been observed at the Gora Uch Kyzyl. Some pottery appears in the upper third of the cross-section (1).	**SU 6=** Fragments of small rocks (limestone conglomerates and sandstone) in a sand matrix. Containing a small amount of pottery, it forms part of a foundation structure alternating layers of compressed clay with fragments of sandstone and limestone conglomerates.
(1) Beneath **N-RB-b**, the sandstone substrate (quite altered) outcrops in the southern part of the trial excavation. SU 4 ends prior to reaching the southern cross-section, so that it does not appear in the sequence of the geological stratigraphy. Similarly, at some points of the excavated area, the archaeological examination has detected SU 5 = "level of compact red clay with pottery remains from the 1st century AD", directly over the sandstone. However, it is not observed in the points taken in the geomorphological survey, possibly because it is part of the underlying unit or because of a local fault.	

Table 2: Correlation between geological and archaeological levels in trial excavation RB

5. Formation of the stratigraphy at Tchinguiz Tepe

5.1. Trial excavation RC

Five phases arise from the geoarchaeological analysis of the stratigraphy of RC. Each is made up of several SUs. Below, their descriptions are organised from oldest to most recent:

1. First phase of occupation

The first phase includes an initial intervention in the sandstone substrate (SU 11 and 12), which shows carving and levelling for the purpose of constructing the fortification foundation (Figure 3). The only structures probably related to this phase are the *pakhsa* walls (SU 8 and 9). Notably, the weathered surface of the sandstone substrate SU 11 is not detected at the eastern end of the trial excavation (beneath SU 23), indicating that no human intervention on the substrate has occurred at its western end, which is the farthest from the fortification wall. This phase also includes SU 23, 22, 21, 19 and 10.

SU 10 (= RC-f), 22 and 19 share some basic characteristics. They are sediments of exclusively sandy composition that appear to have been carried by the wind. However, their stratigraphic relationship makes it necessary to date them to this first phase of human intervention. As noted, SU 22 forms a wedge between SU 23 and SU 21, while SU19 forms a wedge between SU 18 and SU 21. The cracked crust of SU 10 (Figure 5) could be explained as a former floor inside the enclosure.

Figure 5: Trial excavation RC. Top of SU10 showing the formation of a thin cracked surface crust

2. Second phase of occupation

This phase is solely represented by SU 18 an anthropic stratum, part of the foundation of the reinforcement of the interior face of the wall fortification (SU 16).

3*. First phase of abandonment.*

SU 18 and 19 once served as the former surface of use inside the enclosure. However, as previously noted, their top may have suffered erosion that is not detectable in the stratigraphic record. This surface will support a process of accumulation of sediments of varying composition and origin. Their sequence is set out below, ranging from the oldest to the most recent:

- SU 6 (= RC-e). Sand of indeterminate origin packing pottery fragments suggests that this stratum resulted from hill-slope sediment transport. At some points, compact red clay is observed with white patches. This detail appears to increase the weight of the human contribution in the stratum, which includes not only pottery, but also deposits.

- SU 5 (= RC-c + d). Its sandy matrix indicates wind contributions. However, as in the previous stratum, this one contains a significant number of pottery fragments maybe from slope sediment contributions. Phases with low-potential ash indicate human intervention.

- SU 4. This is a stratum of scant size. Based on position and composition, which is solely made up of clay, it is interpreted as adobe-brick remains altered as a consequence of the fortification wall's collapse.

- SU 3. This stratum forms part of the infill of SU 20. Household rubbish with an abundant presence of ash and charcoal alternates with aeolic sand sand in this level. Technically, each of these beds defines a stratum, but they constitute a set of centimetric sheets in its own right. This is an example of a sequence alternating natural and human contributions. Although it remains unlikely, the sand may have been carried by humans.

- SU 2 (RC-g). The stratum contains adobe bricks that have fallen from the fortification wall (Figure 6). The clay matrix arises from the weathering of the adobe itself. The collapse resembles the *rock slides* occurring on slopes, but with an exclusively human source.

4. Third phase of occupation

The third phase of occupation is barely visible in RC. It is solely represented by SU 13 and SU 15, which are part of a wall built after the fortification wall began to fall into ruins, given that it is built on SU 2.

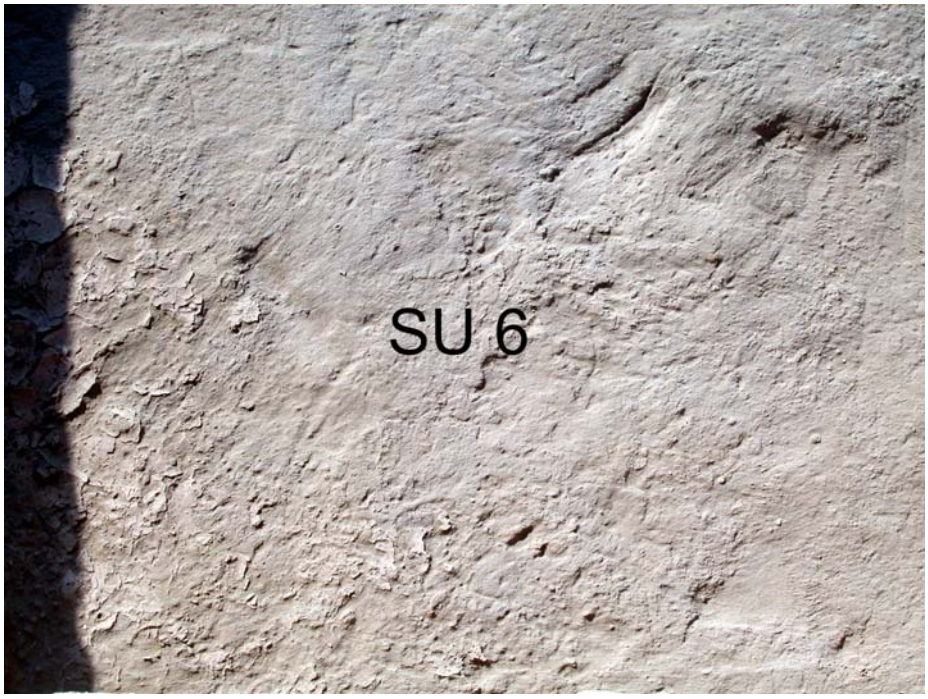

Figure 6: Trial excavation RC. Fallen adobe bricks from the fortification in SU 2

5. Second phase of abandonment

The final sequence of abandonment is solely represented by SU 1 (= RC-a + b). It is the most superficial formation constituted by wind and slope sediment, containing dark gravel that gradually diminishes in lower levels. The pottery remains have reached the stratum by slope dragging from higher elevations.

5.2. Trial excavation RB.

The stratigraphy of trial excavation RB poses interpretation problems arising from the limited surface excavated and the scant potential of the stratigraphy. The oldest documented level is SU 5 (geologically undefined). Basically clay in composition, it would appear to be a deposit. The high number of pottery fragments further supports its likely human association.

Above SU 5 lies SU 6 (= N-RB-b), which is a massive formation of red sand with angular fragments of grey sandstone (highly altered) and ochre or orange lutite and nodules (>1 < 3 cm). The deposit is difficult to interpret. If it were to form part of a foundation jointly with SU 4 and SU5, as first interpreted in the archaeological excavation, then it should be treated as a stratum of human origin. However, the geological stratum does not confirm this fact to the extent that SU 5 is not defined. Rather, it could be the top of a highly developed profile of alteration that may have been moved *in situ* for foundation purposes. Given the absence of conclusive data and the limited excavated surface, no sound reading can be proposed.

SU 4 (not defined geologically) has a composition similar to SU 5. The geological study reveals a matrix broadly natural in origin for both. However, the fundamentally clay composition points to the selection of a deposit. The anthropic component is reinforced by the abundance of pottery provided by this deposit.

SU 2 (=N-RB- f) is the natural infill of a hole (SU 8). It is a level of fine ochre-to-grey sand containing pottery. The processes involved in its formation are hard to determine, but the presence of archaeological material in this deposit should be noted, because it underpins SU 3 (= N-RB-e), a deposit that is difficult to interpret.

SU 3 (= N-RB-e) could be the altered top of the sandstone substrate. Its position over levels of clearly human origin, however, leave the question pending until a new analysis is performed (Figure 7).

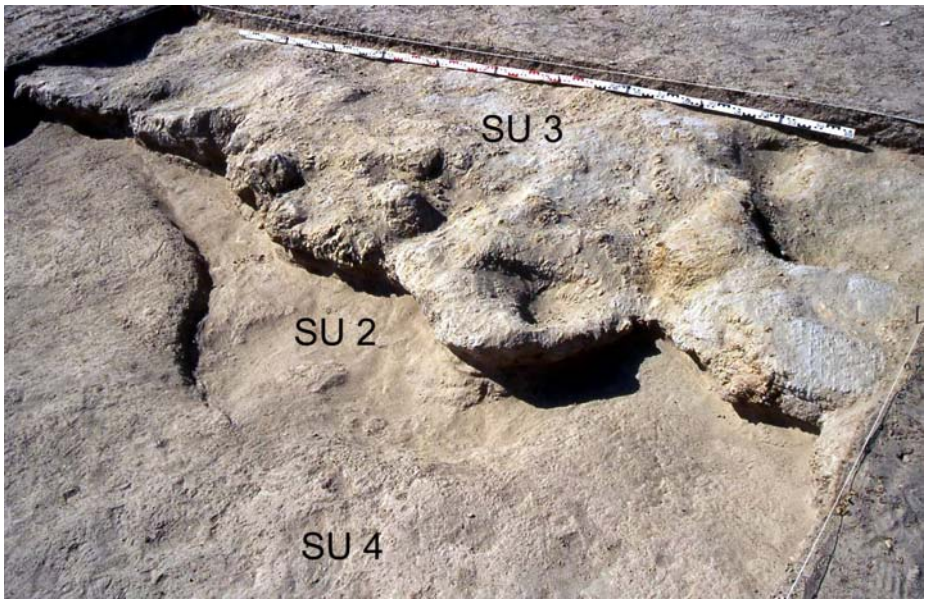

Figure 7: Trial excavation RB. SU 2, 3 and 4. SU 3—likely top of the substrate—can be seen over SU 2, a level of fine sand, ochre to grey in colour, containing archaeological materials

The most recent level SU 1 (= N-RB-a, N-RB-c y N-RB-d) defines the most superficial formation, which is similar to the one uncovered in RC. The geological stratigraphy distinguishes N-RB-c and N-RB-d, the first of which features a direct outcropping where the most superficial covering is discontinuous. Its formation has arisen from wind and slope sediments that may include pottery remains.

5. Stratigraphy of Tchinguiz Tepe and Reading of Geophysical Survey

Logically, georadar readings measure depth relative to the current ground level. The depth readings for the various SUs have been taken from Point 0, which is the reference point for depth of the entire site. For the purposes of comparative analysis, the depths taken during excavation have been corrected by treating the top of SU 1 as depth 0 and using it to measure the potential of each stratum below it. Georadar surveying reaches a depth of -3.00 m. The substrate is located around -1.80 to -2.35 m.

Our main preliminary conclusions are set out below. Firstly, the anomalies observed in the georadar reading for cross-sections 1-5 (0-1.16 m. in depth) correspond quite closely to SU 2 and 4 in the archaeological stratigraphy. As noted early, both of these strata feature a composition made up almost exclusively of a clay matrix. SU 2 also contains adobe bricks or fragments of bricks that have fallen but are well-preserved and form massive accumulations. The top of SU 2 is located at between -0.20 and 0.56 m. of depth and it has a dip slope that follows the slope of the hill. The botton of SU 2 is located at between -1.03 and -1.44 m. Large fragments of adobe brick, located in the central zone of the stratum, have been detected as anomalies by the georadar. SU 4 (depths between -0.34 and -0.59 m.) do not appear in cross-sections 1 and 2, but they do appear in cross-section 3 and, to a lesser extent in cross-section 4. This corresponds to their potential, which is less than SU 2.

No reading corresponds to the archaeological stratigraphy beneath SU 2. Fundamentally clay strata (SU 18, 21 and 23) are not distinguished from the fundamentally sandy strata (SU 19 and 22). Even more notable is the fact that the sandstone, which is located roughly at a depth of -1.80 to -2.35 m, does not appear in the sections taken with georadar (Figure 8).

Lastly, the georadar detected an anomaly in the eastern part of the trial excavation between squares 0 and 2 of the grid. The anomaly appears in all cross-sections. Although it begins diminishing in intensity from 1 metre in depth, it extends throughout the entire stratigraphic sequence. However, it has no correspondence in the archaeological sequence, which is able only to indicate that it lies parallel to the line of fortification.

Figure 8:
Termez project. 2007 season.
Georadar survey at 270MHz.
Grid C Area 3

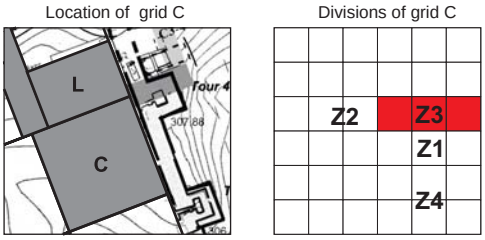

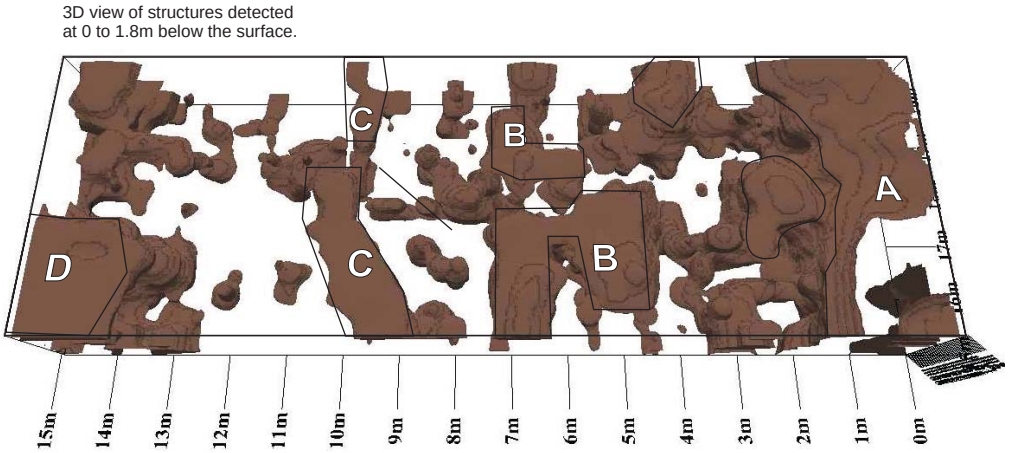

Slide 4 z=0.4-0.6m below the surface.

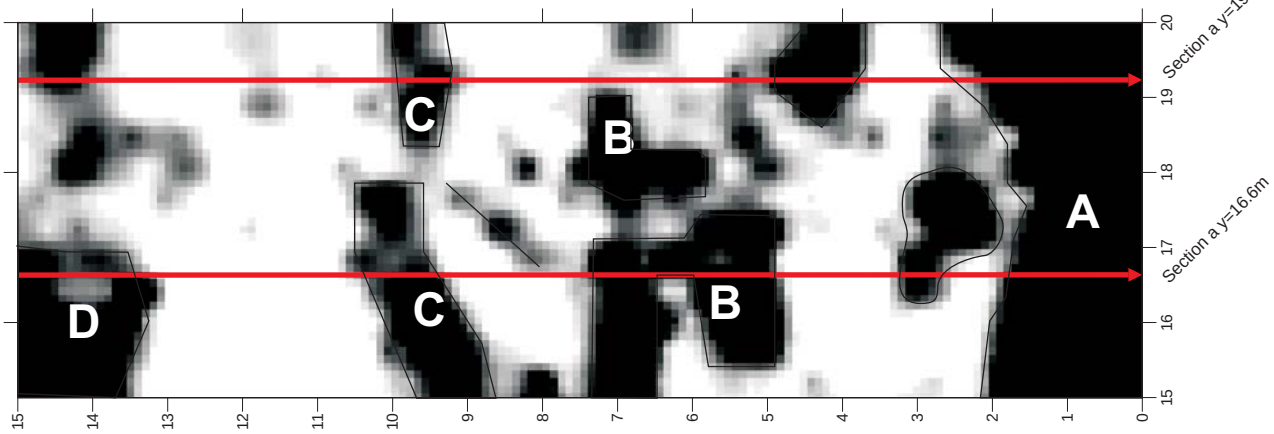

Section a y=19.2m

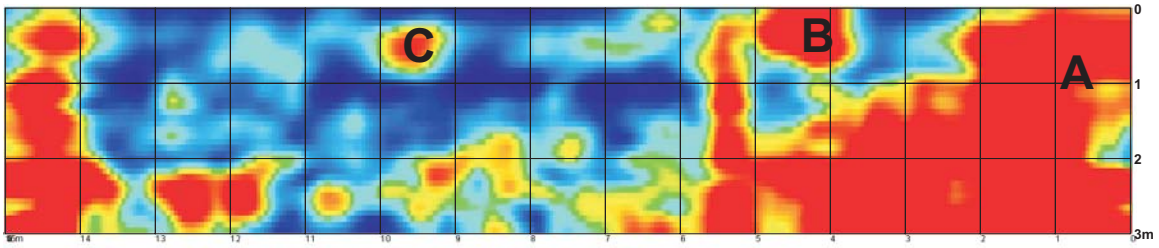

Section a y=16.6m

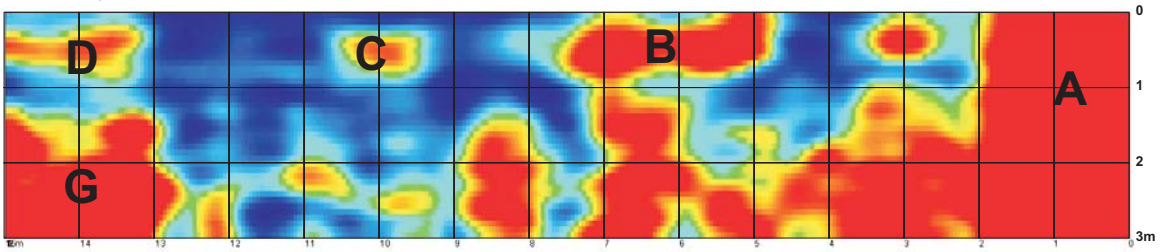

REFERENCE WORKS CITED

Anguita Virella, F. (1988): *Origen e historia de la tierra*, Madrid.

Boroffka, N.; Oberhänsli, H.; Sorrel, Ph.; Demory, F.; Reinhardt, Chr.; Wünnemann, B.; Alimov, K.; Baratov, S.; Rakhimov, K.; Saparov, N.; Shirinov, T.; Krivonogov, S.K.; Röhl, U. (2006): "Archaeology and Climate: Settlement and Lake-Level Changes at the Aral Sea", *Geoarchaeology: An International Journal*, Vol. 21, nº 7, pp. 721-734.

Chen, F.; Holmes, J.; Wünneman, B.; Yu, Z. (2009): "Holocene climate variability in arid Asia: Nature and mechanisms", *Quaternary International*, Vol. 194, pp. 1-5.

Harris, E. C. (1991): *Principios de estratigrafía arqueológica*, (1ª ed. inglesa Londres, 1979).

Goldberg, P. (1979): "Geology of Late Bronze Age mudbrick from Tel Lachish", *Tel Aviv, Journal of the Tel Aviv Institute of Archaeology*, 6, pp. 60-71.

Goldberg, P.; Macphail, R.I. (2006): *Practical and Theoretical Geoarchaeology*, Oxford.

Leriche, P. (2001): "Termez antique et médievale" en Leriche, P.; Pidaev, C.; Gelin, M.; Abdoullaev, K. (Dirs.), avec la collaboration de Fourniau, V., *La Bactriane au carrefour des routes et des civilisations de l'Asie centrale*, Paris, pp. 75-99.

Leriche, P.; Pidaev, Sh. (2007): "Termez in Antiquity", en Hermann, G.; Cribb, J. (Eds.), *After Alexander. Central Asia before Islam*, Oxford, pp. 179-211.

Machalett, B.; Frechen, M.; Hambach, U.; Oches, E.A.; Zöller, L.; Markovic, S.B. (2006): "The loess sequence from Remisowka (northern boundary of the Tien Shan Mountains, Kazakhstan)- Part I: Luminescence dating", *Quaternary International*, Vol.152-153, pp. 192-201.

Oberhänsli, H.; Boroffka, N.; Sorrel, P.; Krivinogov, S. (2007): "Climate variability during the past 2,000 years and past economic and irrigation activities in the Aral Sea basin", *Irrigation and Drainage Systems*, 21, 3-4, pp. 167-183.

Pougatchenkova, G. (2001): "C'était hier; c'était il y a longtemps", en Leriche, P. ; Pidaev, C. ; Gelin, M. ; Abdoullaev, K. (Dirs), avec la collaboration de Fourniau, V., *La Bactriane au carrefour des routes et des civilisations de l'Asie centrale*, Paris, pp. 37-46.

Sorrel, Ph. (2006): *The Aral Sea: a paleoclimatic archive,* doctoral thesis, Institut für Geowissenschaften, Universität Potsdam, Deutschland, Laboratoire PEPS, UMR 5125, Université Claude Bernard – Lyon 1, France.

Yang, B.; Wang, J.; Bräuning, A.; Dong Z.; Esper, J. (2009): "Late Holocene climatic changes in arid central Asia", *Quaternary Internacional*, Vol. 194, pp. 68-78.